Forward Seismic Modelling of Volcanic Intrusions from Independence Fjord - Northeast Greenland

Eli Kristine Sook Austrheim

Abstract

The purpose of this thesis is to investigate the seismic response of large-scale volcanic intrusions by using the technique of forward seismic modelling. The modelled structures are exposed on the south side of Independence Fjord in eastern North Greenland and consist of sandstones cut by mafic intrusions, and overlain by a basaltic lava sequence of plateau basalts.

The modelling algorithm that has been used to generate the synthetic seismic data is based on the elastic wave propagation theory, and the densities and velocities that have been used in the modelling have been determined from the general knowledge of the different lithologies.

The results show that there are strong reflections associated with the layer of plateau basalts, thereby indicating that much of the seismic wave energy is lost due to this layer. Some of the structures beneath are still visible, though not so clear. The high velocity contrasts between the layers in the model also cause numerical instabilities in the modelling algorithm, because the assumptions that the algorithm is based on is not fulfilled.

By removing the layer of plateau basalts and replace it with a sandstone layer, the structures beneath become much clearer, meaning that the plateau basalts obscures the imaging of the structures beneath quite a lot. Since the uppermost volcanic layer that the seismic waves have to propagate through gives the strongest reflections, this indicates that the uppermost volcanic layer influences the imaging of the structures beneath quite a lot. Based on this it is believed that in the presence of several volcanic layers some energy get lost for each volcanic layer that the seismic waves have to propagate through, thereby making it difficult or impossible to see deep in the subsurface when many volcanic layers are present. The high velocities associated with volcanic intrusions also make the resolution of the seismic poorer.

Sammendrag

Hensikten med denne oppgaven er å undersøke den seismiske responsen til storskala vulkanske intrusjoner ved bruk av seismisk framovermodellering. De modellerte strukturene er blottet på sørsiden av Independence-fjorden i det nordøstlige Grønland, og består av sandsteiner som er kuttet av mafiske intrusjoner. En basaltisk lavasekvens bestående av platåbasalter ligger på toppen av sandsteinene.

Modelleringalgoritmen som har blitt brukt til å generere de syntetiske seismiske dataene er basert på elastisk bølgeforplantningsteori, og hastighetene og tetthetene som har blitt brukt i modelleringen er bestemt ved hjelp av den generelle kjennskapen til de ulike litologiene.

Resultatene viser at det forekommer sterke refleksjoner fra platåbasaltlaget, som dermed indikerer at mye seismisk bølgeenergi går tapt på grunn av dette laget. Noen av strukturene under er likevel synlige, selv om de ikke er like tydelige. De høye hastighetsforskjellene mellom lagene i modellen forårsaker også numeriske ustabiliteter i modelleringsalgoritmen, da antagelsene som er gjort i utledningen av algoritmen ikke lenger er oppfylt.

Ved å fjerne platåbasaltlaget og erstatte det med et sandsteinslag, blir strukturene under mye tydeligere, noe som betyr at platåbasaltlaget ødelegger ganske mye for avbildningen av strukturene under. Siden det øverste vulkanske laget som de seismiske bølgene må bevege seg gjennom gir ganske sterke refleksjoner, indikerer dette at det øverste vulkanske laget påvirker avbildningen av strukturene under i stor grad. Basert på dette antas det at når flere vulkanske lag er tilstede, går noe energi tapt for hvert vulkanske lag som de seismiske bølgene må bevege seg gjennom, noe som vil gjøre det vanskelig å se dypt i ned i undergrunnen når mange vulkanske lag er tilstede. De høye hastighetene som er forbundet med vulkanske intrusjoner gjør også at den seismiske oppløsningen blir dårligere.

Preface

This thesis is written as the final part of my master degree in Petroleum Geosciences and Engineering at the Norwegian University of Science and Technology (NTNU). The thesis has been written at the Department of Petroleum Engineering and Applied Geophysics at NTNU.

First of all, I would like to thank my supervisor, Professor Ståle Emil Johansen for his guidance, support and advices throughout the work of this thesis.

I would also like to thank Phd student Espen Birger Raknes and Professor Børge Arntsen for their help and assistance with the modelling and processing the Madagascar software.

Finally, thanks to my fellow students.

Trondheim, June 10th 2012

Eli Kristine Sook Austrheim

Contents

List of Figures

List of Tables

1   Introduction

Seismic data play an important role in the understanding and imaging of the subsurface. Today seismic methods are being used in a number of fields, including mapping of water resources in relation to engineering and environmental studies, mineral exploration and mine planning, and crustal studies. However, the major application for seismic methods is to map and monitor hydrocarbon resources. Marine seismic surveys are among the main tools for petroleum exploration and production offshore. Based on seismic interpretation results, very expensive wells might be drilled. Thus a proper understanding of seismic data is of major importance. One of the difficulties with seismic interpretation is that more than one geological model might fit the seismic data. To improve our understanding of how seismic waves behave the technique of forward seismic modelling is a valuable tool. This allows us to test the relationship between geology and seismic response. In general, seismic modelling can be employed to design the seismic acquisition parameters, prove the seismic processing approaches and validate the seismic interpretation.

Difficulties in imaging the subsurface often arise in relation to volcanic intrusions. Volcanic intrusions usually have very high velocities compared to the host rock such that the interfaces show up as strong reflectors on the seismic data, i.e. bright spots. Because of the strong reflections less energy passes through the intrusions, and thereby makes it more difficult to image the layers beneath. Especially basalt layers cause problems in imaging the subsurface. Basalt layers may consist of several individual flows and may be very inhomogeneous, thus causing much of the seismic energy to be absorbed and scattered within the basalt. This causes problems in looking beneath basalt layers on seismic data.

There have been used to types of software in this thesis, the Petrel software and the Madagascar software. The Petrel software has been used to build a geological model, whereas the Madagascar software has been used in the modelling and processing steps. Because the first intention was to do a 3D modelling, the model building done in Petrel is explained for a 2.5D model, i.e. a 2D model that is constant in the third dimension. However, due to the limited amount of time to finish this thesis it was later decided to do a 2D modelling instead. The results discussed in Chapter 5 are therefore 2D results and not 3D results.

2 Geological setting

2.1 The Independence Fjord Group

The Independence Fjord Group crops out over an area of more than *80 000 km²*, and is found over large areas of eastern North Greenland and North-East Greenland. The group consists of a more than *2 km* thick sandstone sequence, deposited in a continental inland basin that developed around Independence Fjord about *1750 Ma* ago. This basin is the earliest recorded major depositional basin developed on the Greenland shield.
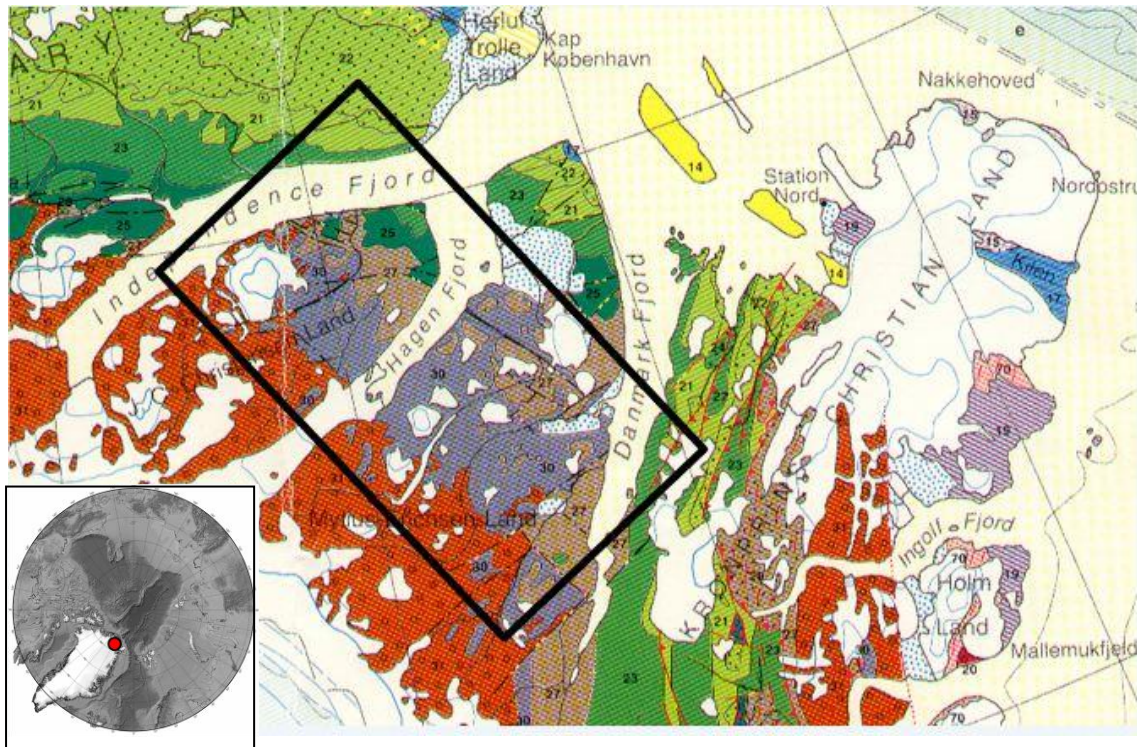
Figure 2.1: Overview of the area around Independence Fjord. The area marked by the rectangle shows the Zig-Zag Dal Basalt Formation (see Chapter 2.2). (From Upton et al, 2005)

The sandstones are mainly found as unfolded layered sequences in the areas west and south of the Palaeozoic fold belts, whereas strongly deformed representatives are found within the Caledonian fold belt in Kronprins Christian Land and areas to the south.

The rocks underlying the sandstones are not exposed, but indirect evidence suggests that they rest on a gneissic basement. The sandstones were originally lake sediments, and include some beds of wind-borne material. Some silty beds alternating with the sandstones also indicate deposition in a salt lake.

2.2   The Midsommersø Dolerites and the Zig-Zag Dal Basalt Formation

The Independence Fjord Group sandstones are everywhere cut by numerous mafic sheets, sills and dykes, the Midsommersø Dolerites (Figure 2.2).

Figure 2.2: Cliffs on the south side of Independence Fjord in North Greenland showing a section through unfolded sandstones of the Independence Fjord Group cut by a network of dark volcanic intrusions that form dykes and flat-lying sills (Midsommersø Dolerites). The dykes and sills are feeder channels to the overlying basaltic rocks (Zig-Zag Dal Basalt Formation), seen at the upper left of the section. Cliffs are about *800 m* high. (From Henriksen, 2005)

The dyke-sill network originates from a major Mesoproterozoic igneous event that occurred either as the beginning of ocean floor spreading north of a Greenland-Canadian continent, or due to the passage of the continent over a volcanic centre in the earth's mantle (a hotspot).

The dolerite intrusions are up to *100 m* thick and dissect the undeformed Independence Fjord Group sandstones. The dolerite dykes were feeders to a thick basaltic lava sequence of tholeiitic flood basalts, the Zig-Zag Dal Basalt Formation, which conformably overlies the Independence Fjord Group (Figure 2.2). The basalt layer is up to *1350 m* thick and is among the oldest well-preserved basalt successions known.
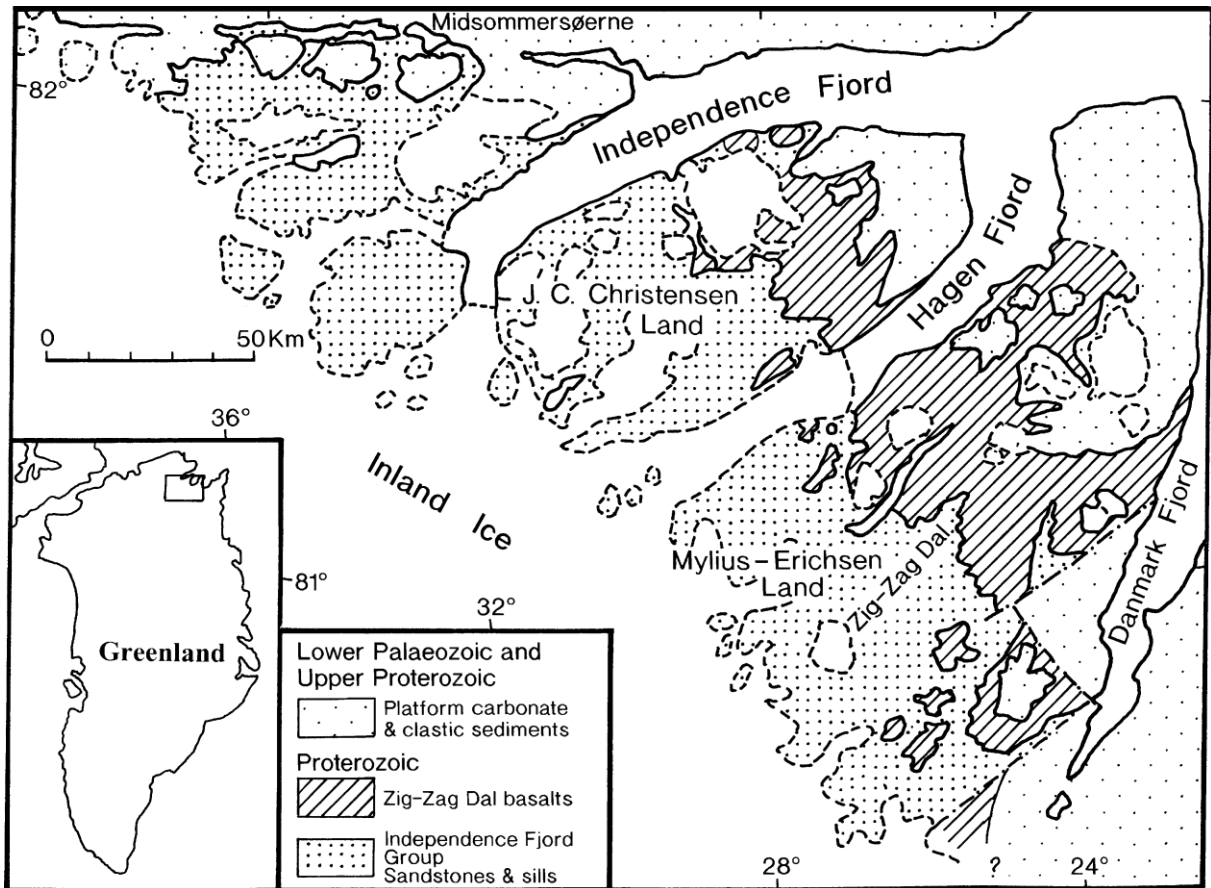
Figure 2.3: Geological sketch map showing the outcrop areas of the Zig-Zag Dal Basalt Formation and the Independence Fjord Formation. (Kalsbeek and Jepsen, 1984 cited in Upton et al., 2005)

The main outcrops are south of Independence Fjord, where it crops out over an area of *10 000 km²* (Figure 2.1 and Figure 2.3). But the local occurrence of similar basalts in eastern Peary Land indicates that the formation once covered a very large part of North Greenland. The Zig-Zag Dal Basalt Formation comprises more than *50* individual flows with thicknesses ranging from *10* to *120 m*. Pillow lava structures in the lower part of the sequence, indicates that some flows were erupted under water, while the upper part of the sequence was clearly extruded onto a land surface. The Midsommersø Dolerites are found to be about *1380 Ma* old, thereby indicating that the Zig-Zag Dal Basalt Formation is of similar age. Hydrothermal activity, associated with the igneous event, caused significant chemical changes both in the sandstones and in many dolerites. This alteration can be seen as reddening in some of the dolerites.

3 Geological modelling

3.1 Geological model

The purpose of a geological model is to show the geological properties like structures and lithology in a certain region. The real earth is very complex, and several assumptions and simplifications have to be done in order to make a geological model. The basis for making a geological model is dependent on the area of investigation and previous studies of the area. A geological model may be made based on outcrops in the field, seismic data, geological samples or other measurements, or a combination of these. In this thesis the geological model from the Independence Fjord area has been made based on a photo showing the outcrops in the field, together with the general knowledge of these kinds of rocks.

Figure 3.1: (Identical to Figure 2.2). Photo showing outcrops in the field. The Independence Fjord Group sandstones are cut by a network of dyke-sill intrusions (the Midsommersø Dolerites) and are overlain by plateau basalts (Zig-Zag Dal Basalt Formation). The height of the cliffs is about *800 m*.

Figure 3.1 (identical to Figure 2.2) shows the outcrops on the south side of Independence Fjord. It shows the Independence Fjord Group sandstones cut by a network of dark volcanic intrusions, the Midsommersø Dolerites. On top of the section the Zig-Zag Dal Basalt Formation conformably overlies the sandstones.

Figure 3.2: Geological model. (Made in Illustrator)

The geological model made from Figure 3.1 is shown in Figure 3.2. It is assumed that at least two events of volcanic intrusions are present in the outcrops from Figure 3.1. This is based on the fact that one of the sills in Figure 3.1 seems to be paler in colour compared to the other intrusions, and that a darker intrusion seems to be cross-cutting the paler intrusion. It is therefore assumed that the paler intrusion is older than the other intrusions. On top the sandstones are overlain by a layer of plateau basalts with varying thickness. The sharp change in colour between the sandstones and the volcanic intrusions make it quite easy to distinguish between the different lithologies. However, small changes are difficult to observe just based on a photo. The resolution of the photo is limited, and in addition slumping of the sandstones along the cliffs makes it difficult to see the thinnest intrusions, and smaller lithology changes. The structures of the volcanic intrusions are therefore simplified, and it is assumed that the photo of the cliffs shows a nearly vertical section. This is of course not *100 %* correct, but it is believed that it gives an acceptable model, as the purpose of this thesis is to study large-scale structures.

3.2 Geophysical model

The values for the velocities and densities that have been used in the modelling are all assumptions based on theoretical values for the different lithologies. Accurate estimation of the velocities and densities were impossible, as no samples or measurements from the outcrops of Independence Fjord were available. Velocities and densities for a given lithology can vary a lot, depending on factors like porosity, fluids, deformation, cracks and faults. In determining the velocities and densities it is assumed that no major cracks or faults are present in the area, if so the chosen velocities and densities would have to be considerably lower. It is also taken into consideration that the impedance contrast between the sandstones and the volcanic intrusions is quite large, as this is one of the difficulties with seismic from volcanic intrusions.

In order to make the model applicable for a marine seismic survey, the rocks are assumed to be water saturated. The layer of plateau basalts is overlain by a layer of weak sandstone to make the model more likely to appear in offshore marine settings. The ocean bottom is also not made completely flat in order to make the model more realistic.

The chosen velocities and densities are listed in Table 3.1 below, together with the V_p/V_s-ratios. It is assumed that the "Dolerite 1st intrusion", which is believed to be the oldest intrusion, has a bit lower velocities than the "Dolerite 2nd intrusion".

Table 3.1: P-wave velocities, S-wave velocities and densities selected for use in the model. The values have been selected based on the papers: Gary Mavko – Stanford rock physics laboratory p.74 and Rune M. Holt, Lecture Notes TPG4170 Rock Acoustics, NTNU, 2004 p. 17

Lithology/facies association	P-velocity	S-velocity	Density	V_p/V_s
Sea water	1.48	0	1.027	-
Upper sandstone	2.3	1.1	2.0	2.091
Plateau basalts	4.2	2.3	2.5	1.826
Sandstone	2.5	1.3	2.2	1.923
Dolerite 1st intrusion	4.7	2.7	2.7	1.741
Dolerite 2nd intrusion	4.9	2.8	2.7	1.75

E   W

Upper sandstone

- Plateau basalts
- Sandstone
- Dolerite 1st intrusion
- Dolerite 2nd intrusion
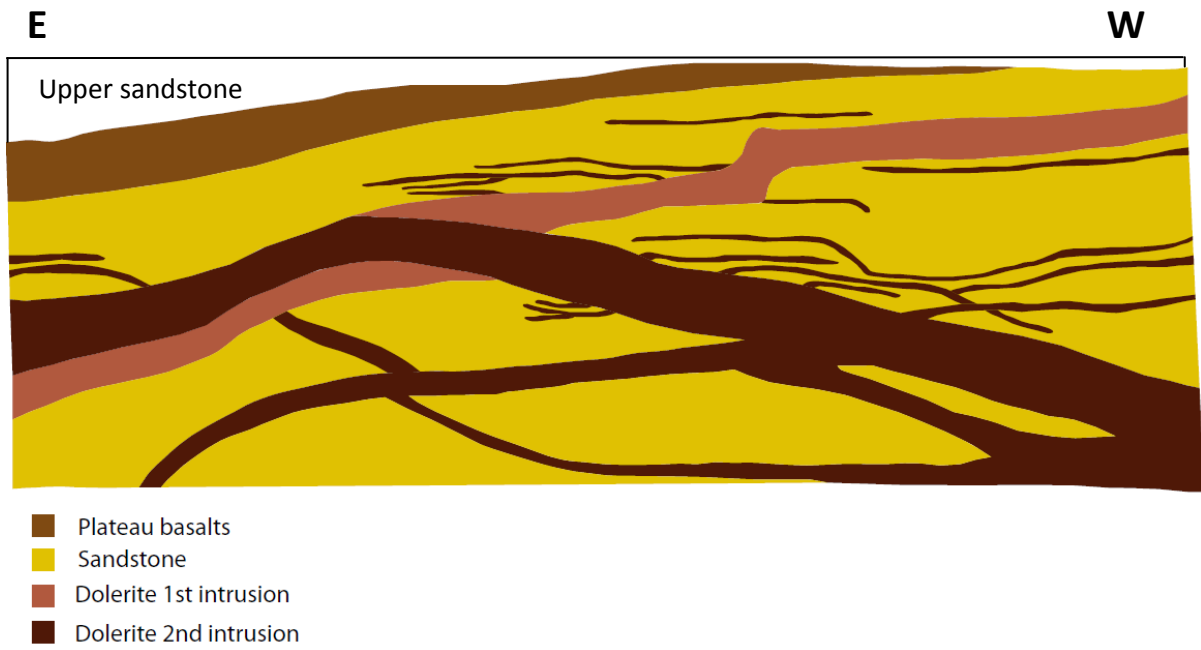
Figure 3.3: Geophysical model. A weak sandstone is inserted on top of the plateau basalts (Upper sandstone) to make the model more likely to appear in offshore marine settings.

3.3   Model building in Petrel

(For a more detailed description of the model building in Petrel see Appendix A)

One of the main stages in seismic modelling is geological model building, as the quality of the computed seismic response is partly related to the type of model that is built. In this thesis the Petrel software has been used to build the model. Petrel is a Schlumberger owned Windows PC software application intended to aggregate oil reservoir data from multiple sources (www.wikipedia.org).

3.3.1   Handmade model

The first step in the model building was to make a geological model for hand based on the photo shown in Figure 2.2.
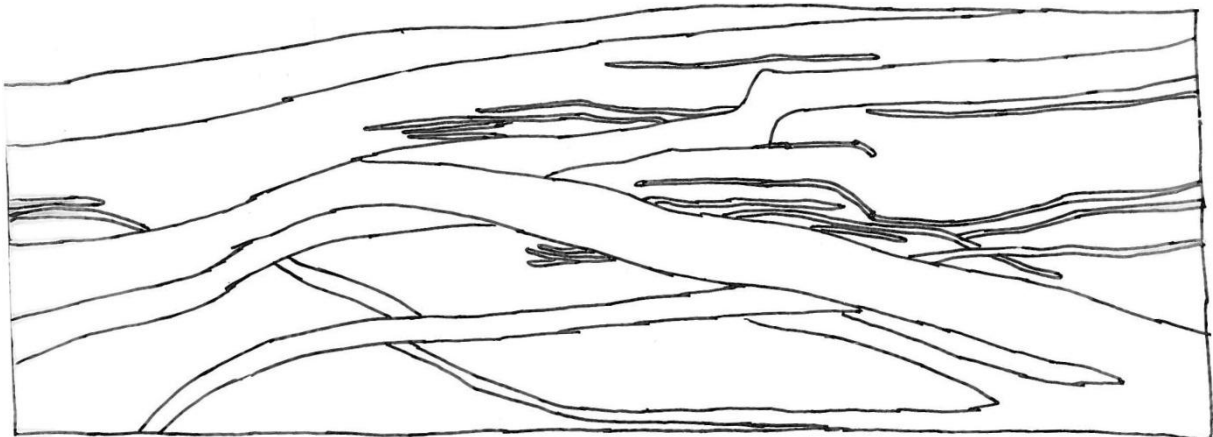
Figure 3.4: Geological model made for hand, based on the photo shown in Figure 2.2.

To do this a transparent paper was placed on top of the photo, and the visible structures were drawn with a pen. The result is shown in Figure 3.4 above. This is of course, as mentioned in Chapter 3.1, a simplification of the real system.

3.3.2   Importing image into Petrel

The handmade geological model was then scanned and imported into the Petrel software as a bitmap. Coordinates were assigned to the corners of the image to specify the actual size of the model. The size of the model shown in Figure 3.4 is not known exactly, and the specified size must therefore be considered as an approximation. The height of the cliffs shown in Figure 2.2 is said to be about *800 m*, therefore the height of the model shown in Figure 3.4 is specified to be *800 m.* Further, it is assumed that the horizontal scale of the photo shown in Figure 2.2 is equal the vertical scale, therefore the length of the model in Figure 3.4 is specified to be *2350 m*. Thus the size of the model is set to be *800 m x 2350 m* in the z- and x-direction respectively. It is assumed that the specified size gives a quite realistic size of the geology in the area around Independence Fjord. The thicknesses of the volcanic intrusions in the model do also match the thicknesses described in several articles and papers about the geology around Independence Fjord.

3.3.3   Digitize the image

The next step in the model building process was to digitize all the horizons in the model by creating polygons. First the image was shown in a 3D window in Petrel, and then polygons were created by following the structures in the imported image.

Figure 3.5: Two digitized polygons (Generated in Petrel).

Figure 3.5 shows two horizons that have been digitized by creating polygons in Petrel.

3.3.4   Make surfaces

When all the horizons had been digitized by polygons, surfaces were made from the polygons by using the ***Make/edit surface*** process in Petrel. In order to get full fold of the synthetic seismic data, the model should be extended with at least one streamer length on each side of the model. This was simply done by extending all the surfaces in the model by a constant value, see Figure 3.6. An easier way would be to extend the model after importing it to the Madagascar software by using the function ***sfspan.*** However at this point I wasn't aware of that function, so all my surfaces are extended in Petrel.
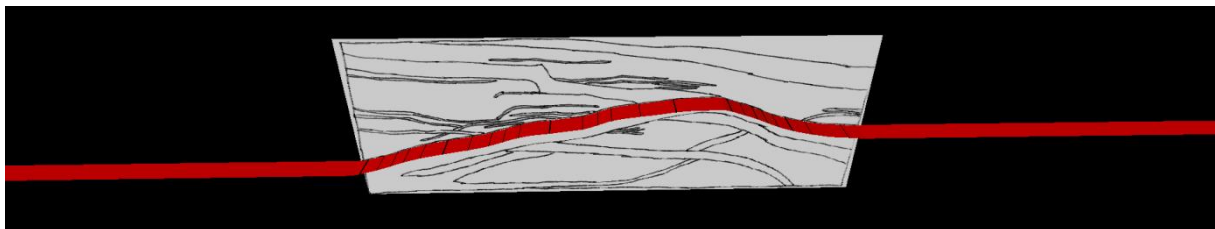
Figure 3.6: In order to get full fold of the synthetic seismic data, the model needs to be extended with one streamer length on each side of the model. (An easier way to extend the model would have been to use the function *sfspan* in the Madagascar software).

To get a 3D effect of the seismic modelling the model thickness in the y-direction was in this case set to be *125 m*. The thickness of the model was chosen such that the model consisted of approximately *20* cells in the y-direction. The size of the cells was chosen according to Nyquist (see Chapter 4.1.2), i.e. $f_{max} < \frac{c_{min}}{2 \cdot \Delta x}$, where c_{min} is the lowest velocity in the model and Δx is the size of the cells. By choosing Δx=5 m and using c_{min}=1100 m/s found from Table 3.1 we get $f_{max} < \frac{c_{min}}{2 \cdot \Delta x}$ = 110 Hz, which means that it will be possible to use a Ricker wavelet with a peak frequency of *30 Hz* in the modelling.

The surfaces were set to be constant in the y-direction, thus the model is said to be 2.5D. The reason for choosing a 2.5D model instead of a 3D model, was that no data were available for how the structures were changing in the third dimension, and in addition to give the surfaces a constant value in the y-direction is quite easy and fast to do and gives at the same time some 3D effect on the synthetic seismic.
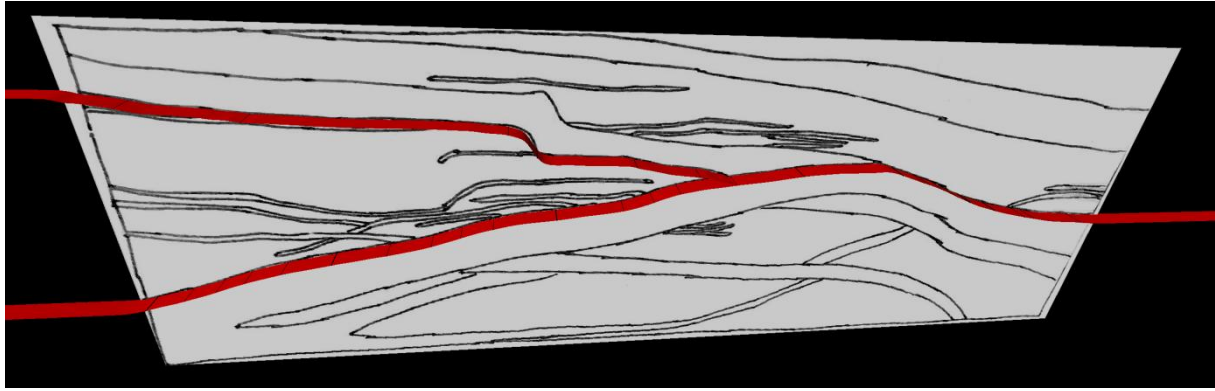
Figure 3.7: Showing two surfaces that overlap each other.

One other important thing to remember is that all the surfaces have to be continuous throughout the whole model, which in principle means that some surfaces have to overlap each other, see Figure 3.7.

To make it possible to insert a water layer on top of the model, all the surfaces were moved down with a constant value equal to the desired water depth. In this case a *1000 m* thick water layer was inserted on top of the model (this was later modified to *200 m*, see Chapter 4.3.1). The purpose by inserting such a deep water layer was to avoid multiples from the ocean bottom .The ocean bottom was made from a polygon drawn for hand instead of making it completely horizontal in order to make the model a bit more realistic (see Chapter 3.2). At last a top and a bottom surface defining the extent of the model were defined.

3.3.5   3D Grid Construction
In order to generate 3D cells for the model, the model needs a lattice. This lattice can be built in three ways in Petrel:

1. Make simple grid
2. Corner point gridding
3. Structural framework

To use the modelling algorithm implemented in the Madagascar software, the model needs a regular grid. Therefore the **Make simple grid** process was chosen as the grid process. The **Make simple grid** process creates vertical pillars in the xy-plane, so in order to make regular cells instead of pillars the **Layering** process was used to specify the number of layers (i.e. number of layers in the z-direction).

The size of the grid cells was set to be *5x5x5 m*.

3.3.6   Inserting properties between the layers (Geophysical model)
To create the geophysical model, the **Geometrical modeling** process was used to assign velocities and densities between the surfaces. Velocities and densities were assigned according to Table 3.1. Figure 3.8 shows the gridded model created in Petrel.

Figure 3.8: Model created in Petrel. The model is extended with *6 km* on each side of the actual model (area of interest). The figure above only shows part of the extension.

4 Seismic modelling

4.1 Forward seismic modelling

Forward seismic modelling is a technique used for simulating how seismic waves will propagate through the real earth. The objective is to predict the seismogram that a set of sensors would record, given an assumed structure of the subsurface. Thus it is in a sense the opposite of the inverse modelling approach in which the parameters of the geological model are computed from the acquired data.
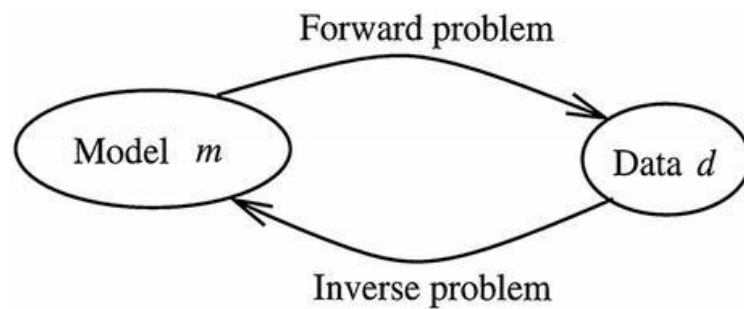
Figure 4.1: Forward modelling problem. (From Scale and Snider, 2000)

The results from the simulation are useful in understanding how seismic waves behave and propagate and are therefore a valuable tool for seismic interpretation and an essential part of seismic inversion algorithms. Another important application of seismic modelling is the evaluation and design of new seismic surveys.

In order to perform seismic modelling, the subsurface as well as the wave propagation procedure needs to be simplified. Due to the complexity of the real earth it would be impossible to create a geological model that includes all details and all properties of the real subsurface. The earth is therefore divided into layers or separated volumes in which approximately the same properties can be assigned to each of them.

Seismic modelling is based on a wave propagation theory. Several wave propagation theories exist, but the most common theories are probably the acoustic wave theory and the elastic wave theory. The main difference between these two theories is that the elastic wave theory includes shear waves (S-waves) in addition to pressure waves (P-waves), whereas the acoustic wave theory only includes pressure waves. The wave field can therefore be represented by a scalar for the acoustic case, and as a vector for the elastic case.

For each wave theory there are a number of possible wave equations, and several methods for solving the wave equations exist. In, general the solving methods can be classified into three main categories:

1. Direct methods
2. Integral-equation methods
3. Ray-tracing methods

Direct methods are also called grid methods or full-wave equation methods. In general, direct techniques are methods that give an answer in a fixed number of steps, subject only to round-off errors. The geological model is for this case approximated by a numerical mesh. Advantages with

direct methods are that no restrictions on the material variability are given and the method can be very accurate when a sufficiently fine grid is used. A disadvantage is that direct methods can be more expensive than analytical and ray methods in terms of computer time. Examples of direct methods are finite difference (FD), finite element (FE) and pseudospectral (PS) methods.

Integral-equation methods represent the wave field on integral form. These methods are based on Huygens' principle, stating that every point on a wave front may be considered a source of a new wave.

Ray-tracing methods are methods where the waves are approximated by rays that obey Snell's law at boundaries. These methods do not take the complete wave field into account, but they are very efficient, making them a popular choice in seismic modelling and imaging.

4.1.1 The wave equation

Newton's second law of motion states that the unbalanced force equals the mass times the acceleration, $\sum F = ma$
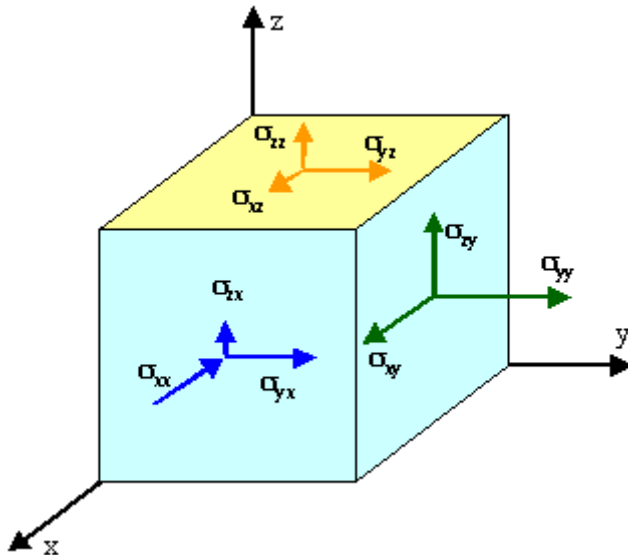
Figure 4.2: Components of stress. (From www.tf.uni-kiel.de)

Thus the equations of motion along the x, y and z-axis can be given as follows

$$\rho \frac{\partial^2 u_x}{\partial t^2} = \frac{\partial \sigma_{xx}}{\partial x} + \frac{\partial \sigma_{xy}}{\partial y} + \frac{\partial \sigma_{xz}}{\partial z},$$

$$\rho \frac{\partial^2 u_y}{\partial t^2} = \frac{\partial \sigma_{yx}}{\partial x} + \frac{\partial \sigma_{yy}}{\partial y} + \frac{\partial \sigma_{yz}}{\partial z}, \qquad (4.1)$$

$$\rho \frac{\partial^2 u_z}{\partial t^2} = \frac{\partial \sigma_{zx}}{\partial x} + \frac{\partial \sigma_{zy}}{\partial y} + \frac{\partial \sigma_{zz}}{\partial z}$$

, where ρ is the density, *(u_x, u_y, u_z)* is the displacement vector and $(\sigma_{xx}, \sigma_{yy}, \sigma_{zz}, \sigma_{xy}, \sigma_{yz}, \sigma_{zx})$ is the stress tensor.

Hooke's law states that a given strain is directly proportional to the stress producing it, when the strains are small. The strains involved in seismic waves are usually less than 10^{-8} except very near the source, so that Hooke's law holds (Sheriff & Geldart, 1995).

For isotropic and elastic media Hooke's law can be expressed as

$$
\begin{array}{ll}
\sigma_{ii} = \lambda\Delta + 2\mu\varepsilon_{ii} & (i = x, y, z) \\
\sigma_{ij} = \mu\varepsilon_{ij} & (i, j = x, y, z; i \neq j)
\end{array}
\tag{4.2}
$$

, where λ and μ are the Lamé coefficients, and Δ is the dilatation given by $\Delta = \varepsilon_{xx} + \varepsilon_{yy} + \varepsilon_{zz}$

For a general, anisotropic media Hooke's law can be expressed as a tensor equation

$$
\boldsymbol{\sigma} = \boldsymbol{C\varepsilon} \tag{4.3}
$$

, where **C** is the stiffness. This system of equations has *21* independent constants. However, for the isotropic case the number of independent constants reduces to *2*.

By expressing the strains in terms of displacements in Equation (4.2) we get

$$
\sigma_{xx} = (\lambda + 2\mu)\frac{\partial u_x}{\partial x} + \lambda\left(\frac{\partial u_y}{\partial y} + \frac{\partial u_z}{\partial z}\right)
$$

$$
\sigma_{yy} = (\lambda + 2\mu)\frac{\partial u_y}{\partial y} + \lambda\left(\frac{\partial u_x}{\partial x} + \frac{\partial u_z}{\partial z}\right)
$$

$$
\sigma_{zz} = (\lambda + 2\mu)\frac{\partial u_z}{\partial z} + \lambda\left(\frac{\partial u_x}{\partial x} + \frac{\partial u_y}{\partial y}\right)
$$

$$
\sigma_{xy} = \mu(\frac{\partial u_y}{\partial x} + \frac{\partial u_x}{\partial y}) \tag{4.4}
$$

$$
\sigma_{yz} = \mu(\frac{\partial u_z}{\partial y} + \frac{\partial u_y}{\partial z})
$$

$$
\sigma_{zx} = \mu(\frac{\partial u_x}{\partial z} + \frac{\partial u_z}{\partial x})
$$

By symmetry $\sigma_{xy} = \sigma_{yx}$, $\sigma_{yz} = \sigma_{zy}$ and $\sigma_{zx} = \sigma_{xz}$

Further, by using the fact that the velocity is the derivative of the displacement, $\boldsymbol{v} = \frac{\partial \boldsymbol{u}}{\partial t}$, the systems of equations in (4.1) and (4.4) can be transformed into the following first order hyperbolic system

$$\frac{\partial v_x}{\partial t} = \frac{1}{\rho} \left(\frac{\partial \sigma_{xx}}{\partial x} + \frac{\partial \sigma_{xy}}{\partial y} + \frac{\partial \sigma_{xz}}{\partial z} \right),$$

$$\frac{\partial v_y}{\partial t} = \frac{1}{\rho} \left(\frac{\partial \sigma_{yx}}{\partial x} + \frac{\partial \sigma_{yy}}{\partial y} + \frac{\partial \sigma_{yz}}{\partial z} \right),$$

$$\frac{\partial v_z}{\partial t} = \frac{1}{\rho} \left(\frac{\partial \sigma_{zx}}{\partial x} + \frac{\partial \sigma_{zy}}{\partial y} + \frac{\partial \sigma_{zz}}{\partial z} \right),$$

$$\frac{\partial \sigma_{xx}}{\partial t} = (\lambda + 2\mu) \frac{\partial v_x}{\partial x} + \lambda \left(\frac{\partial v_y}{\partial y} + \frac{\partial v_z}{\partial z} \right),$$

$$\frac{\partial \sigma_{yy}}{\partial t} = (\lambda + 2\mu) \frac{\partial v_y}{\partial y} + \lambda \left(\frac{\partial v_x}{\partial x} + \frac{\partial v_z}{\partial z} \right), \qquad (4.5)$$

$$\frac{\partial \sigma_{zz}}{\partial t} = (\lambda + 2\mu) \frac{\partial v_z}{\partial z} + \lambda \left(\frac{\partial v_x}{\partial x} + \frac{\partial v_y}{\partial y} \right),$$

$$\frac{\partial \sigma_{xy}}{\partial t} = \mu \left(\frac{\partial v_y}{\partial x} + \frac{\partial v_x}{\partial y} \right),$$

$$\frac{\partial \sigma_{yz}}{\partial t} = \mu \left(\frac{\partial v_z}{\partial y} + \frac{\partial v_y}{\partial z} \right),$$

$$\frac{\partial \sigma_{zx}}{\partial t} = \mu \left(\frac{\partial v_z}{\partial x} + \frac{\partial v_x}{\partial z} \right)$$

The medium is supposed to be in equilibrium at time $t = 0$, i.e. stress and velocity are set to zero everywhere in the medium.

4.1.2   Finite difference modelling

The modelling algorithm implemented in the Madagascar software is based on finite differences. A finite difference method proceeds by replacing the derivatives in the differential equations with finite-difference approximations. This gives a large, but finite algebraic system of equations to be solved in place of the differential equation, something that can be done on a computer. For instance, three different approximations for $\frac{\partial u}{\partial x}$ are given by

Forward
approximation:
$$D_+ u(x) = \frac{u(x+h) - u(x)}{h} \qquad (4.6)$$

Backward
approximation:
$$D_- u(x) = \frac{u(x) - u(x-h)}{h} \qquad (4.7)$$

Centred
approximation:
$$D_0 u(x) = \frac{u(x+h) - u(x-h)}{2h} \qquad (4.8)$$

16
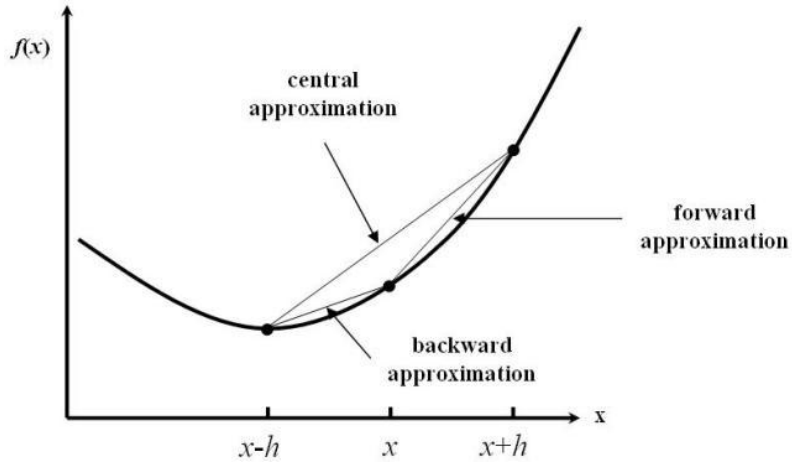
Figure 4.3: Various approximations to u'(x) interpreted as the slope of secant lines. (From www.goddardconsulting.ca)

From Figure 4.3 it should be clear that we would expect $D_0 u(x)$ to give a better approximation than either of the one-sided approximations. Other approximations for $\frac{\partial u}{\partial x}$ are possible as well.

The finite difference scheme for the system of equations in (4.5) implemented in the Madagascar software is based on centred differences. To simplify a bit the discretisation is showed for the 2D case instead of for the 3D case, this is simply done by omitting the y-direction in Equations (4.1), (4.4) and (4.5). Discretising the elastodynamic equations in (4.5) for a vertical 2D medium with a horizontal x-axis and a vertical z-axis pointing downwards gives

$$U_{i,j}^{k+1/2} = U_{i,j}^{k-1/2} + \frac{1}{R_{i,j}}\frac{\Delta t}{\Delta x}\left(\Sigma_{i+1/2,j}^{k} - \Sigma_{i-1/2,j}^{k}\right)$$
$$+ \frac{1}{R_{i,j}}\frac{\Delta t}{\Delta z}\left(\Xi_{i,j+1/2}^{k} - \Xi_{i,j-1/2}^{k}\right),$$

$$V_{i+1/2,j+1/2}^{k+1/2} = V_{i+1/2,j+1/2}^{k-1/2} + \frac{1}{R_{i+1/2,j+1/2}}\frac{\Delta t}{\Delta x}\left(\Xi_{i+1,j+1/2}^{k} - \Xi_{i,j+1/2}^{k}\right)$$
$$+ \frac{1}{R_{i+1/2,j+1/2}}\frac{\Delta t}{\Delta z}\left(T_{i+1/2,j+1}^{k} - T_{i+1/2,j}^{k}\right),$$

$$(4.9)$$

$$\Sigma_{i+1/2,j}^{k+1} = \Sigma_{i+1/2,j}^{k} + (L+2M)_{i+1/2,j}\frac{\Delta t}{\Delta x}\left(U_{i+1,j}^{k+1/2} - U_{i,j}^{k+1/2}\right)$$
$$+ L_{i+1/2,j}\frac{\Delta t}{\Delta z}\left(V_{i,j+1}^{k+1/2} - V_{i,j}^{k+1/2}\right),$$

$$T_{i+1/2,j}^{k+1} = T_{i+1/2,j}^{k} + (L+2M)_{i+1/2,j}\frac{\Delta t}{\Delta z}\left(V_{i,j+1}^{k+1/2} - V_{i,j}^{k+1/2}\right)$$
$$+ L_{i+1/2,j}\frac{\Delta t}{\Delta x}\left(U_{i+1,j}^{k+1/2} - U_{i,j}^{k+1/2}\right),$$

17

$$\Xi^{k+1}_{i,j+1/2} = \Xi^{k}_{i,j+1/2} + M_{i,j+1/2}\frac{\Delta t}{\Delta z}\left(U^{k+1/2}_{i,j+1} - U^{k+1/2}_{i,j}\right)$$
$$+ M_{i,j+1/2}\frac{\Delta t}{\Delta x}\left(V^{k+1/2}_{i+1,j} - V^{k+1/2}_{i,j}\right)$$

, where k denotes the index for the time discretisation, i for the x-axis discretisation and j for the z-axis discretisation. Δt, Δx and Δz are the grid steps in time, in the x-direction and in the z-direction, respectively. Numerical velocity $(U, V) = (v_x, v_z)$ at time $(k + 1/2)\Delta t$, and numerical stress $(\Sigma, \Xi, T) = (\sigma_{xx}, \sigma_{zz}, \sigma_{xz})$ at time $(k + 1)\Delta t$ are computed explicitly from velocity at time $(k - 1/2)\Delta t$ and stress at time $k\Delta t$. R represents the density inside the medium, while L, M represent Lamé coefficients (λ, μ) as shown in Figure 4.4.
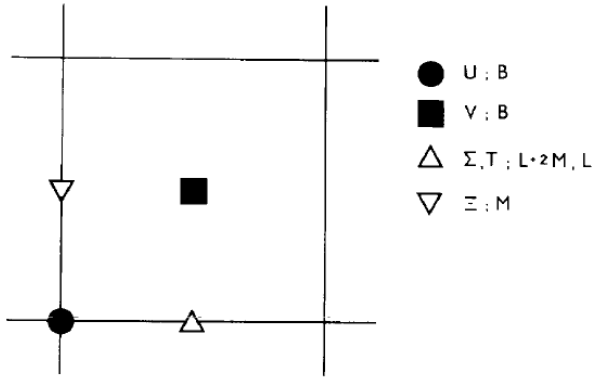
Figure 4.4: Discretisation of the medium on a staggered grid. Black symbols are for velocities, $(U, V) = (v_x, v_z)$ and buoyancy, $B=1/R$, where R denotes the density, at time $k\Delta t$. Whites symbols are for stresses $(\Sigma, \Xi, T) = (\sigma_{xx}, \sigma_{zz}, \sigma_{xz})$ and Lamé coefficients, L, M at time $(k+1/2)\Delta t$. (From Virieux, 1989).

By using operators from Holberg (1987) and spectral analysis, the following numerical stability condition for Equations (4.9) is obtained

$$\frac{c_{max}\Delta t}{\Delta x} \leq \frac{\sqrt{2}}{\pi} \tag{4.10}$$

, where c_{max} is the maximum P- or S-wave velocity.

In addition the Nyquist criterion needs to be fulfilled

$$f_{max} \leq \frac{c_{min}}{2\Delta x} \tag{4.11}$$

Here f_{max} is the maximum frequency of the frequency spectrum, and c_{min} is the minimum P- or S-wave velocity.

As stated in the derivations above, this applies to an elastic, isotropic and homogeneous medium.

For the 3D case the stability criterion in Equation (4.10) becomes

$$\frac{c_{max}\Delta t}{\Delta x} \leq \frac{2}{\sqrt{3}\pi} \tag{4.12}$$

4.1.3   Perfectly Matched Layer (PML)

The boundary conditions for the algorithm implemented in Madagascar are based on the Perfectly Matched Layer (PML) approach. A viscoelastic material is implemented on the edges of the model in order to absorb the wave fields travelling away from the interior of the grid. Thus the PML acts as an absorbing material. The PML is constructed such that waves incident upon the PML from a non-PML medium is strongly absorbed, whereas there is no loss in the direction tangential to the interface.
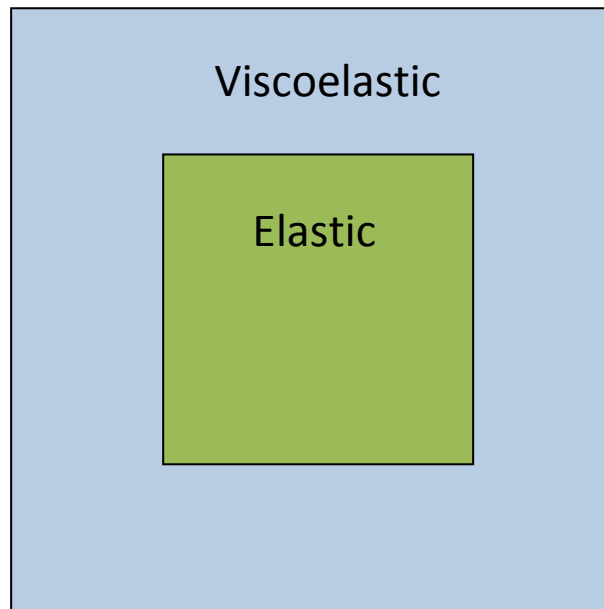
Figure 4.5: Illustration showing the principle of the Perfectly Matched Layer (PML) approach.

4.2   Seismic data processing

Acquired seismic data need to be processed in order to image the subsurface. The purpose of seismic processing is to improve the quality of the data i.e. increase the signal/noise ratio, and to give an image of the subsurface that can be used to infer the subsurface structures.

During seismic processing the data is manipulated by applying a series of computer routines. Processing routines generally fall into one of the following categories

- Enhancing signal at the expense of noise
- Providing velocity information
- Collapsing diffractions and placing dipping events in their true subsurface locations (migration)
- Increasing resolution

Some of the most important processes are discussed below.

4.2.1   Muting

Real seismic data often contain unwanted signals for near offsets and short recording times. Noisy signals are very often associated with strong mode conversions at the ocean bottom, water bottom reverberations, low frequent wave noise (swell-noise) etc. It is therefore normal to zero out or mute such areas. Since these unwanted signals very often have high amplitudes, the effect of not applying muting is dramatic.

4.2.2 CMP

The initial display of seismic profile data is normally in groups of seismic traces recorded from a common shot, known as shot gathers. Traces within one shot gather will be reflected from different points in the subsurface. By combining traces from different shots it is possible to choose traces with a symmetric ray path, see Figure 4.6. Such traces representing a common midpoint are called a CMP-gather (Common MidPoint Gather).
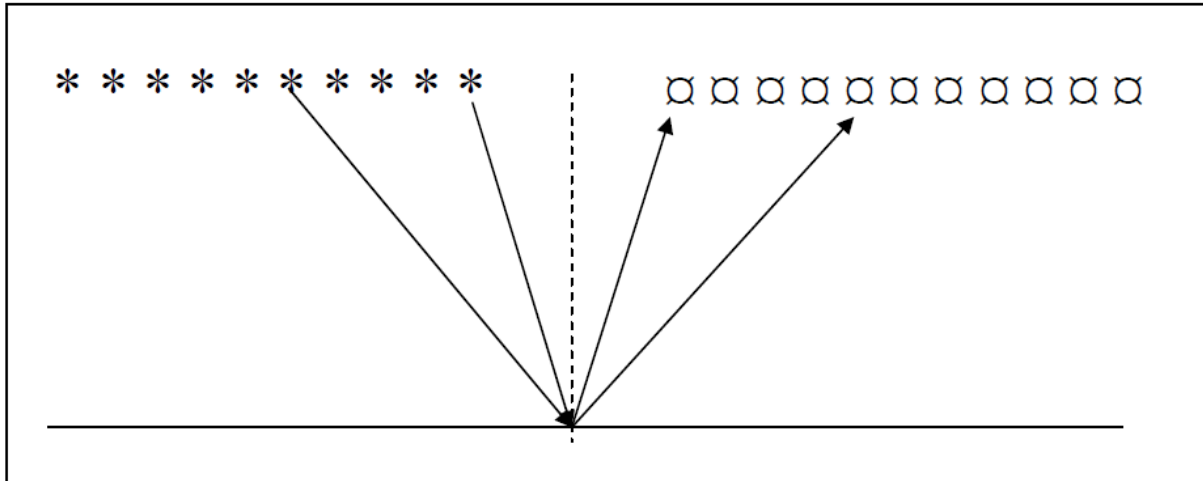
Figure 4.6: Schematic sketch showing two shots of a CMP-gather (∗ = shot ¤ = receiver). (From Landrø, 2008)

The advantage by sorting the data into CMP-gathers is that all the traces within one CMP-gather roughly represent the same location, thus it is easier to image the subsurface. In 3D seismic this sorting is known as binning, where all the data that have a common midpoint falling into one binning cell are grouped together.

4.2.3 Normal MoveOut correction (NMO)

A shot gather consists of many traces, where the distance between the source and receiver (offset) increases gradually from one trace to the next. This means that the travel time of a reflection from a horizontal surface at depth is gradually delayed from one trace to the next. The relationship between travel time and offset is hyperbolic, as seen in Figure 4.7.
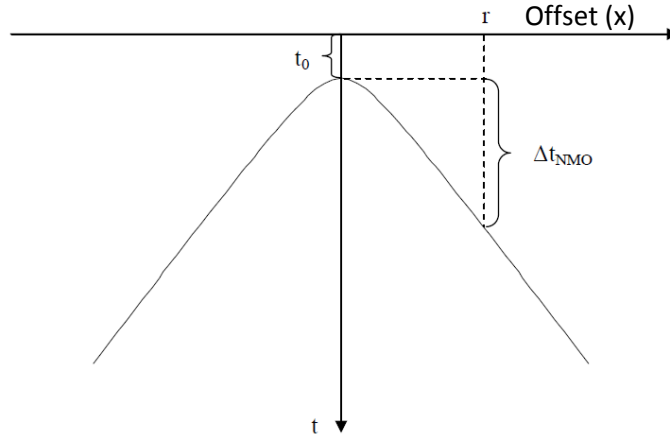
Figure 4.7: Travel time curve for a plane horizontal reflector. (From Tjåland, TPG4125 Seismic waves, NTNU, 2010)

The purpose of Normal MoveOut (NMO) correction is to move all the reflections to the same time, such that the events become horizontal as a function of offset instead of hyperbolas. The NMO-correction can therefore be seen as a measure for the curvature of the travel time hyperbola for a plane layer model ($\theta=0$). Based on this the NMO-correction is given as

$$\Delta t_{NMO} = [t(r) - t_0]|_{\theta=0} \tag{4.13}$$

, where $t(r)$ is the travel time for offset $x=r$ and t_0 is the zero-offset travel time ($x=0$).
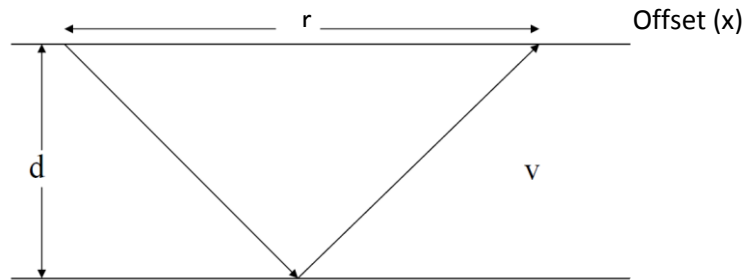
Figure 4.8: Sketch of a seismic reflection from an interface. It is assumed that source and receiver are at the same depth, that the vertical distance from source to the interface is d, and that the offset between source and receiver is r. v is the velocity of the layer. (From Landrø, 2008)

For a flat, horizontal reflector, the travel time equation is

$$t = \frac{2}{v}\sqrt{d^2 + \frac{r^2}{4}} \tag{4.14}$$

, where v is the velocity, d is the vertical depth from source to the interface, and r is the offset (see Figure 4.8). By using the zero-offset travel time (vertical two-way travel time) $t_0 = \frac{2d}{v}$ and assuming $r \ll d$ the correction which needs to be applied in order to get the travel times for all offsets to be equal to the one for zero offset becomes

$$\Delta t_{NMO} \approx \frac{r^2}{4vd} = \frac{r^2}{2t_0 v^2} \tag{4.15}$$

For a dipping reflector a Dip MoveOut (DMO) correction needs to be performed. Dip moveout is defined as the difference in time for a given offset between a dipping reflector and a horizontal reflector, and is defined as

$$\Delta t_{DMO} = t(r) - t(r)|_{\theta=0} \tag{4.16}$$
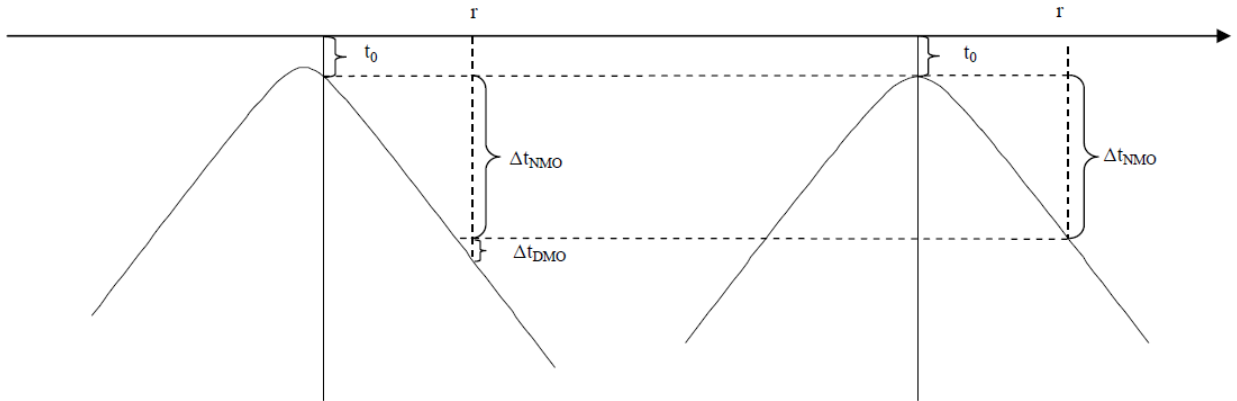
Figure 4.9: Difference between travel time curve for a dipping reflector (left) and a horizontal reflector (right). (From Tjåland, TPG4125 Seismic waves, NTNU, 2010)

Based on the above the travel time for a dipping layer is given as

$$t = t_0 + \Delta t_{NMO} + \Delta t_{DMO} \tag{4.17}$$

In order to perform NMO and DMO-correction, a velocity model is needed, which can be found by velocity analysis.

4.2.4 Velocity analysis

Velocity analysis is a systematic way of estimating velocities as a function of two-way travel time. Information about velocity is necessary for stacking, imaging and is also a lithology indicator. The main objective in velocity analysis is to obtain stacking velocities that can be used in a normal moveout correction algorithm prior to stacking or summing the seismic traces belonging to a certain CMP-gather.

In velocity analysis one uses the fact that the curvature of the hyperbolic travel time curves are dependent on the velocity. The more a seismic event is bending, the lower is the velocity (see Equation (4.14)).

There are several methods to determine the velocity

- $(t^2\text{-}x^2)$ analysis
- Constant velocity panels
- Constant velocity stacks
- Analysis of velocity spectra

The (t^2-x^2) *analysis* is based on the fact that the moveout expression for the square of t and x result in a linear event (see Equation (4.14)). By plotting different values for t^2 and x^2, the slope can be used to determine v^2.

For **Constant Velocity Panels (CVP)** an NMO correction is applied by using different velocities, and the velocity that flattens the hyperbolic travel time curve best is chosen as the velocity for a certain reflector.

Constant Velocity Stacks (CVS) is also based on the NMO-correction, but after the NMO-correction is performed the data is stacked, and the velocity that yields the best stacking response for a seismic event is selected.

One common way to determine the **Velocity spectrum** is the semblance function. In semblance analysis the hyperbolic moveout is used for determining RMS (Root Mean Square) velocities. The semblance function returns a value between *0* and *1*, where a higher semblance values give a higher probability that the velocity is correct.

4.2.5   Stacking

After NMO-correction it is normal to sum up the traces in each CMP-gather. This is called stacking, and one of the major objectives is to increase the signal to noise ratio, another objective is multiple attenuation.

4.2.6   Migration

Migration is an imaging method that involves repositioning of data elements to make their locations appropriate to the locations of the associated reflectors or diffracting points. To migrate the data, the velocity model needs to be known. Several migration algorithms exist including

- Kirchhoff migration (diffraction stacking)
    - Integral solution of the wave equation
- f-k migration
    - Fourier domain solution of the wave equation
- Finite difference migration
    - Derivative solution of the wave equation

4.3 The Madagascar software

The software used for the modelling and processing of the synthetic seismic data in this thesis is the Madagascar software.

Madagascar is an open-source software package for multidimensional data analysis and reproducible computational experiments. Its mission is to provide

- A convenient and powerful environment
- A convenient technology transfer tool

for researchers working with digital image and data processing in geophysics and related fields (www.reproducibility.org).
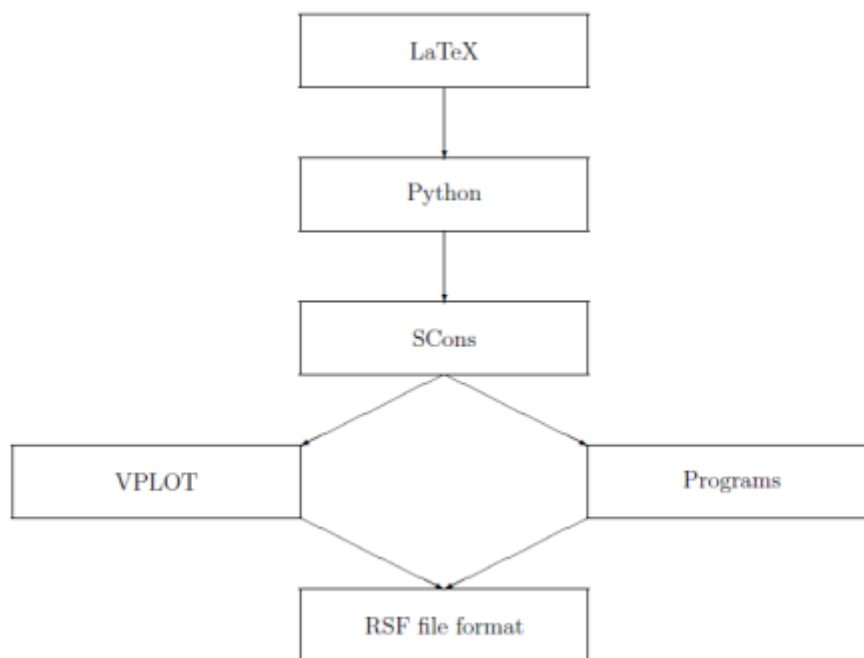
Figure 4.10: The hierarchy of Madagascar. At the lower-most level is the RSF file format, which is the common exchange format for all the Madagascar programs. At the next level are the actual Madagascar programs that manipulate RSF files to process data. VPLOT is a graphics library which allows the user to plot and visualise RSF files. Python and SCons are the scripting utilities, allowing the user to make scripts. The last level is the support for LaTeX. (From www.reproducibility.org).

Madagascar's design consists of a few levels. The lowest level is the RSF file format, which is the format used to exchange information between Madagascar programs. The RSF files are defined by two files, the header and the binary file. The header file contains information about the dimensionality of the data as well as information about the data contained in the binary file, whereas the binary file contains the actual data. The next level of Madagascar is the Madagascar programs and the VPLOT graphics library. The Madagascar programs manipulate RSF files to process data, and VPLOT allows users to plot and visualise the RSF files. Further, the next level includes the scripting utilities in Python and SCons, which allows the user to make scripts. The last level is the support for LaTeX.

Madagascar programs follow the standard UNIX conventions for reading and writing RSF files. For example a Madagascar program can be used by the following command

```
command < input.rsf  key=val > output.rsf
```

, where *command* denotes the Madagascar program to be used, *key* is the name of the parameter we want to set in the program and *val* is the value of the parameter.

It is also possible to chain multiple commands together without writing intermediate Madagascar RSF files in the process. This is called piping.

```
command1 < input.rsf | command2 > output.rsf
```

Here the result from *command1* is piped to command*2*. By using pipes the number of files that need to be saved to the disk reduces, and because there is no limit of the number of statements that can be piped together piping can be very powerful.

The main scripting option in Madagascar is SCons, which is a build manager written in *100%* Python. SCons scripts are called SConstructs. These are composed of four commands: Fetch, Flow, Plot and Result. A flow creates the relationship between the input file, the output file and the processing command used to create the output file from the input file. The syntax for a Flow is

```
 Flow(output file, input file, command)
```

, where command is a string containing the Madagascar program to be used, along with the command line parameters needed for the program to run.

Plot and Result are used to visualise the data. The syntax is as follows

```
Plot(input file, command)
```

```
Result(input file, command)
```

4.3.1 Convert the data from Eclipse (ASCII) format to RSF file format

In order to do the modelling the geophysical model made in Petrel (see Chapter 3.3) has to be imported into the Madagascar software. Because the geophysical model exported from Petrel is in Eclipse (ASCII) format the model needs to be converted to RSF file format before we can do the modelling. This is simply done by using the Madagascar program *sfpetread*.
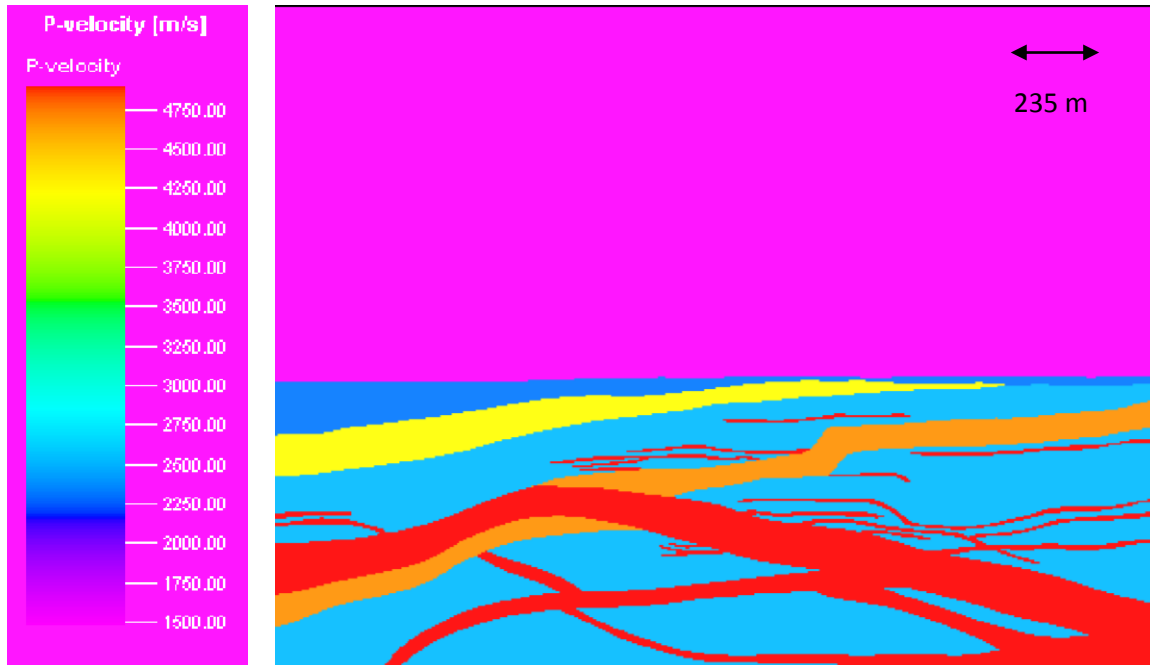
Figure 4.11: P-wave model made in Petrel. The horizontal length is *2350 m* and the vertical depth is *1800 m*. The upper half of the image (purple colour) shows a *1000* m thick water layer.
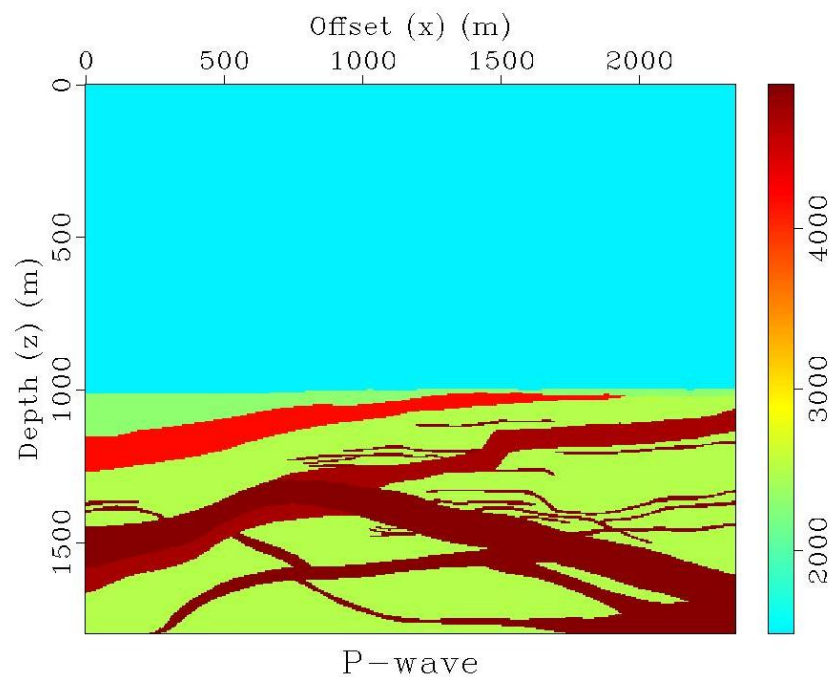
Figure 4.12: P-wave model in Madagascar after conversion to RSF file format.

Figure 4.11 and Figure 4.12 show the P-wave model in Petrel and Madagascar respectively. As mentioned in Chapter 3.3.4 the intention by inserting a *1000 m* thick water layer on top of the model

was to avoid ocean bottom multiples, but because this increases the amount of data to handle, and thus the running time of the modelling significantly, the water layer was reduced to *200 m* by using the Madagascar program ***sfwindow***. *200 m* water depth is also representative for the North Sea. The P-wave, S-wave and density model after reducing the water depth to *200 m* are shown in Figure 4.13, Figure 4.14 and Figure 4.15 respectively.
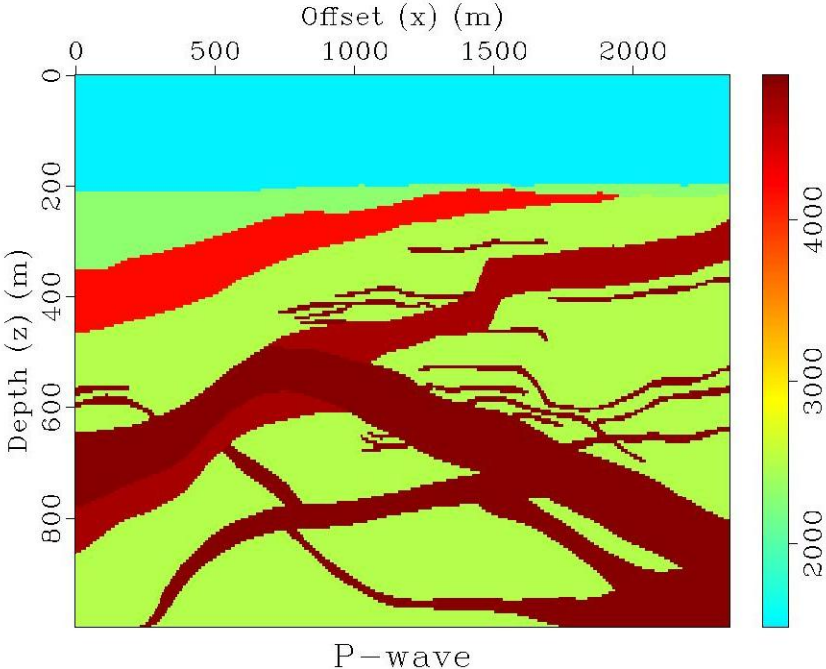
Figure 4.13: P-wave model after reducing the water depth to *200 m*. (Generated in Madagascar).
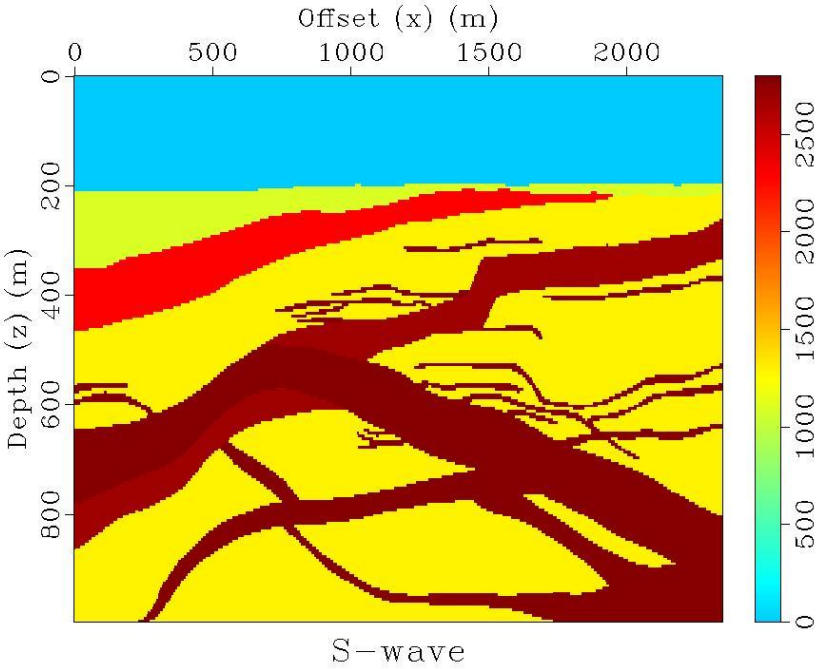
Figure 4.14: S-wave model after reducing the water depth to *200 m*. (Generated in Madagascar).
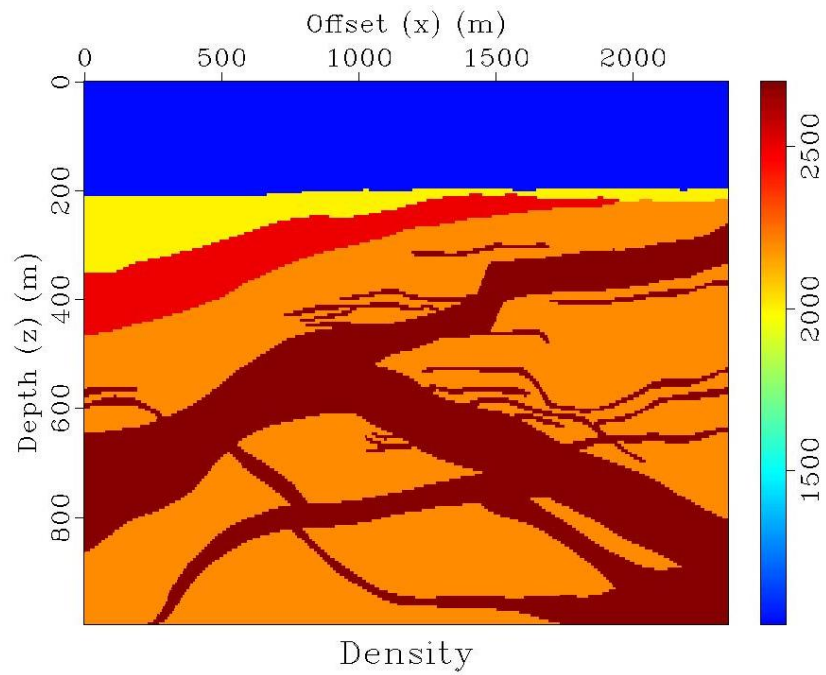
Figure 4.15: Density model after reducing the water depth to *200 m*. (Generated in Madagascar).

4.3.2 The supercomputer Kongull

Seismic modelling requires computer hardware. Because of the big amount of data that need to be handled in multiple shots modelling the supercomputer Kongull has been used for the modelling in Madagascar. Kongull is a relatively big computer that is shared between different institutes at NTNU and SINTEF.

5 Results

This chapter is divided into three parts. The first section deals with the single shot modelling. The second section is about multiple shots modelling, and in the last section the processing of the synthetic seismic data is discussed.

As mentioned in the Introduction in Chapter 1, the modelling is performed in 2D, instead of 3D, which was the first intention.

The Madagascar scripts used for the modelling and processing can be seen in Appendix B.

5.1 Single shot modelling

The purpose by doing single shot modelling was to see how the wave field behaved and to test out the Madagascar script before doing multiple shots modelling on Kongull. In this way the influence of the different parameters used in the modelling could be tested out. Such parameters might be frequency, thickness of the PML layers, free surface, position of source and receivers etc.

The Madagascar program *sffd2dewe*, which is a time domain 2D finite difference modelling for the elastic wave equation (see Chapter 4.1) was used to do the modelling.

Single shot modelling can be done relatively quickly by resampling the data, by using the program *sfwindow*. However, we need to be sure that the resampling and frequency used in the modelling fulfil the Nyquist criterion given in Equation (4.11)

$$f_{max} \leq \frac{c_{min}}{2\Delta x}$$

During the model building in Petrel the size of the grid cells were set to be *5x5x5 m*, and from Table 3.1 we see that the lowest velocity in the model is *1100 m/s*, which corresponds to the S-wave velocity in the upper sandstone layer.
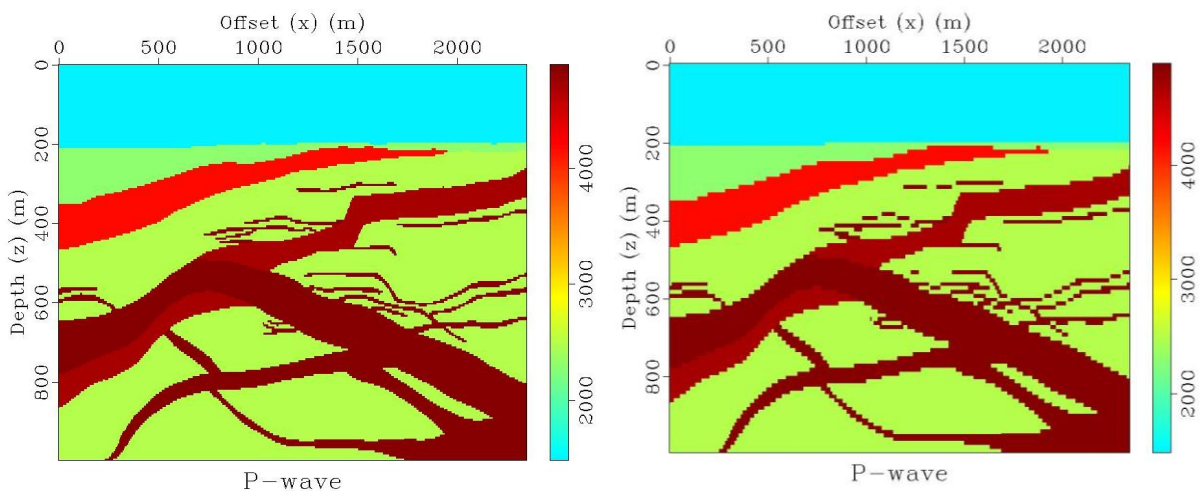
Figure 5.1: P-wave model. Left: initial model with grid cells of *5x5 m*. Right: Resampled model with grid cells of *10x10 m*.
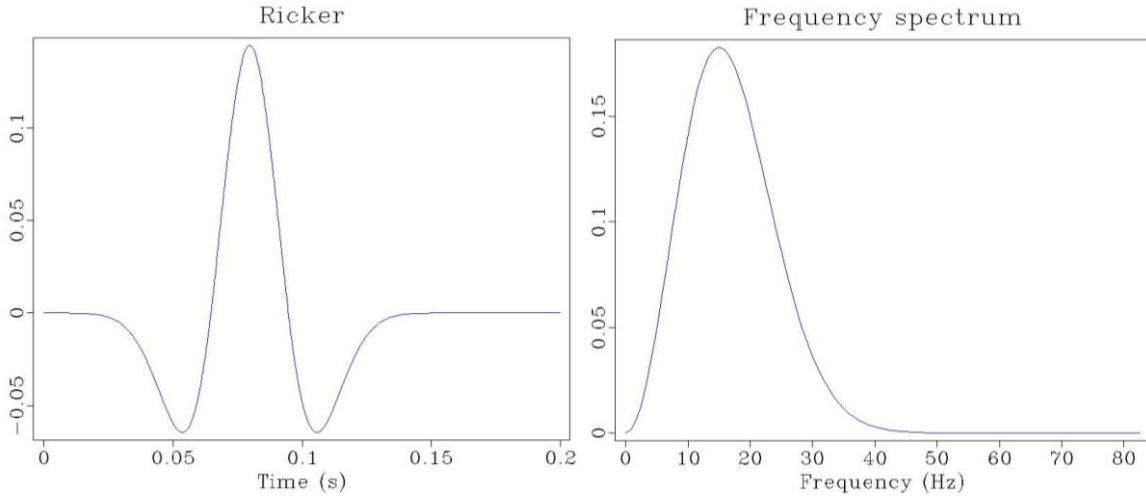
Figure 5.2: Left: Ricker wavelet with a peak frequency of *15 Hz* centred at *t=0.08 s*. Right: Frequency spectrum for a Ricker wavelet with a peak frequency of *15 Hz*, the maximum frequency is approximately *45 Hz*. (Generated in Madagascar).

If we resample to *10 m* (Figure 5.1) we find that the Nyquist criterion is fulfilled if $f_{max} \leq 55\ Hz$. This is fulfilled by using a Ricker wavelet with a peak frequency of *15 Hz*, where $f_{max} \approx 45\ Hz$ (see Figure 5.2).

In addition for the modelling to be stable the time step *Δt* has to fulfil the criterion shown in Equation (4.10)

$$\frac{c_{max}\Delta t}{\Delta x} \leq \frac{\sqrt{2}}{\pi}$$

From Table 3.1 we see that the maximum velocity in the model is the P-wave velocity of the 2nd Dolerite intrusion, which is set to be *4900 m/s*. With $\Delta x = 10\ m$ we get that $\Delta t \leq 0.9$ for the modelling algorithm to be stable.

To avoid reflections from the ocean surface, and thus ocean bottom multiples, the free surface option was turned off. By doing so direct waves will show up on the synthetic seismic data, but these can easily be muted away during the processing of the seismic data.

Since we only want to look at a single shot, there is no need for using the extended model. Therefore the extensions on each side of the model have been removed for the case of single shot modelling by using *sfwindow*.
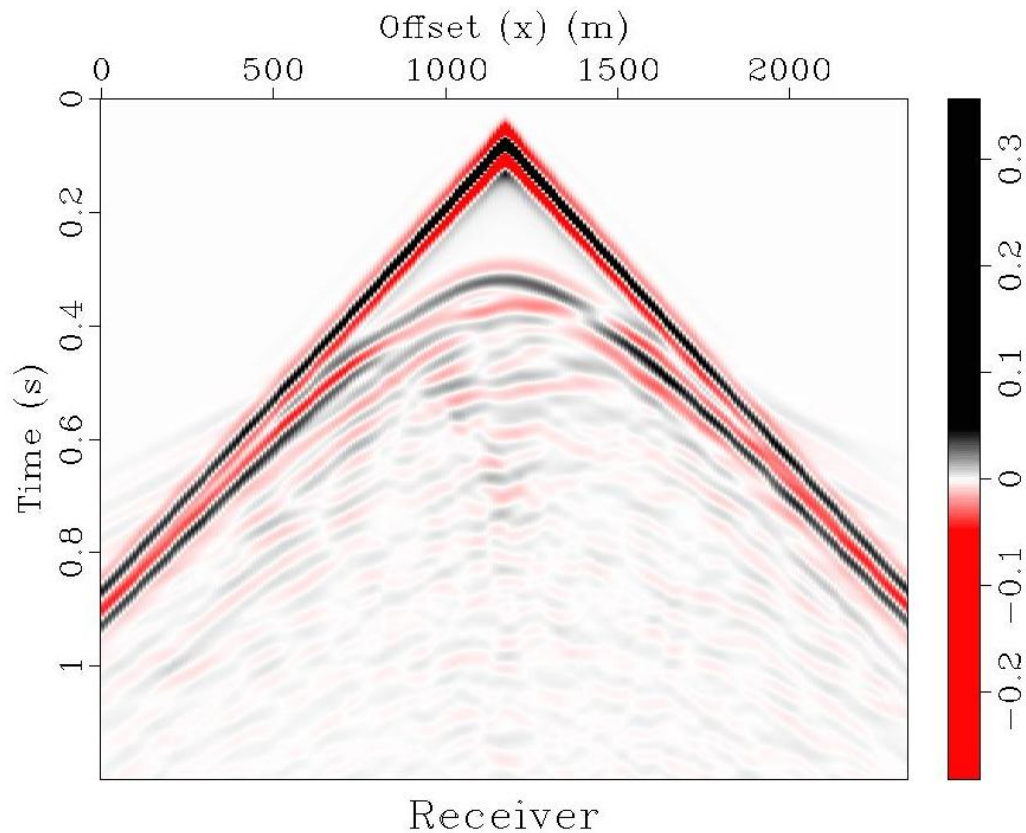
Figure 5.3: Shot record over the model with *10 m* resampling. The source is placed in the middle of the model at a depth of *10 m*, whereas receivers are placed every *10 m* over the whole model at a depth of *20 m*. A time sampling of *0.4 ms* is used.

Figure 5.3 shows the result of shooting a single shot over the model with *10 m* resampling. The source is placed approximately in the middle of the model (*x=1170 m*) at *10 m* depth, and receivers are placed every *10 m* over the whole model at *20 m* depth. A time sampling interval of *0.4 ms* has been used. The direct wave is clearly seen as strong linear events on each side of the source position. Beneath the direct wave we observe the reflected and refracted waves from the ocean bottom. The events below are harder to recognize due to the strong amplitudes of the direct wave.
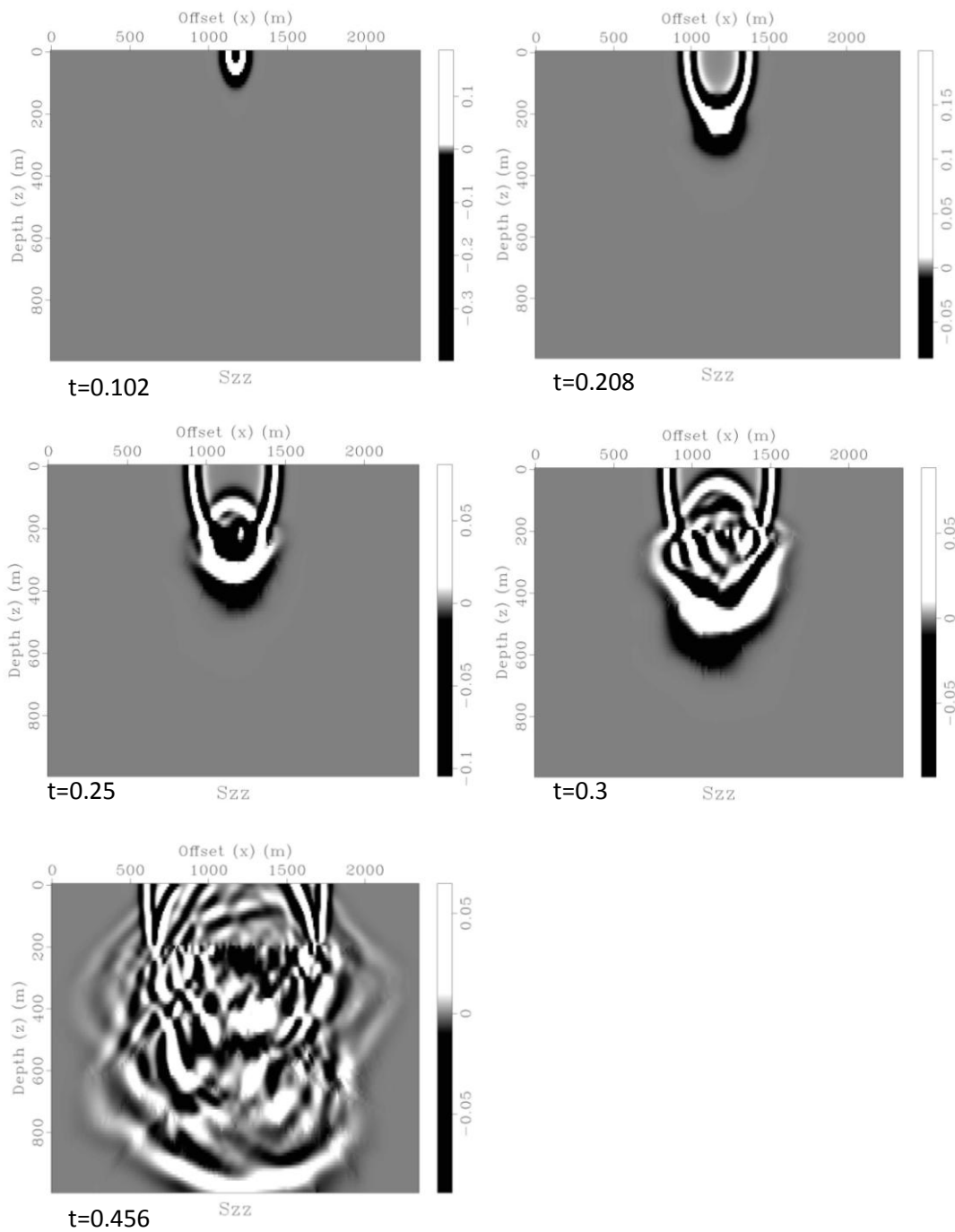
Figure 5.4: Images of the vertical component of the wave field for different times. (Generated in Madagascar)

Figure 5.4 shows the vertical component of the wave field at different times. At the first image the signal has just been emitted and the wave field starts to move downwards in the model. The second image shows the wave field reaching the ocean bottom, and at the third image the wave field has reached the layer of plateau basalts, and starts reflecting off. The fourth image shows both the ocean bottom reflection as well and the reflection from the layer of plateau basalts moving upwards towards the receivers. We observe that when the wave field reaches the volcanic intrusions it moves quite fast due to the high velocities in these layers, which causes the wave fronts to become wider. The complex structures of the volcanic intrusions together with the high impedance contrasts

32

between the intrusions and the sandstones causes the wave field to spread in all directions after some time, and at the last image the wave field shows up as quite messy.

5.2   Multiple shots modelling

As mentioned in Chapter 4.3.2 the multiple shots modelling has been performed on the supercomputer Kongull. For the multiple shots modelling the option for local models has been used, which simply means that the model is split up into several smaller models. The local models can overlap, and each local model has the same size and source and receiver geometry. According to this, one local model for each shot has been made, and the distance between one local model and the next is specified to be the same as the distance between each shot.

During the acquisition of the synthetic seismic data, the receiver length has been chosen such that it is equal to the depth of the model, i.e. *1000 m*.
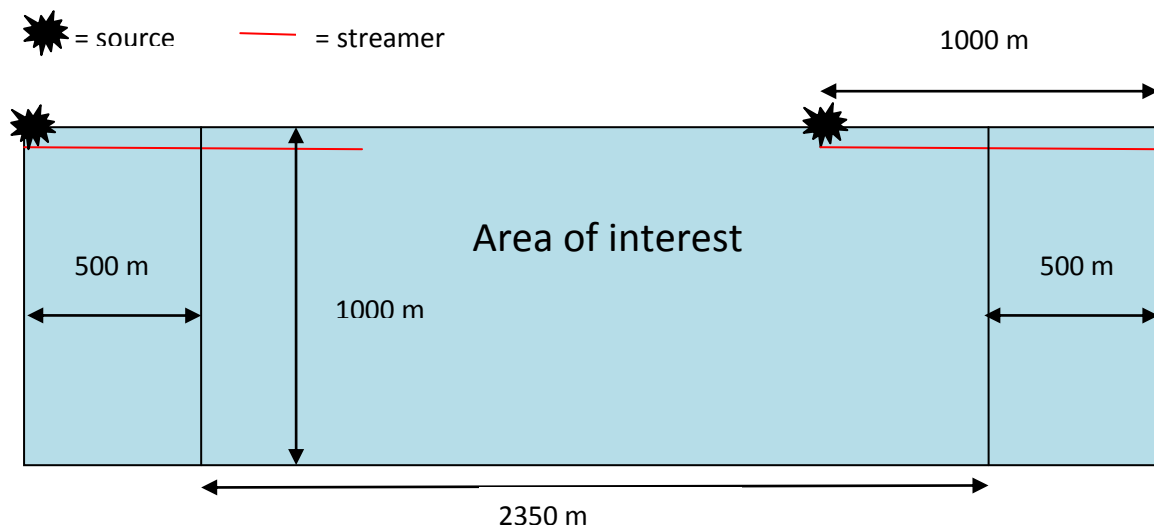
Figure 5.5: Sketch showing the shot and receiver positions for the first and last shot over the model.

Source and receiver points have been placed a half streamer length outside of the actual model (area of interest), see Figure 5.5. Because the model made in Petrel has been extended with *6 km* on each side of the actual model this means that the first shot has to be placed on *x=5500 m*, according to Figure 5.5.
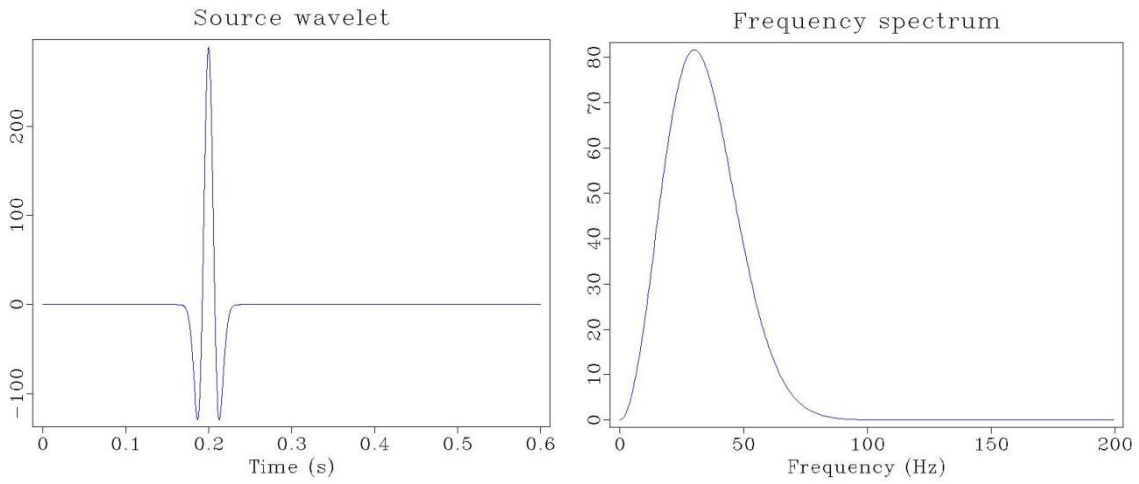
Figure 5.6: Left: Ricker wavelet with a peak frequency of *30 Hz* centred at *t=0.2 s*. Right: Frequency spectrum for a Ricker wavelet with a peak frequency of *30 Hz*, the maximum frequency is approximately *90 Hz*.

A Ricker wavelet with a peak frequency of *30 Hz* has been used in the modelling. Figure 5.6 shows the wavelet and the corresponding frequency spectrum. The maximum frequency is about *90 Hz*. To satisfy the stability conditions given in Equation (4.10) and (4.11) *Δx* must be set to *5 m* (i.e. no resampling), and *Δt* must be less than *0.46 ms*.

5.2.1 Modelling 1 – shot interval: 25 m

Figure 5.7 shows the shot record for a shot located at *x=6625 m* and *20 m* depth. We observe that the direct wave first appears on time *t=0.2 s*, which is due to the time delay of the Ricker wavelet shown in Figure 5.6. The distance between each shot is set to be *25 m*, which means that the distance between one local model and the next is *25 m*. The streamer is placed at *10 m* depth with a receiver spacing of *10 m.* The time sampling that has been used is $\Delta t = 0.4\ ms$. All the parameters used in the modelling are listed in Table 5.1 below.
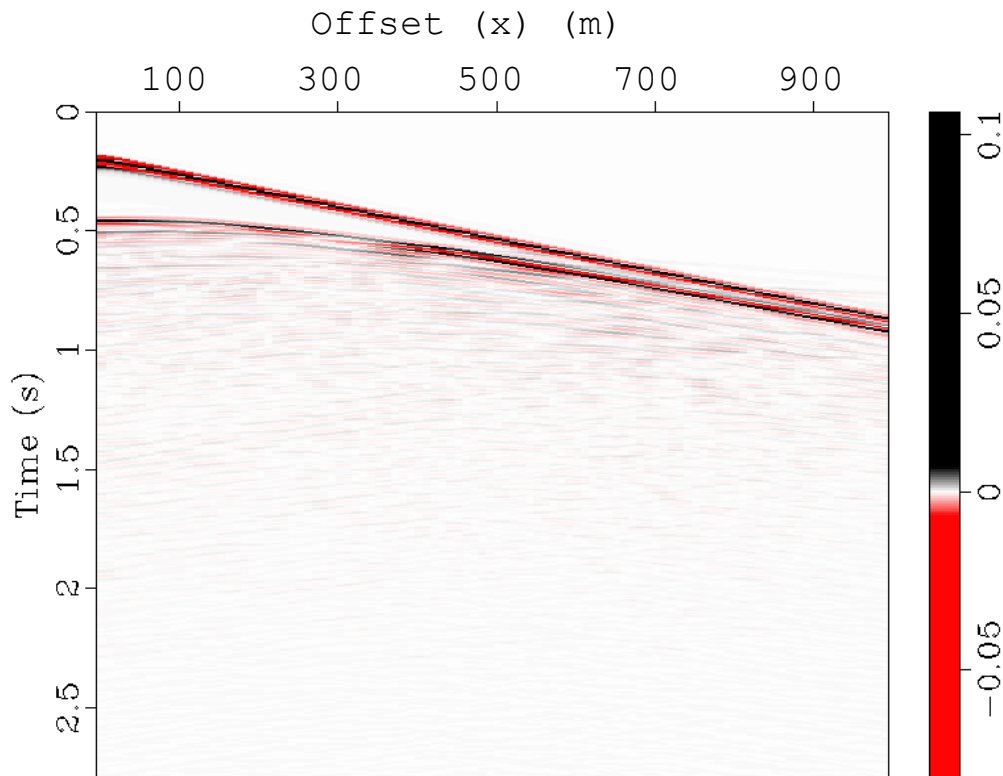
Figure 5.7: A shot record from the multiple shots modelling. The shot is located at *x=6625 m* and *20 m* depth. All the parameters used in the modelling are listed in Table 5.1.

Table 5.1: Parameters used in modelling 1.

Parameter	Value
Size of grid cells, Δx · Δz	5 · 5 m
Time sampling interval, Δt	0.4 ms
Peak frequency, f	30 Hz
Source depth	20 m
Shot interval	25 m
Streamer depth	10 m
Near offset	0 m
Far offset	1000 m
Receiver spacing	10 m
Record length	2.6 s

5.2.2   Modelling 2 – shot interval: 10 m

Because the actual model (area of interest) is only *2350m* long, a shot spacing of *25 m* is quite sparse. Therefore another forward seismic modelling has been done, where the shot spacing is set to be *10 m*. In addition the time sampling interval has been reduced from *0.4 ms* to *0.1 ms*. The reason for doing that, was that *0.4 ms* was right beneath the limit for the stability criterion given in Equation 4.10 ($\Delta t \leq 0.46\ ms$). For the modelling discussed in Chapter 5.2.1, there also was a depth distance of *10 m* between the streamer and the source. Theoretically we should correct for this in the processing, but because a distance of only *10 m* together with the P-wave velocity in the water, which is set to be *1480 m/s*, the effect of correcting for this is very small. But to be sure to avoid this effect the streamer and the source are placed at the same depth, i.e. *10 m*. All the other parameters in the modelling are equal to the ones used for the modelling discussed in Chapter 5.2.1. The parameters used in the modelling are summarised in Table 5.2 below. The parameters that are different from the modelling discussed in Chapter 5.2.1 are marked in blue.

Table 5.2: Parameters used in the modelling.

Parameter	Value
Size of grid cells, Δx · Δz	5 · 5 m
Time sampling interval, Δt	0.1 ms
Peak frequency, f	30 Hz
Source depth	10 m
Shot interval	10 m
Streamer depth	10 m
Near offset	0 m
Far offset	1000 m
Receiver spacing	10 m
Record length	1.45 s

5.2.3   Modelling 3 – check the influence of the layer of plateau basalts

Another interesting feature to check out would be the influence of the layer of plateau basalts. It is believed that much energy is lost due to this layer. To check out the influence of this layer another forward modelling has been done, where the properties of the layer of plateau basalts has been changed to sandstone properties. To distinguish the layer from the upper sandstone and sandstone in Table 3.1, the layer has been given properties which are slightly different from those.

Table 5.3: P-wave velocities, S-wave velocities and densities used to model the effect of the layer of plateau basalts. The layer where the properties have been changed is marked in blue.

Lithology/facies association	P-velocity	S-velocity	Density	V_p/V_s
Sea water	1.48	0	1.027	-
Upper sandstone	2.3	1.1	2.0	2.091
Plateau basalts changed to sandstone	2.4	1.2	2.1	2.0
Sandstone	2.5	1.3	2.2	1.923
Dolerite 1st intrusion	4.7	2.7	2.7	1.741
Dolerite 2nd intrusion	4.9	2.8	2.7	1.75

The velocities and densities that have been used to model the effect of the layer of plateau basalts are given in Table 5.3. The initial layer of plateau basalts where the properties have been changed to sandstone properties is marked in blue. The parameters used for the modelling are the same as those used for modelling 2, see Table 5.2.

5.3   Processing of the synthetic seismic data

The processing flow that has been applied to the seismic data from Chapter 5.2 consists of muting, CMP-sorting, NMO-correction, stacking and migration. The purpose by muting the data is to remove the direct wave, as there are very large amplitudes associated with this wave. The NMO-correction and migration require a velocity model, which has been made by first converting the P-wave depth velocity model seen in Figure 4.13 to time, and thereafter transforming the interval velocities to RMS velocities. The NMO-correction and stacking of the NMO-corrected data are therefore used as a quality control of the data, i.e. check the velocity model, before performing migration of the data, which is the most time consuming step in the processing. The migration algorithm that has been used is 2D prestack Kirchhoff time migration. The Kirchhoff migration, also called diffraction stacking uses the integral form of the wave equation, and treats each element of an unmigrated reflection as a portion of a diffraction.

Before the processing of the data has been performed, the data have first been resampled according to the Nyquist sampling criterion

$$\Delta t \leq \frac{1}{2 f_{max}} \tag{5.1}$$

The frequency spectrum used in the modelling has a maximum frequency of about *90 Hz* (see Chapter 5.2). By inserting f_{max} = *90 Hz* this into Equation (5.1) above, we get that *Δt ≤ 5.5 ms*. Based on this and the time sampling used in the modelling in Chapter 5.2, *Δt* is resampled to *4 ms*.

5.3.1 Modelling 1 – shot interval: 25 m

Figure 5.8 shows a shot record before muting to the left, and after muting to the right.
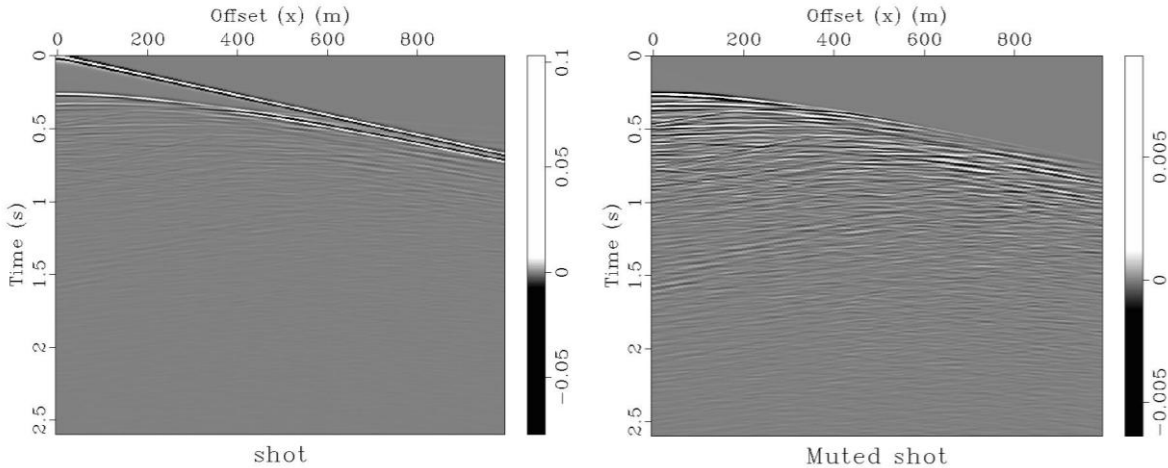
Figure 5.8: Left: Shot record from modelling 1 *(x=6500***). The direct wave is shown as a linear event in the uppermost part of the image. Right: Shot record with the direct wave muted away.**

In the right image the direct wave has been muted away, simply by zeroing out the data for *t <f(x)*, where *f(x)* is a linear function specified by the user. Due to the removal of the large amplitudes of the direct wave the other waves can be seen much more clearly in the muted image to the right, compared to the unmuted image to the left.
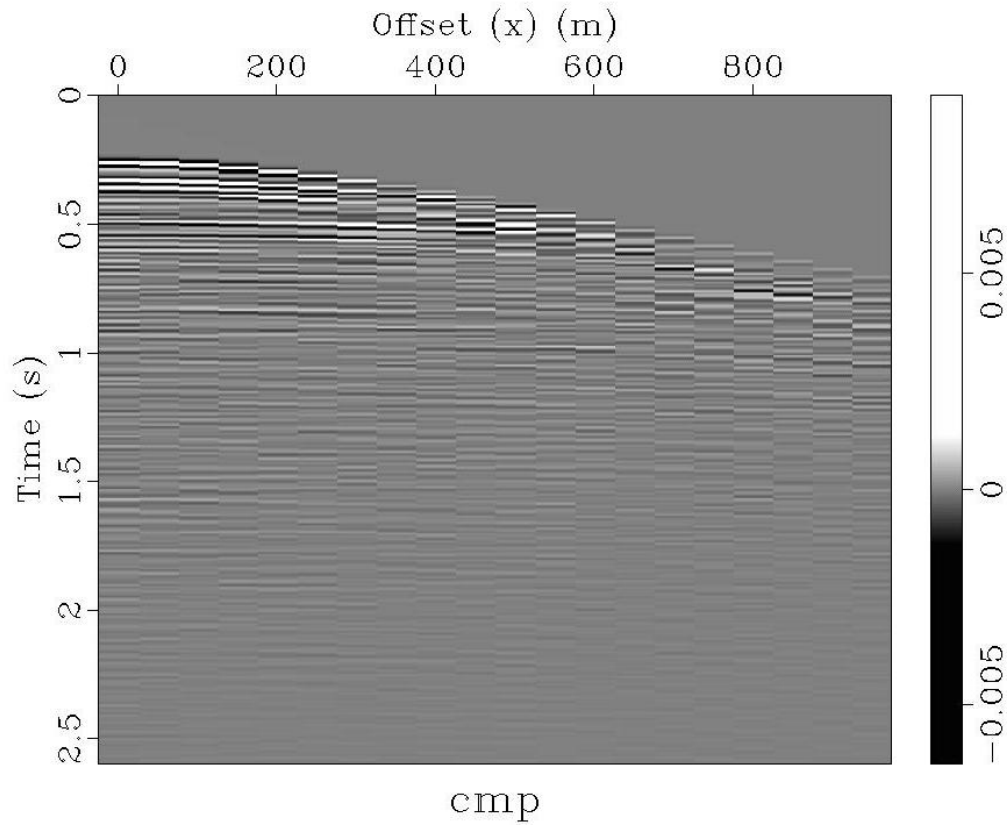
Figure 5.9: CMP-gather from modelling 1. The CMP-offset, which is twice the shot spacing, is *50 m.*

Figure 5.9 shows a CMP-gather from the seismic data. The CMP offset is twice the shot spacing, that is *50 m* for this case, which we see is a bit sparse.

The fold is defined as the number of times the same point on a reflector is sampled. Maximum fold for this survey of *94* shots with *25 m* spacing and *100* receivers with *10 m* spacing is *20*, which is a bit small.
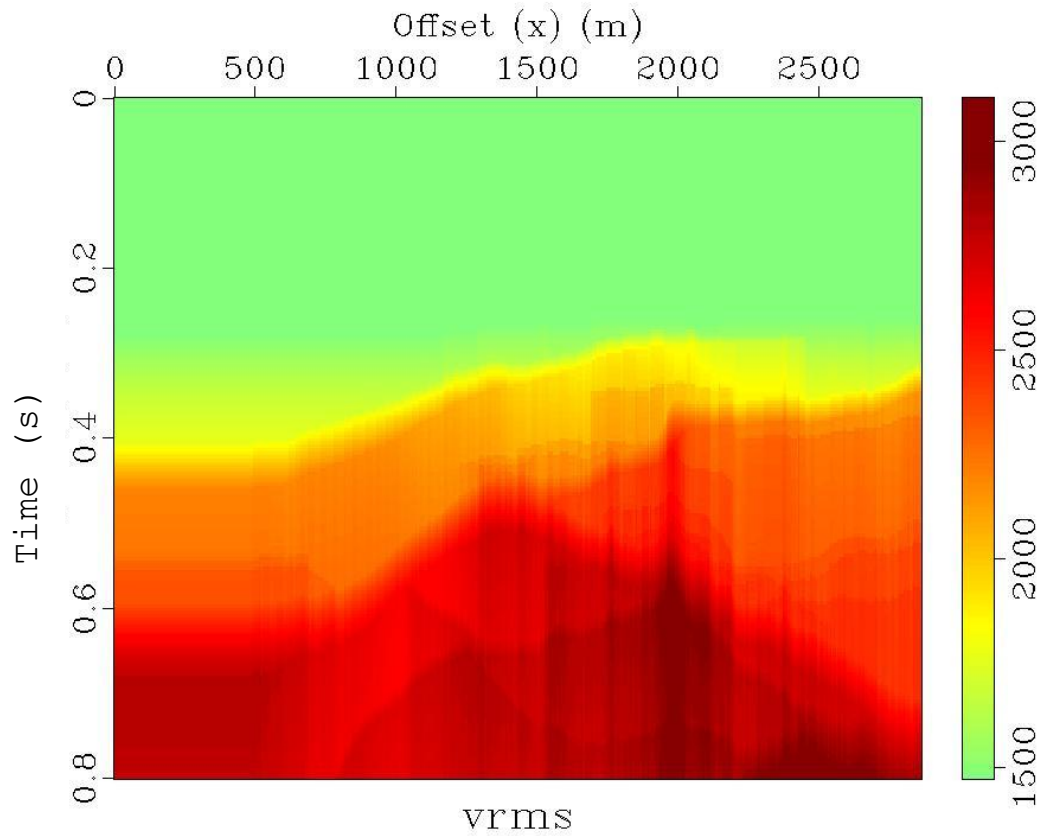
Figure 5.10: RMS-velocities for the P-wave velocities used in modelling 1.

Figure 5.10 shows the RMS-velocities (Root-Mean-Square velocities), that has been calculated by first converting the P-wave depth velocity model shown in Figure 4.13 to time, and thereafter transforming the interval velocities to RMS velocities. We see that the RMS-velocities gradually increases with depth as it should.
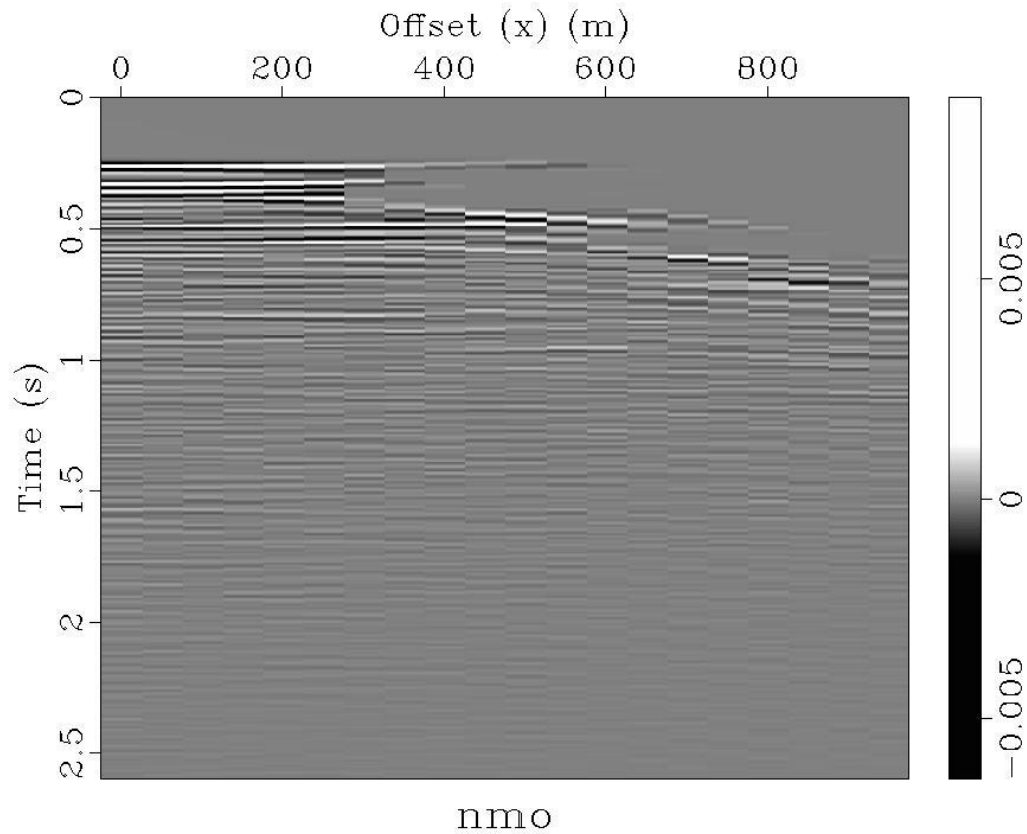
Figure 5.11: NMO-correction.

To quality check the data before performing the migration, the data have been NMO-corrected by using the RMS-velocities shown in Figure 5.10 and thereafter stacked. An NMO-correction from modelling 1 is shown in Figure 5.11. We see that the ocean bottom flattens out quite well. The reason that it's not entirely flattened, but seems to move a bit upwards around *x=400* is due to the non-flat ocean bottom.
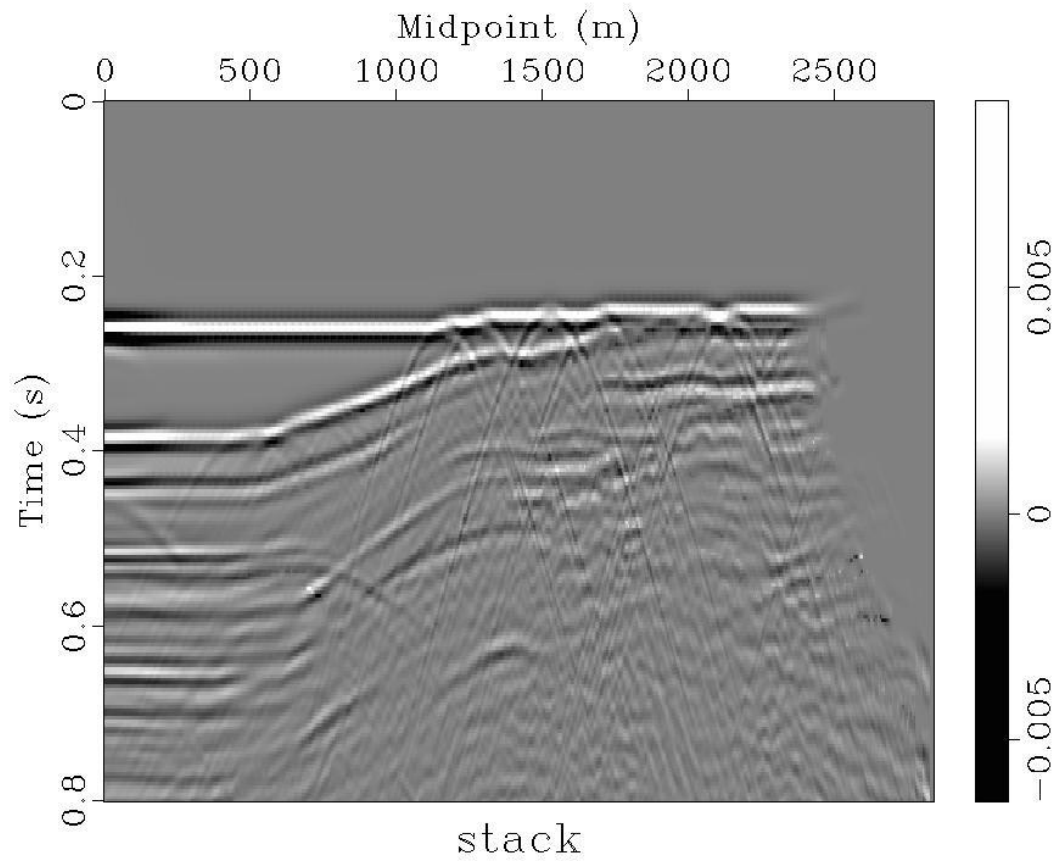
Figure 5.12: Stacking of the NMO-corrected data.

Figure 5.12 shows the stacking of the NMO-corrected data, which seems quite reasonable. Hyperbolas are still present, because migration hasn't been performed yet. We observe several diffraction hyperbolas at the ocean bottom, due to small troughs and peaks that act as seismic spreaders. The area with apparently no data to the right is caused by the fact that there are no shots directly above that area.
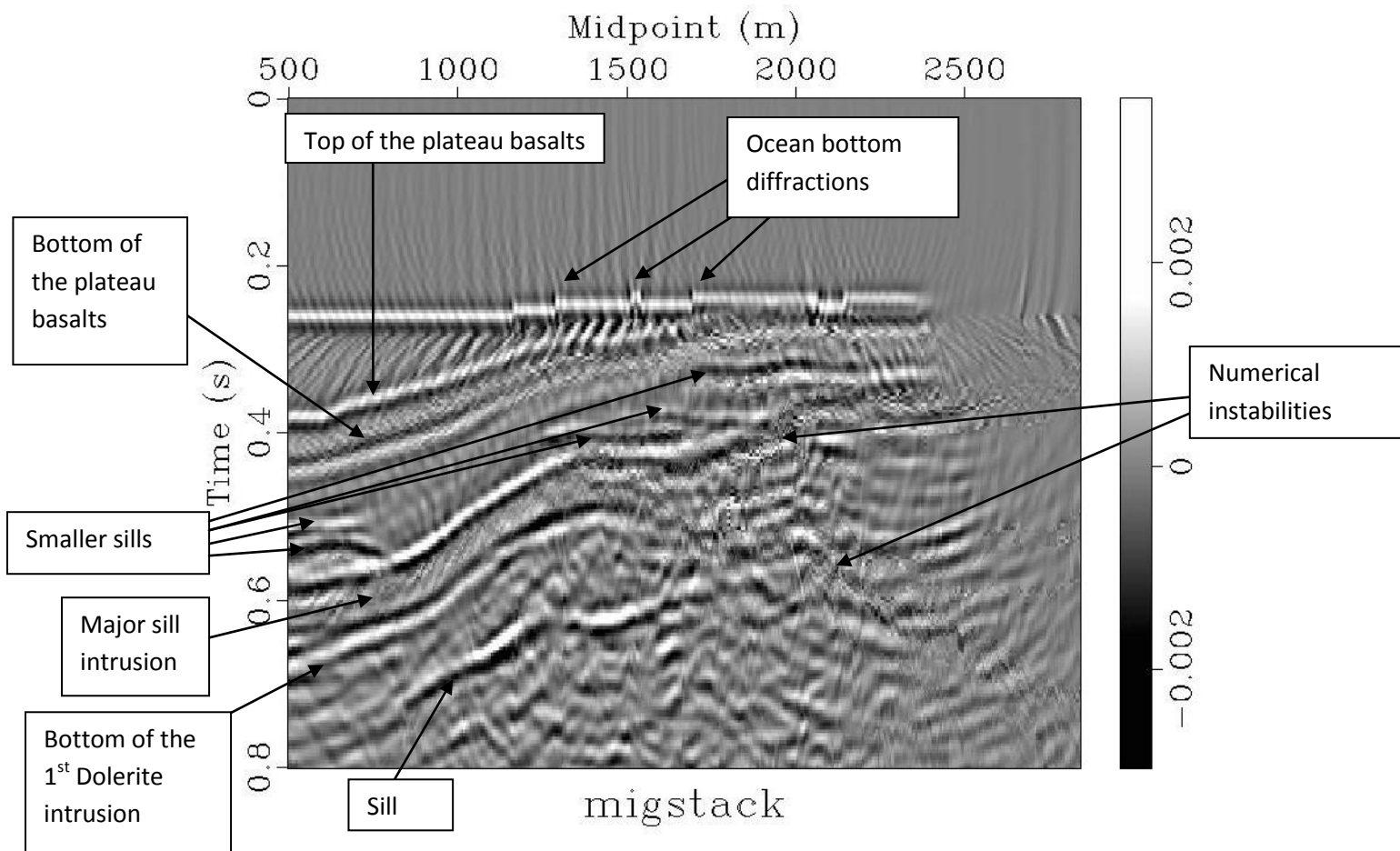
Figure 5.13: Migrated section from modelling 1.

Figure 5.13 shows the result after migrating the data. As discussed for the stacking in Figure 5.12 ocean bottom diffractions are also seen in the migrated section. Comparing the migrated image with the time converted velocity model shown in Figure 5.14 we see that the top of the plateau basalt layer show up as a strong reflector. The bottom of the plateau basalts is visible as well. Beneath the plateau basalts we recognise some of the smaller sills. The major sill intrusion (2nd Dolerite intrusion) gives strong reflections. It's also possible to distinguish between the 1st and 2nd Dolerite intrusion in the left part of the image. In the right part of the image, where there should be several smaller sills we observe numerical instabilities. This is caused by the large impedance changes between the sandstone and the intrusions, which gives instabilities in the modelling algorithm, because the homogeneous media assumption in Chapter 4.1 is not fulfilled.
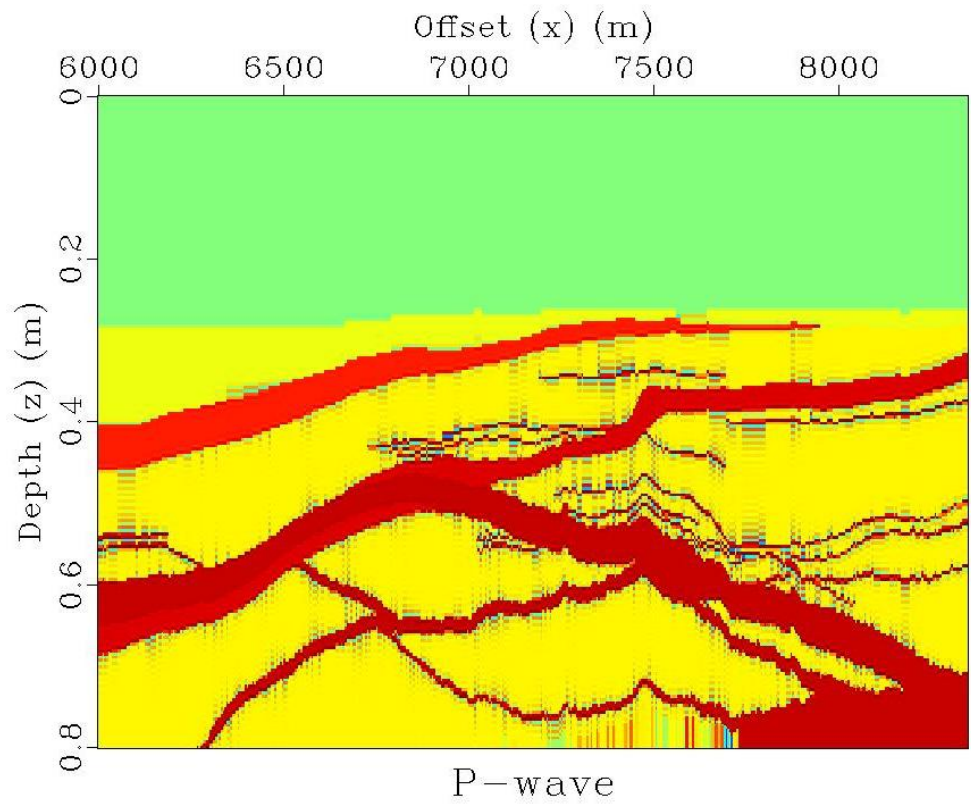
Figure 5.14: Time converted P-wave velocities.

5.3.2 Modelling 2 – shot spacing: 10 m

Because of denser shot spacing it is expected that the data from modelling 2 should give better resolution and thus, better results.
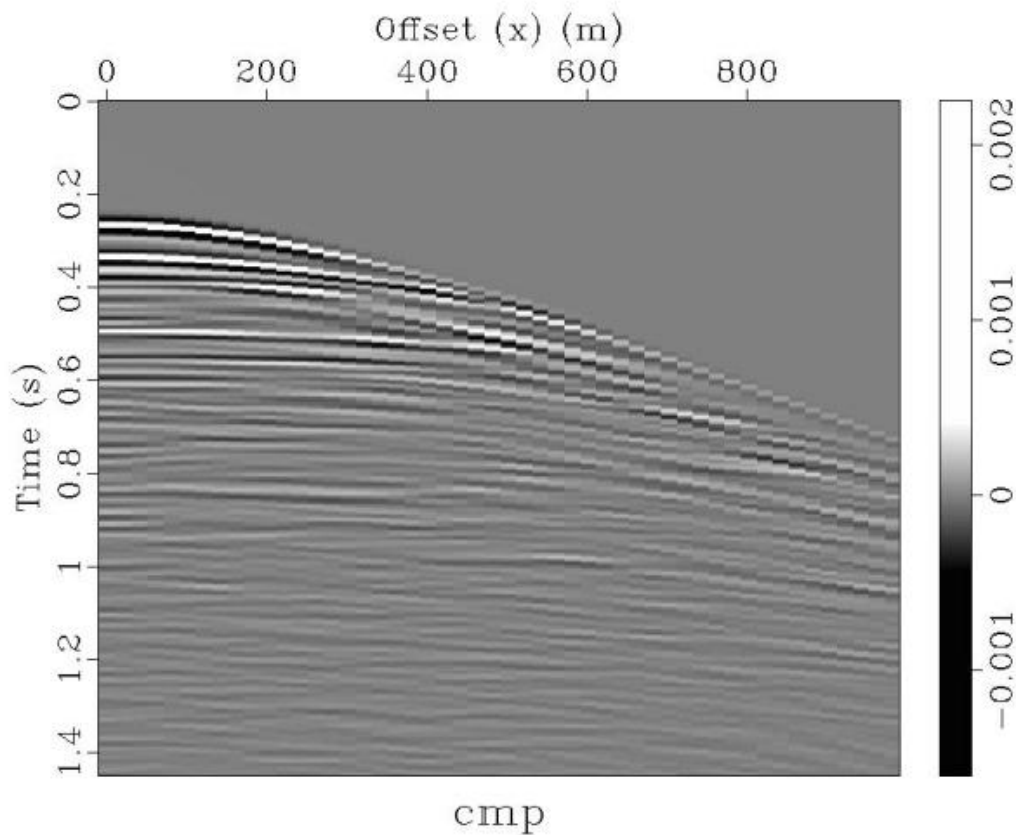
Figure 5.15: CMP-gather from modelling 2. The CMP-offset, which is twice the shot spacing is 50 m.

Figure 5.15 shows a CMP-gather from modelling 2, and we see quite clearly that the number of CMPs has increased compared to modelling 1 in Chapter 5.3.1 The CMP-offset is now *20 m* instead of *50 m* as in Figure 5.9

The maximum fold for this modelling is calculated to be *50*, which is a big increase compared to the maximum fold for modelling 1, which was *20*.

Because the only difference between modelling 1 and modelling 2 is the acquisition parameters, the velocity model used in modelling 2 is the same as the one used for modelling 1. The RMS-velocity model used for modelling 2 is therefore identical to the one shown i Figure 5.10.

Figure 5.16: Migrated section from modelling 2.
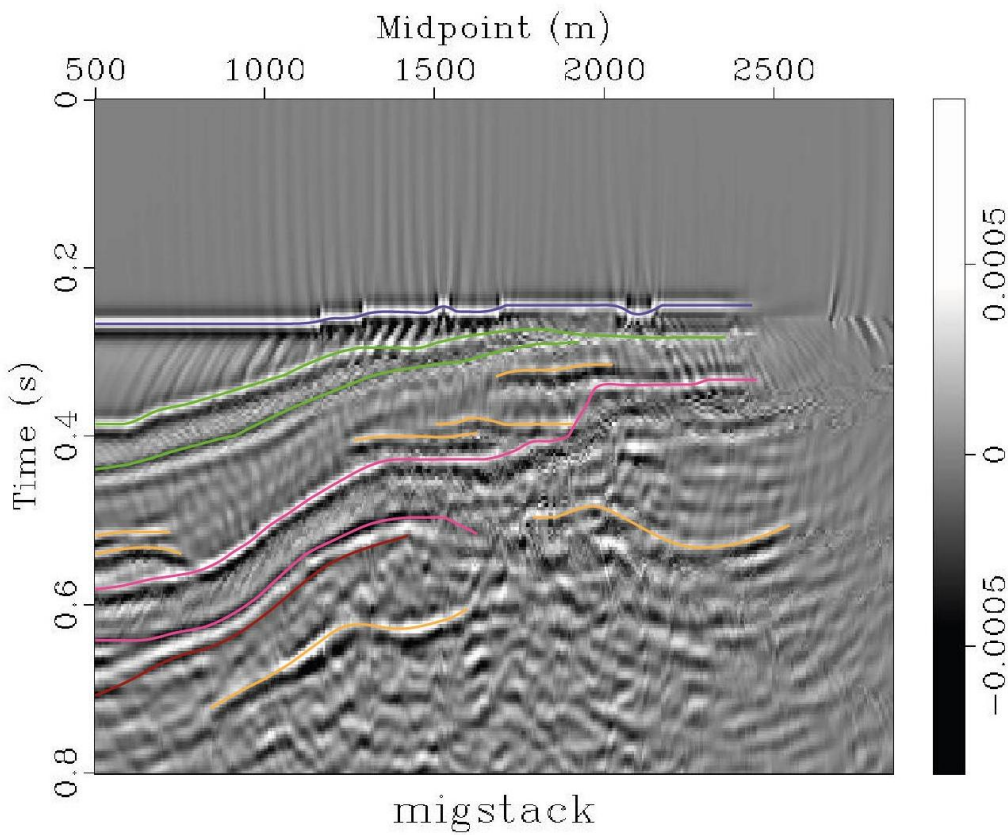
Figure 5.17: Interpretation of the migrated section shown in Figure 5.16.

The result after migration is shown in Figure 5.16 and the corresponding interpretation of the migrated section is shown in Figure 5.17 (for larger images see Appendix C). Essentially the same structures as those observed for modelling 1 are visible, but the reflectors are much clearer in Figure 5.16 compared to Figure 5.13. Especially the areas above the ocean bottom and in the upper sandstone are seen more clearly. The layer of plateau basalts is easily recognised, but as this layer gradually thins out to the right of the image, the amplitudes of the top and bottom of the layer starts to interfere and eventually makes it impossible to distinguish the top and bottom. This is called tuning effects. For the thinnest sill intrusions tuning effects occur as well. The intrusions are so thin that it's impossible to distinguish the top and bottom of the intrusions. Some of the intrusions are also so close that they all show up as one reflector. Not all the volcanic intrusions are visible on the migrated section, especially in the right part of the image it is difficult to see the intrusions. It is believed that much of the energy is scattered between the many volcanic intrusions that are present in the right part of the image (see Figure 5.14), and thus make it difficult to image the structures. Numerical instabilities in this area of the migrated section make it even more difficult to interpret the area.
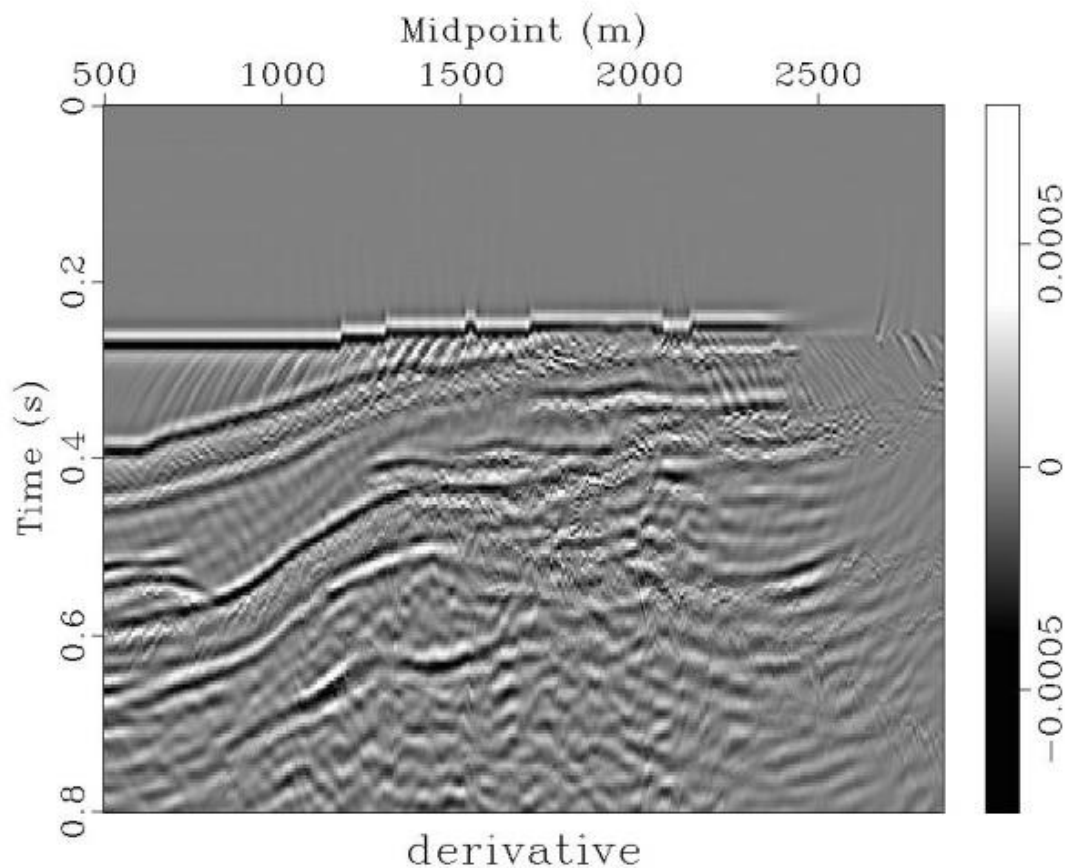
Figure 5.18: Showing the first derivative of the migrated image in Figure 5.16. We see that the ocean bottom diffractions have almost disappeared, and that the reflectors become clearer. The scaling of the image is, however wrong, due to the differentiation.

By calculating the first derivative of the migrated image in Figure 5.16, and thus look at the amplitude changes instead of the actual amplitudes itself, we see that the structures become a bit clearer. The ocean bottom diffractions have almost disappeared, and the reflectors become clearer as well. Of

course we must keep in mind that the scaling of the image is incorrect when we have differentiated it.

5.3.3 Modelling 3 – check the influence of the layer of plateau basalts

As mentioned in Chapter 5.2.3, the plateau basalts have now been changed to a sandstone layer, see Table 5.3. This means that the velocity model has changed, and the resulting RMS-velocities for modelling 3 can be seen in Figure 5.19. Compared to the RMS-velocities used for modelling 1 and 2 shown in Figure 5.10, we see that the RMS-velocities now are a bit lower, as expected.
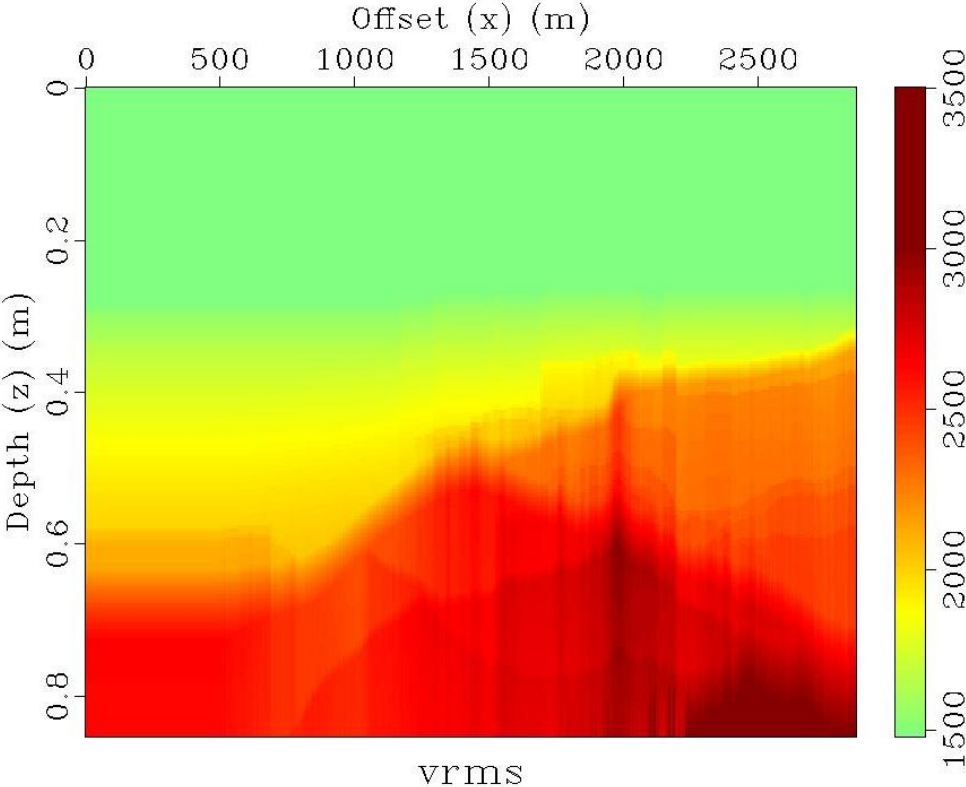
Figure 5.19: RMS-velocities for modelling 3.

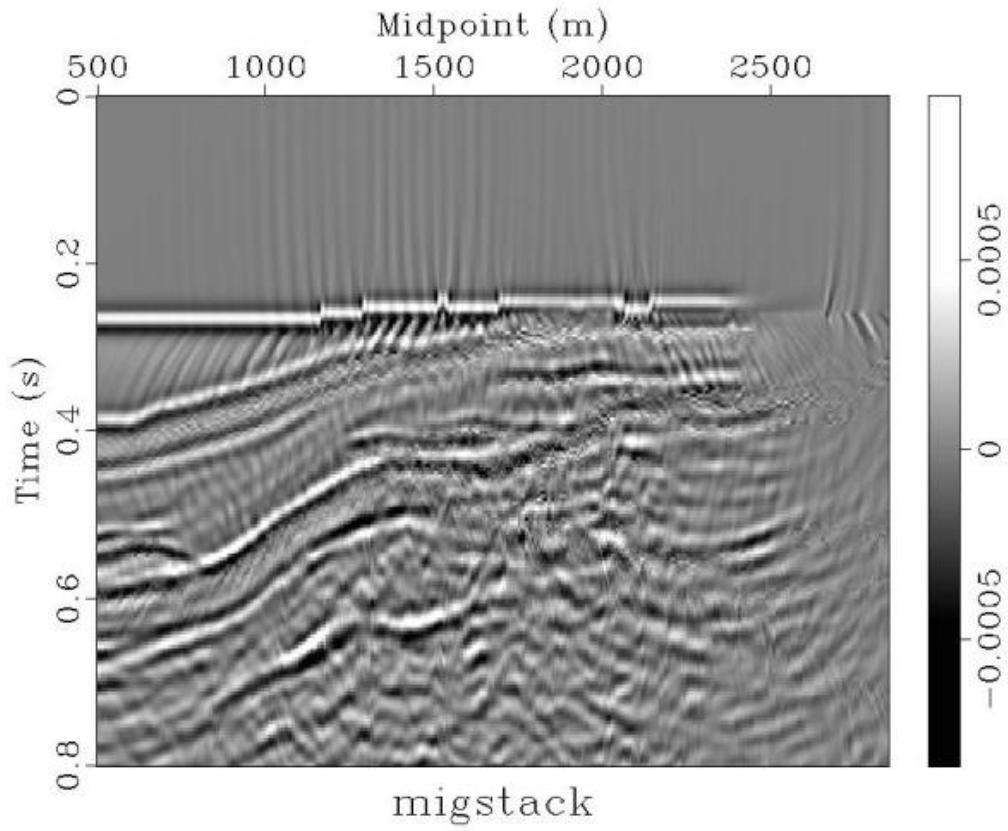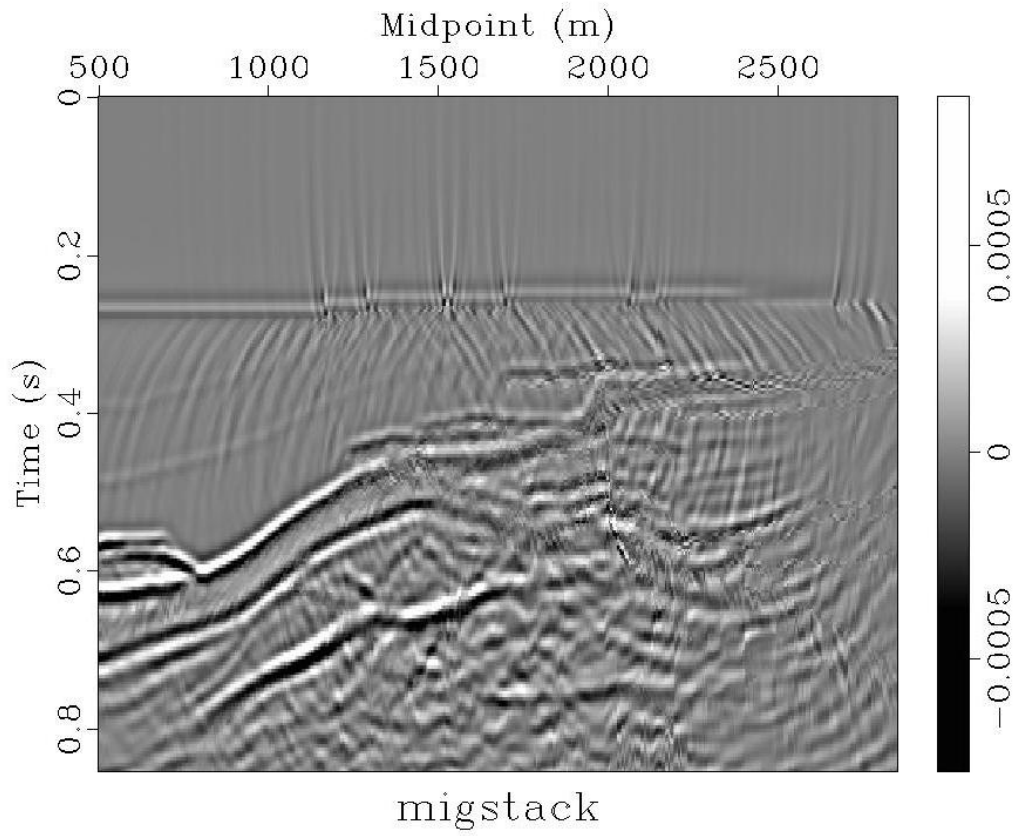**Figure 5.20: Migrated section from modeling 3.**
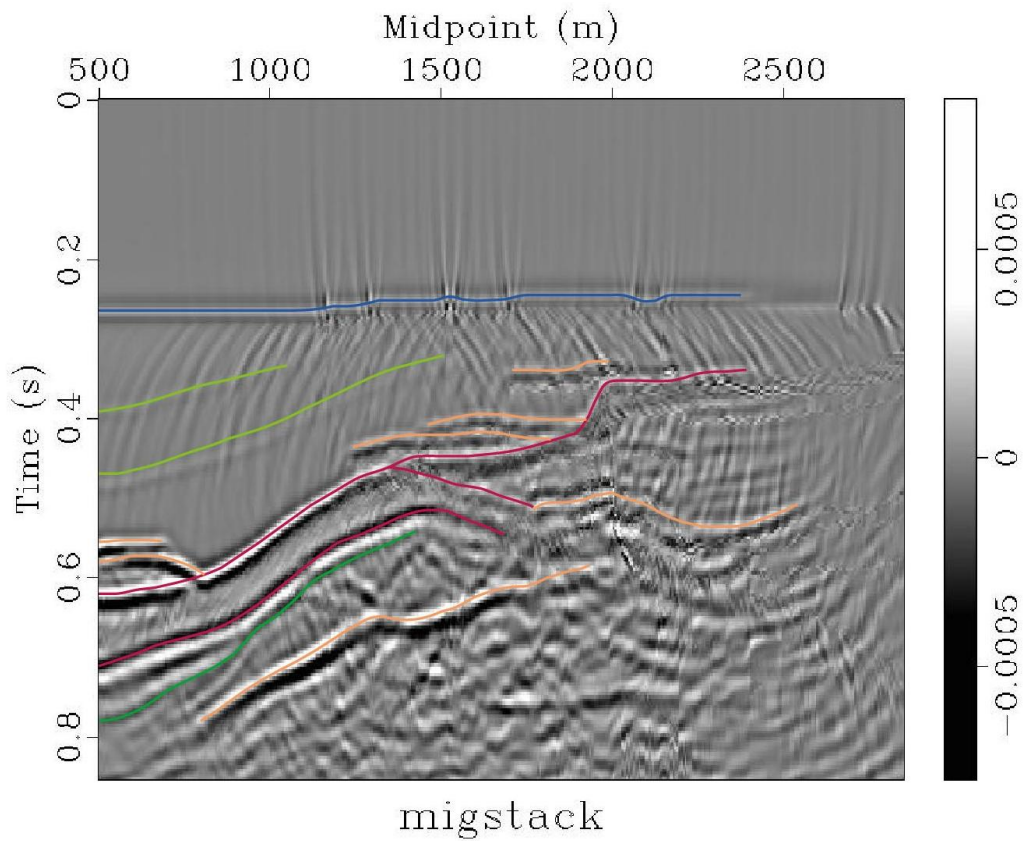
Figure 5.21: Interpretation of the migrated section shown in Figure 5.20

The migrated image from modelling 3 and the corresponding interpretation of the image are shown in Figure 5.20 and Figure 5.21, respectively (for larger images see Appendix C). The structures beneath the previously plateau basalts are now clearer, due to only weak reflections from the layer where the plateau basalts were. We observe that the reflections from the small sills between the plateau basalts and the major sill intrusion (1st and 2nd Dolerite intrusion) are clearer. The major sill intrusion shows clearer reflections as well, and it is easier to distinguish the 1st and 2nd Dolerite intrusions in the left part of the image. It's also easier to follow the top of the 1st Dolerite intrusion in the right part, though the bottom of the 1st Dolerite intrusion is still difficult to see in right part of the image. Basically all the reflectors beneath the plateau basalts are now clearer, which means that much energy is lost due to the plateau basalts.

6 Discussion

In order to perform the modelling that has been done in this thesis several assumptions and simplifications had to be taken into consideration.

First of all, as discussed in Chapter 3, the geological model is based on a photo, which means that the different lithologies and structures have been interpreted purely based on the photo and the general knowledge of these rocks. The sharp colour change between the sandstones and the volcanic intrusions make it quite easy to distinguish these two lithologies, however as the resolution of the photo is limited and slumping of the sandstones along the cliffs occur, it's difficult to observe small changes and smaller intrusions. There might for instance also be small changes within the sandstones or within the volcanic intrusions that are not visible on a photo. For this reason the structures of the volcanic intrusions had to be simplified. It is also assumed that the cliffs show a nearly vertical section and that the horizontal scale on the photo is the same as the vertical scale. Though, the size of the outcrops in the field must be considered an approximation it is believed that the specified size gives a quite realistic size of the geology in the area around Independence Fjord, such that it doesn't affect the modelling in that it gives unrealistic size and form of the geological structures. The purpose of this thesis was also to study large-scale structures. The peak frequency of the Ricker wavelet used in the modelling was fairly low-frequent (*30 Hz*), and thus it would have been impossible to distinguish thin layers on the synthetic seismic data by using this frequency. The limit of separability is defined as a quarter of a wavelength $d = \frac{\lambda}{4}$, where $\lambda = \frac{v}{f}$. Due to the large velocities used in the model the limit of separability becomes about *35-40 m* for the volcanic intrusions. The reason for choosing such a low frequency was because of the high impedance contrasts and the fact that high frequencies are more absorbed than low frequencies. So based on the low resolution of the seismic it would had make no sense to make a geological model with many thin layers.

During the model building in Petrel the model is divided into layers or separate volumes that can be assigned the same properties. This is of course a big simplification, it would however be impossible to create a geological model that includes all details and all properties of the real subsurface.

The properties that have been assigned to each of the layers are all based on theoretical values for the different lithologies, and it is assumed that no major cracks or faults are present in the area. Because there are big variations in density and velocities for a given lithology, the uncertainties in assigning properties to the layers are quite big. It is however, taken into consideration that the impedance contrast between the sandstones and the volcanic intrusions is quite large, as this is one of the difficulties with seismic from volcanic intrusions.

Further, the modelling algorithm that is implemented in the Madagascar software is based on elastic wave theory, where the wave equation and the numerical solution that have been derived yields for elastic, isotropic and homogeneous media. That means that the modelling algorithm doesn't take anisotropy, heterogeneity or absorption effects into account. This is believed to be a major source of error, as real earth is always anisotropic and heterogeneous. Due to the very high impedance contrasts that are associated with the volcanic intrusions, the assumption of homogeneity is clearly broken. This causes numerical instabilities in the modelling algorithm, which can be seen on the migrated sections in Chapter 5.3. Despite of the simplifications, it is however believed that the modelling gives an indication of what we can expect to see on seismic data in relation to volcanic intrusions.

The Ricker wavelet used in the modelling is also idealised, and a real seismic wavelet would probably have a broader frequency spectrum as well.

In the processing flow the travel times haven't been corrected for the fact that the source and receivers have different depth in modelling 1, however because the distance is only *10 m* it is believed to only have a minor effect. Furthermore, the source and receivers are placed at the same depth in modelling 2 and 3, thus avoiding the need of this correction.

One major assumption that has been done in the processing is that it is assumed that the velocity model is known, as the RMS-velocities used in the processing are found by first converting the P-wave depth velocity model to time. For real seismic surveys the velocity model is usually not known, and a velocity analysis have to be performed. This means that the velocity model used in the processing in this thesis may be better than one would have obtained from real seismic data, and thus influences the result by better giving a better migration.

7 Conclusions

It is found that the layer of plateau basalts that overlies the Independence Fjord Group clearly affects and obscures the imaging of the structures beneath. However, it is possible to see several volcanic intrusions beneath the plateau basalts, though the reflectors are not as clear as for the layer of plateau basalts. Several smaller sills are also visible on the seismic, but due to tuning effects it's impossible to distinguish the top and bottom of them. Ocean bottom diffractions are observed because of small troughs and peaks at the ocean bottom that act as seismic spreaders.

By removing the layer of plateau basalts and replace it with a sandstone layer, all the other reflectors become much clearer, which means that the plateau basalts affect the imaging of the structures beneath quite a lot. Since the uppermost volcanic layer that the seismic waves have to propagate through give the strongest reflections, this indicates that the uppermost volcanic layer have a big influence on the imaging of the structures beneath. Based on this, it is believed that in the presence of several volcanic layers some energy get lost for each volcanic layer, making it difficult or impossible to see deep in the subsurface when many volcanic layers are present.

Numerical instabilities from the modelling algorithm are also observable on the migrated sections in Chapter 5.3. This is caused by the large impedance contrasts that are present in the model, such that the assumption about homogeneous media in Chapter 4 is not fulfilled.

It is believed that there are big uncertainties related to the layer of plateau basalts. The plateau basalts consist of several individual flows and are usually very inhomogeneous, something that is not taken into account in the modelling that is done in this thesis. Thus, it is expected that much more energy is absorbed and scattered within the plateau basalts in reality than what is observable on the synthetic seismic in Chapter 5. One could therefore expect that the layers beneath the plateau basalts on real seismic are less visible, if visible at all, than what the results in Chapter 5 show.

8   References

(n.d.). Retrieved June 2013, from http://www.bairdpetro.com/pdf_files/p58-62.pdf#page=1&zoom=auto,0,842

Arntsen, B. (2011). *Geophysical Analysis Lecture Notes.* NTNU.

Avseth, P., Mukerji, T., & Mavko, G. (2005). *Quantitative Seismic Interpretation: Applying Rock Physics Tools to Reduce Interpretation Risk.* Cambridge University Press.

Bingen, B., Andersson, J., Söderlund, U., & Möller, C. (2008, March). The Mesoproterozoic in the Nordic Countries. *Episodes, Vol. 31, No. 1* , pp. 29-34.

Brown, A. R. (2010). *Interpretation of Three-Dimensional Seismic Data.* AAPG.

Carcione, J. M., Herman, G. C., & Kroode, A. t. (2002). Seismic modeling. *Geophysics vol. 67, no. 4* , pp. 1304-1325.

Henriksen, N. (2005). *Geological History of Greenland - Four billion years of Earth evolution.* GEUS.

Henriksen, N., Higgins, A., Kalsbeek, F., & Pulvertaft, T. C. (2000). Greenland from Archaean to Quaternary. *Geology of Greenland Survey Bulletin nr. 185* , pp. 24-52.

Holberg, O. (1987). Computational Aspects of the Choice of Operator and Sampling Interval for Numerical Differentiation in Large-scale Simulation of Wave Phenomena. *Geophysical Prospecting 35* , pp. 629-655.

Holt, R. M. (2004). Lecture Notes: TPG4170 Rock Acoustics, NTNU. Trondheim, Norway.

Johansen, S. E., Kibsgaard, S., Andresen, A., Henningsen, T., & Granli, J. R. (1994). Seismic Modeling of a Strongly Emergent Thrust Front, West Spitsbergen Fold Belt, Svalbard. *AAPG Bulletin, V. 78, No. 7* , pp. 1018-1027.

Johansen, S. E., Wicklund, T. A., & Amundsen, H. E. (2007, March). Interpretation example of marine CSEM data. *The Leading Edge* .

Johansen, S., Granberg, E., Mellere, D., Arntsen, B., & Olsen, T. (2007). Decoupling of seismic reflectors and stratigraphic timelines: A modeling study of Tertiary strata from Svalbard. *Geophysics vol. 72, no. 5* , pp. SM273-SM280.

Kalsbeek, F., & Frei, R. (2006). The Mesoproterozoic Midsommersø dolerites and associated high-silica intrusions, North Greenland: crustal melting, contamination and hydrothermal alteration. *Contrib Mineral Petrol 152* , pp. 89-110.

Kearey, P. (2001). *The New Penguin Dictionary of Geology.* Penguin Books.

Krebes, E. S. (2004, April). Seismic Forward Modeling. *CSEG Recorder* , pp. 28-39.

Landrø, M. (2008). *Anvendt geofysikk i TPG4100 Fysikk og Geofysikk.* NTNU.

Landrø, M. (2011). *Seismic Data Acquisition and Imaging.* NTNU.

LeVeque, R. J. (2007). *Finite Difference Methods for Ordinary and Partial Differential Equations: Steady-State and Time-Dependent Problems.* SIAM.

Madagascar. (n.d.). Retrieved 2013, from www.reproducibility.org

Margrave, G. F., & Manning, P. M. (2004). Seismic Modelling: An Essential Interpreter's Tool. *2004 CSEG National Convention* .

Mavko, G. (n.d.). *Stanford Rock Physics Laboratory.* Retrieved June 2013, from Parameters that influence seismic velocity: Conceptual overview of rock and fluid factors that impact seismic velocity and impedance: https://pangea.stanford.edu/courses/gp262/Notes/8.SeismicVelocity.pdf

Misaghi, A. (2011). Lecture Notes - TPG4190 Seismic Data Acquisition and Processing, NTNU. Trondheim, Norway.

Nitsche, F., & Kruk, J. v. (n.d.). Retrieved June 2013, from http://e-collection.library.ethz.ch/eserv/eth:25462/eth-25462-01.pdf

Petrel TIPS&TRICKS from SCM. (n.d.). Retrieved June 2013, from Import and Digitize Bitmaps - Petrel 2010: http://www.scminc.com/port/SCM_Scan_Register_Digitize_Bitmap_Petrel_2010.pdf

Schneider, J. (n.d.). *Chapter 11: Perfectly Matched Layer*. Retrieved 2013, from http://www.eecs.wsu.edu/~schneidj/ufdtd/chap11.pdf

Sheriff, R. E., & Geldart, L. P. (1995). *Exploration Seismology.* Cambridge University Press.

Upton, B. G., Rämö, O. T., Heaman, L. M., Blichert-Toft, J., Kalsbeek, F., Barry, T. L., et al. (2005). The Mesoproterozoic Zig-Zag Dal basalts and associated intrusions of eastern North Greenland: mantle plume-lithosphere interaction. *Contrib Mineral Petrol 149* , pp. 40-56.

Virieux, J. (1989). P-SV wave propagation in heterogeneous media: Velocity-stress finite-difference method. *Society of Exploration Geophysicists* , pp. 889-901.

Appendix A –Detailed description of the model building in Petrel

(From outcrops in the field to input to the Madagascar software)

As discussed in Chapter 3, the starting point for making the geological model was a photo showing the outcrops in the field (Figure A.1).

Figure A.1: (Identical to Figure 2.2). Photo showing the outcrops in the field.

A.1 Handmade model

Based on the photo shown in Figure A.1 above a geological model for hand was made, simply by placing a transparent paper on top of the photo and drawing the visible structures, see Figure A.2.
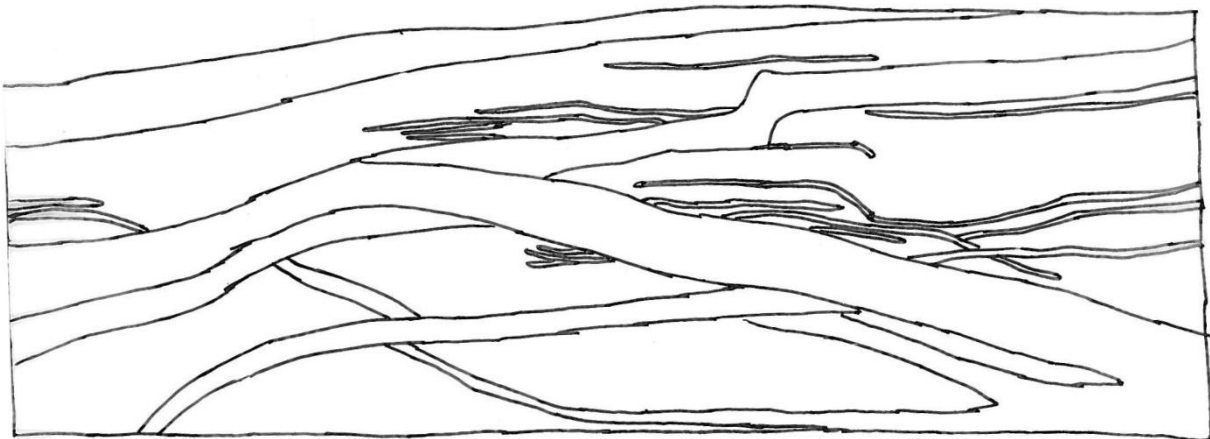

Figure A.2: (Identical to Figure 3.4). Geological model made for hand.

A.2 Import image into Petrel

The handmade geological model was thereafter scanned and imported into the Petrel software as a bitmap. The image formats accepted by Petrel are BMP, JPG, TIFF, GIF and PNG, so if the scanned image has another format it has to be converted to one of the formats accepted by Petrel. As the image in Petrel has to be registered to a coordinate system it is easiest to crop and rotate the image properly before it is imported into Petrel. A screen capture tool such as Snipping Tool or Snagit, or a graphic editing tool such as Adobe Photoshop can be used to rotate and crop the image if needed. The image should be rotated so that the x-axis is horizontal and the z-axis (depth) is vertical.

The prepared image was imported into Petrel by using Import (on selection):

1. Create a folder
2. Right click on the folder
3. Select Import (on selection)
4. Use the Bitmap image format
5. Select the file
6. Click Open to import
7. The file is placed in the folder

A.3 Assign coordinates

After the image has been imported into the Petrel software, it has to be assigned to a coordinate system. It is not necessary to select a Coordinate Reference System (CRS), but the real size of the image has to be known.
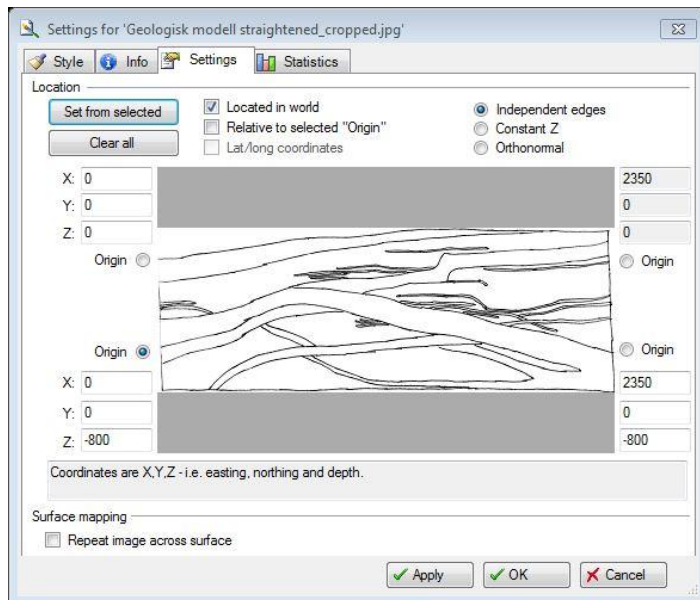
Figure A.3: Settings dialog of the imported image where coordinates are assigned.

To assign coordinates to the image, double click on the imported file and go to the *Settings* tab. Check the box in front of *Located in world*. Select the *Independent edges* radio button, and enter the coordinates for the corners of the image. If you rather want to assign coordinates to specific marks on the image, you have to place tick marks on the image before scanning, follow the procedure

above to assign coordinates and then move the coordinates to the correct spot by adjusting the coordinates.

A.4 Digitize the data

The next step is now to digitize the image, by using polygons. Open a 3D window and toggle on the image to show it.

Figure A.4: Showing two digitized polygons.

To create polygons go to the processes pane →*utilities* and make the **Make/edit Polygons** process

active. Click on the *Start a new set of points/polygons* icon ☐ and digitize the first horizon. Do the same for the other horizons. A top and bottom for the model should be made as well in order to define the extent of the model.

A.5 Make surfaces

Surfaces can be made by using the **Make/edit surface** process under the *Utilities* tab in the Processes pane.
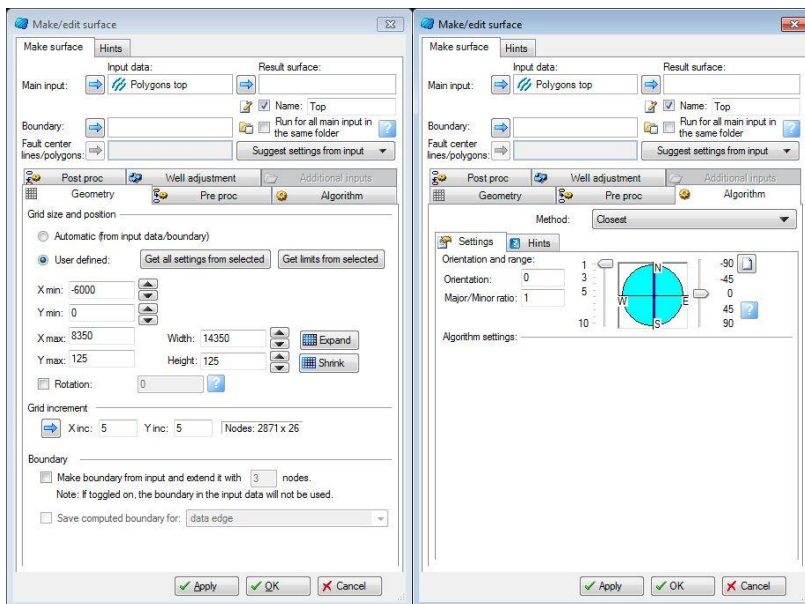
Figure A.5: Make/edit surface process.

Use the polygons as input. Under the *Geometry* tab toggle on the radio button for *User defined*. It is possible to make an extended model by extending the surfaces constantly in the x-direction, simply by specifying X min and X max to the desired values (Figure A.5). Because the polygons are not extended, this means that the surfaces in the extended area get the same values as the polygons have at the edges of the model, see Figure A.6

Figure A.6: Showing a surface that has been extended constantly on each side of the model in the x-direction. (An easier way to extend the model is to use the program sfspan in the Madagascar software).

To get a 3D effect of the seismic modelling the model thickness in the y-direction should be set such that the model consists of at least 20 cells in the y-direction. See Chapter 3.3.4 for how to determine the size of the cells.

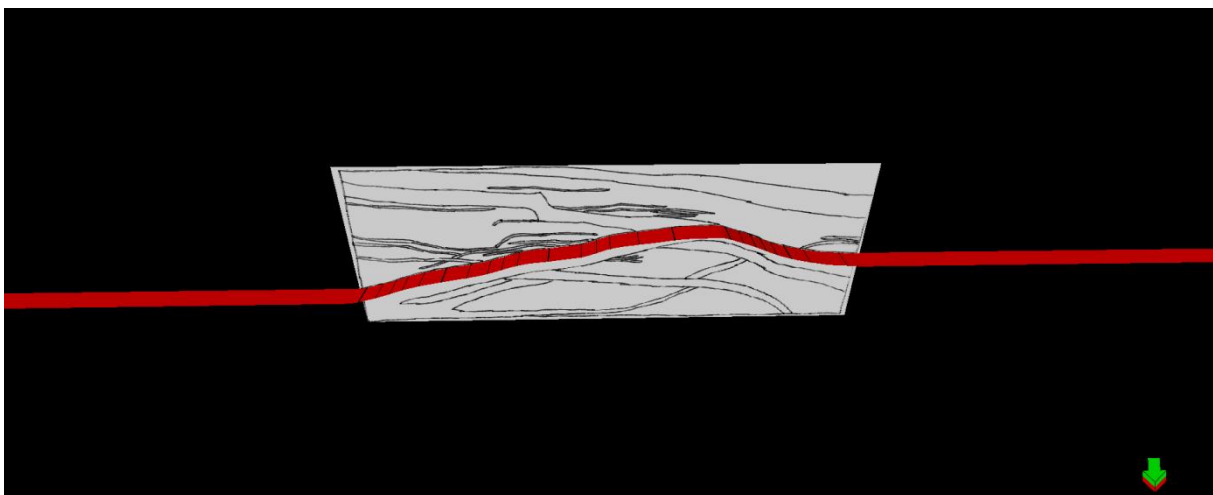Under the *Algorithm* tab you can specify which algorithm that should be used to create the surfaces from the polygons. In this thesis the algorithm *closest* was used. This algorithm uses the closest input point for the created surface, and assigns each node with the closest observation. The model will then have constant values in the y-direction (2.5D model). The default settings for the algorithm was used, see Figure A.5.

For the gridding purposes of the geological model all the surfaces should be made continuous through the whole model, that is, each surface should go from the left side of the model to the right side. This means that some of the surfaces have to overlap each other, something that can be done by using the *Calculations* tab under the *Settings* of the given surface, see Chapter A.5.1.

In order to be able to make a regular grid (see Appendix A.7) it is also important that the top and bottom which defines the extent of the model are made completely horizontal. A regular grid is needed in order to use the modelling algorithm implemented in the Madagascar software.

To get rid of peaks and troughs created by the *Make/edit surface* algorithm the surfaces probably have to be smoothed.
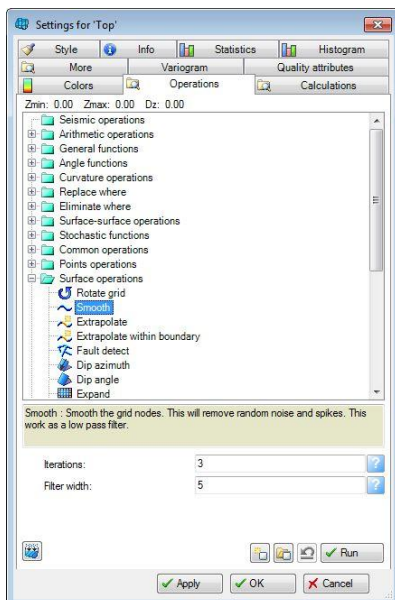
Figure A.7: Smooth surfaces.

This can be done by going to the *Settings* for the chosen horizon, click on the *Operations* tab, expand *Surface operations* and select *Smooth*. Here it is possible to select different values for the number of iterations and the filter width. Larger numbers give higher smoothing. It is also possible to do local smoothing, but then you may lose the property that the model is kept constant in the y-direction. Local smoothing can be done by highlighting the **Make/edit surface** process and clicking the *Smooth area* or *Peak remover* icon.
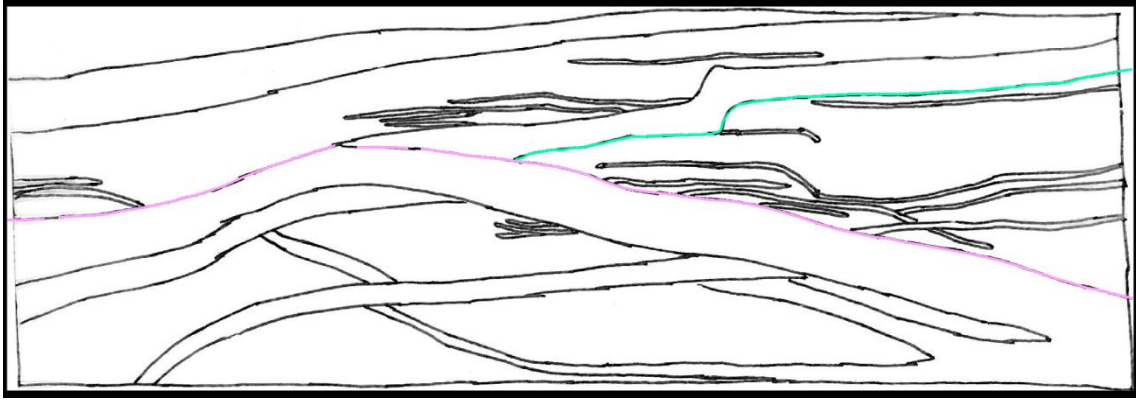
Figure A.8: Overlapping surfaces.

To extend some of the surfaces from one side to the other, it may be necessary to overlap some of the surfaces. For instance in Figure A.8 above, one possibility to extend the surface corresponding to the green line all the way to the left of the model would be to let this surface follow the surface corresponding to the pink line. This can be done under the *Calculations* tab under the *Settings* for the given surface. An example is shown beneath.
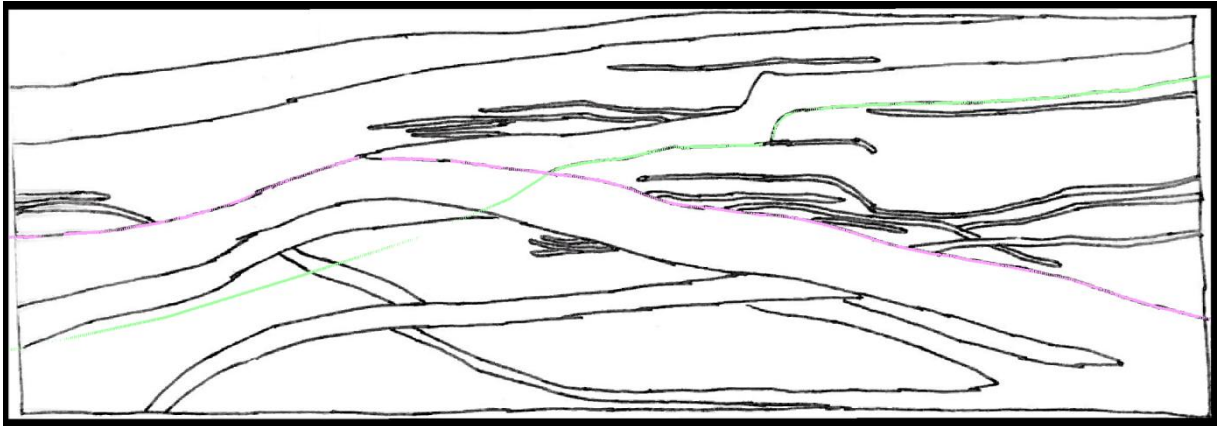
A.5.1 Example

Figure A.9: Two polygons drawn upon the handmade model imported into Petrel.

Figure A.9 above shows the handmade model imported into Petrel together with two polygons drawn upon it. Because we want the surfaces to be continuous throughout the whole model, the polygon for the uppermost surface (green line) is drawn consequently beneath the polygon for the lowermost surface (pink line) to the left of the point of intersection. We now want the uppermost surface to follow the lowermost surface to the left of the point of intersection. The possibility of drawing the polygon for the uppermost surface directly on the lowermost surface will involve more uncertainties, as it is very difficult to exactly follow the same path. It would also be more time consuming.
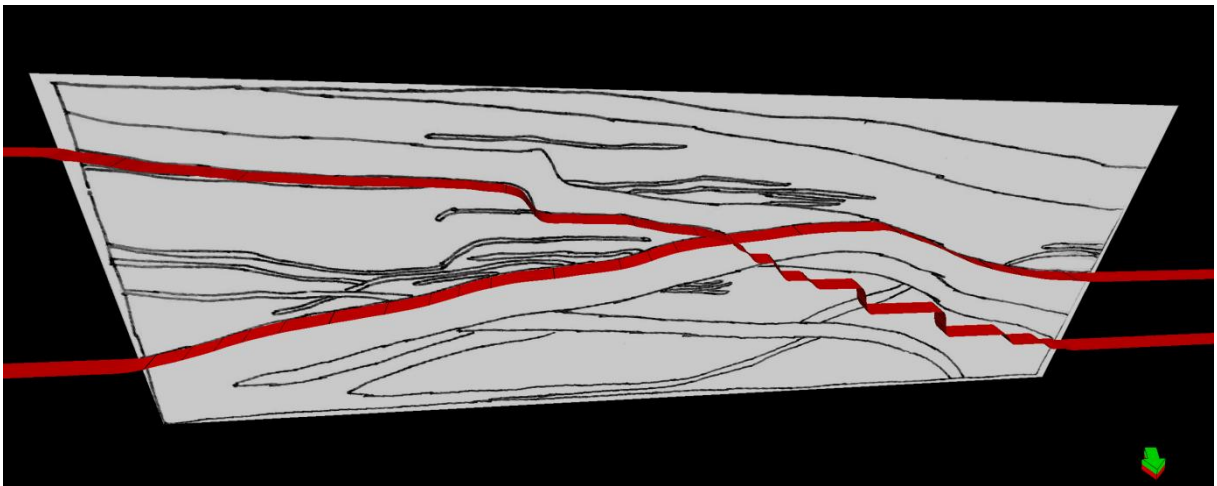
Figure A.10: Two smoothed surfaces that are not overlapping.

First we make surfaces for the two horizons and smooth them. The result is shown in Figure A.10 above.

After smoothing the surfaces, we go to the *Settings* for the uppermost horizon and click on the *Calculations* tab.
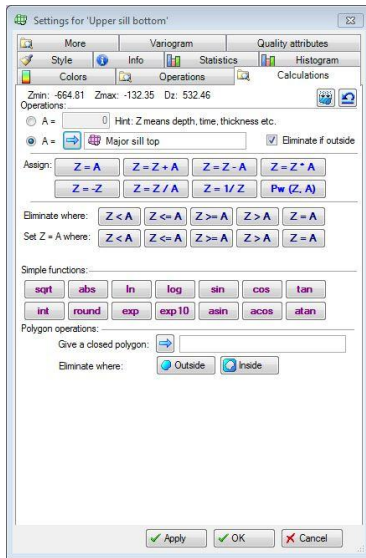
Figure A.11: Calculations tab.

We take in the lowermost surface as input under A=, and then click the button set Z=A where: Z<=A.
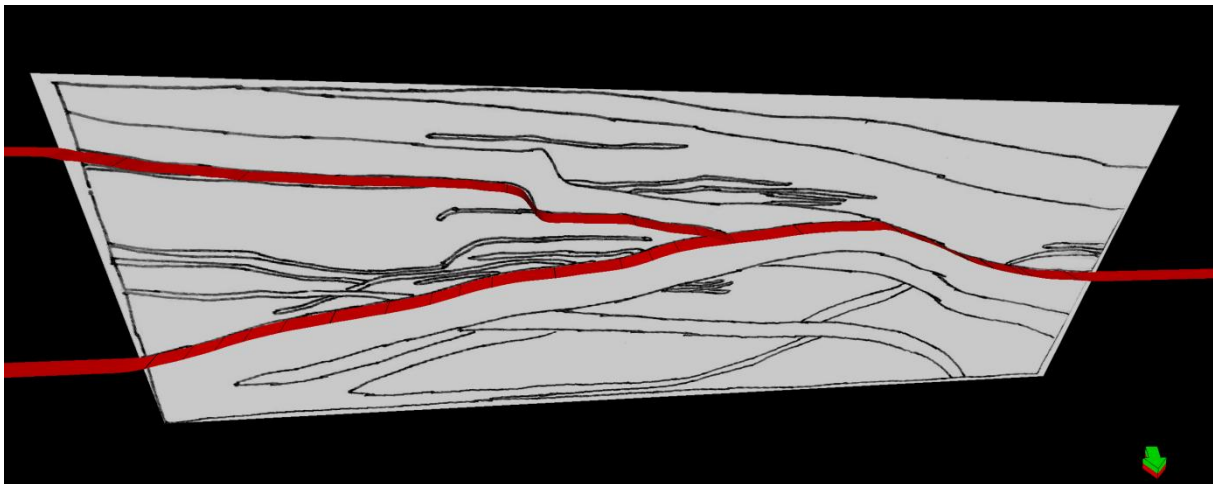
Figure A.12: Two surfaces partly overlapping each other.

The result is shown in the Figure A.12 above. With this method the uppermost surface will follow the lowermost surface perfectly and we don't need to worry about any differences between the surfaces in the part where they are supposed to overlap each other.

A.6 Inserting a water layer on top

A water layer can be inserted on top of the model by moving all of the surfaces down with a constant (equal the desired water depth).

Figure A.13: The surface is moved down by 1000 m.

This can be done in the *Calculations* tab under the *Settings* for each surface. Type in the thickness of the water layer you want to add and click on *Assign Z=Z-A*, to move the surface down. This has to be done for all the surfaces.

A.7 Gridding

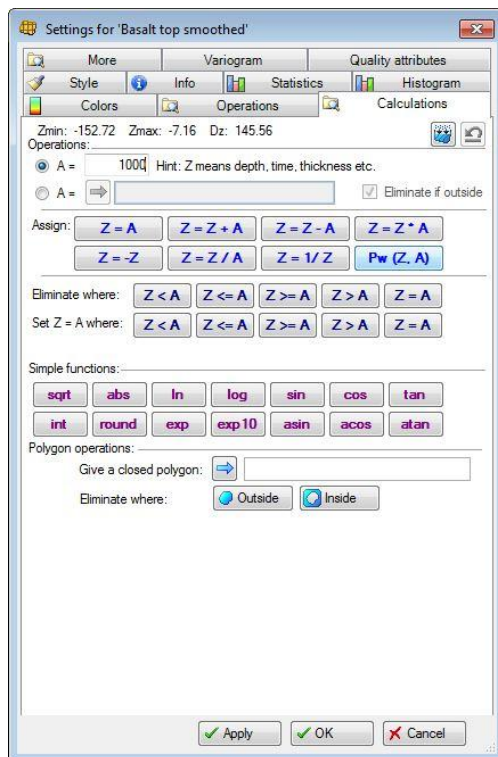Petrel has several gridding options, and the simplest one is the **Make simple grid** process, which has been used in this thesis. **Make simple grid** is the simplest gridding process in Petrel, and the process only accepts surfaces as input, which means that no faults are taken into account. However, as long as the model is not going to be used to do any flow modelling, this gridding process can also be used in the presence of faults.
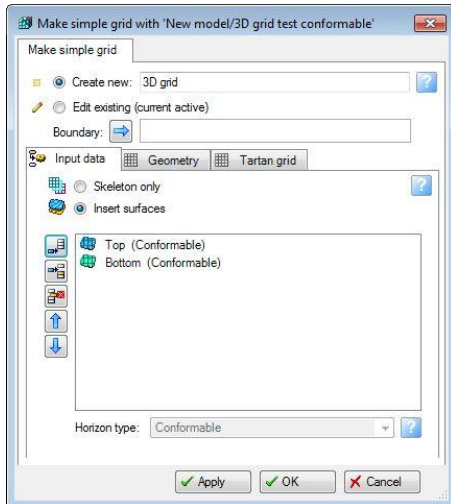
Figure A.14: Make simple grid – input data.

Double-click on the **Make simple grid** process under *Utilities* in the *Processes* pane. Click on *insert surfaces* in the *Input data* tab and insert the top and bottom of the model. This will define the extent of the model. The reason why we choose not to insert all the surfaces is that this will result in a grid that is not regular, the grid will instead follow the different surfaces. For this reason it is important that the top and bottom of the model are completely horizontal.

Figure A.15: Make simple grid – geometry.

Go to the *Geometry* tab, click the radio button for *user defined* and specify the geometry. It's easiest to mark one of your surfaces and click *Get limits from selected*, but it's also possible to specify them manually. Under *Grid increment* type in the desired grid increment.

The model has now been gridded in the xy-plane, and the grid consists of vertical pillars in the xy-plane. So in order to make regular cells out of these pillars, we need to specify the number of layers in the z-direction. Double-click on **Layering** under *Corn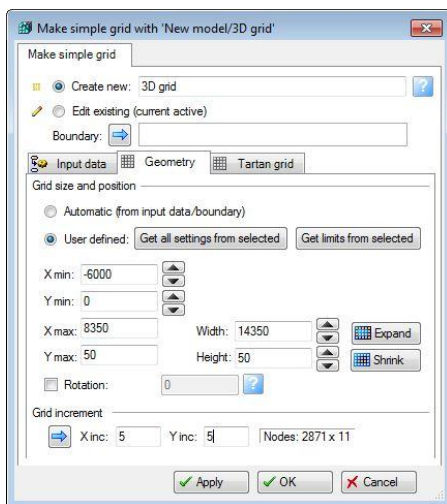er point gridding* in the *Processes* pane. Under *Zone division* change the number of layers so that the cells get the same size in all three dimensions. In this case the model is 1800 m deep and we have chosen a gridding of 5x5 m so the number of layers is: $\frac{1800\,m}{5\,m} = 360$.
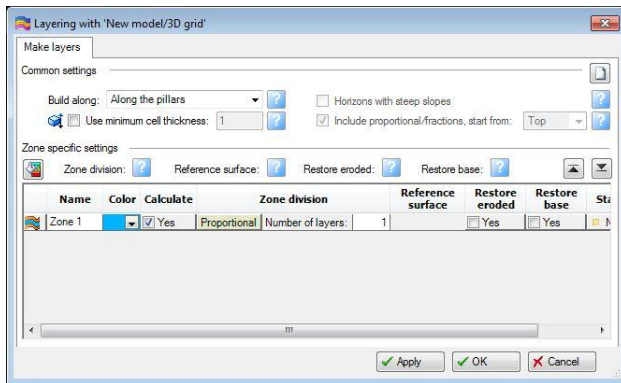
Figure A.16: Specify the number of layers.

A.8 Inserting properties between the layers

To create a geophysical model, velocities and densities needs to be assigned to the model. This can be done under **Geometrical modeling**, which can be found under *Property modeling* in the Processes pane.
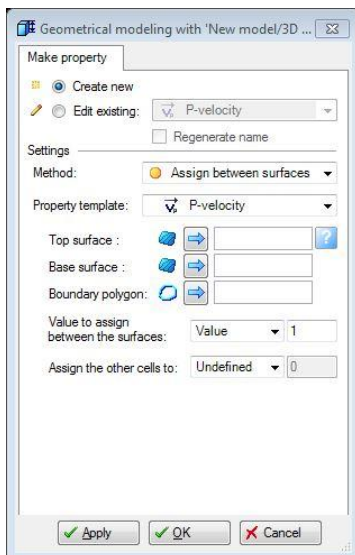
Figure A.17: Geometrical modelling.

Under *Method* select *Assign between surfaces and polygons* and choose which property to assign under *Property template.* Select the top and the base surface you want to fill in the property between and assign the values by typing in a value under *Value to assign between surfaces*. It's also possible to give the remaining cells a value, by selecting *value* under *Assign the other cells to* and type in a value. Click apply. Repeat the procedure to assign other values between other surfaces, but

66

remember to select unchanged under *Assign the other cells to*, otherwise the cells you have already assigned will be changed.
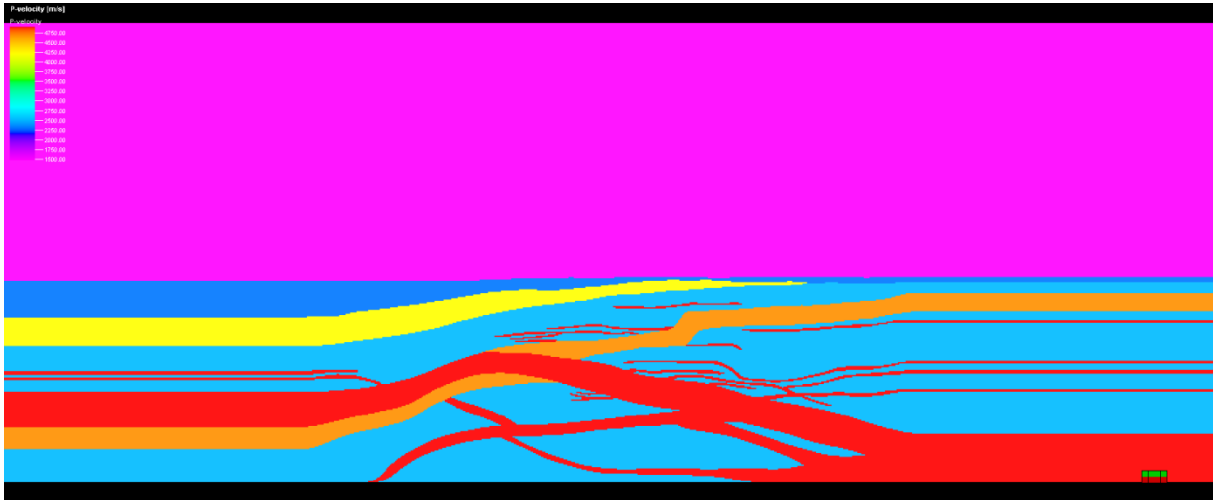
Figure A.18: P-wave velocities.

Figure A.18 shows the P-wave velocities after completing the **geometrical modelling** process. The Grid cells can also be shown by highlighting the model under the *Models* pane and click on

Show/hide grid lines.

A.9   Exporting data
When the geophysical model in Petrel has been completed, the data can be exported.
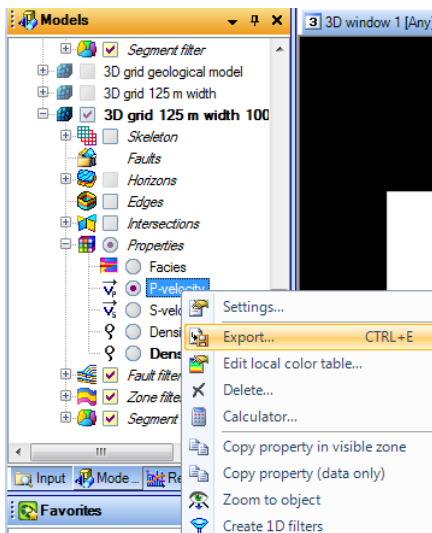
Figure A.19: Exporting data from Petrel.

This is done by right clicking on the property you want to export under the Models pane and then click Export…
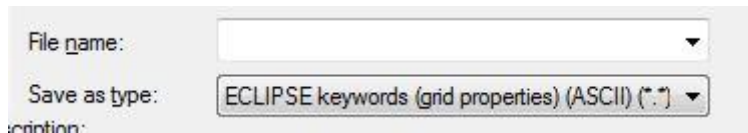
Figure A.20: Eclipse (ASCII) format.

Select the ECLIPSE (ASCII) format and click Save.

A.10   Convert the file from Eclipse (ASCII) format to RSF format

To be able to use the Madagascar software to do the modelling, the files have to be converted from Eclipse (ASCII) format to RSF format, which is the format excepted by Madagascar. In order to do this the Madagascar program *sfpetread* has been used.

The syntax to use sfpetread is as follows

```
sfpetread > Fmod.rsf petfile=inputfile
```

, where Fmod.rsf is the name of the output file and input file is the Eclipse (ASCII) file from Petrel.

Appendix B – Madagascar scripts

B.1 Modelling scripts

B.1.1 Modelling 1

```
##### Importing libraries

from rsf.proj import *

from rsf.recipes import msimmod


### Setup model

Flow('rho','rho-cut','window j1=1 j2=1')

Flow('vp','vp-cut','window j1=1 j2=1')

Flow('vs','vs-cut','window j1=1 j2=1')


Result('rho','grey bias=1750 scalebar=y color=j title="Density"')

Result('vp','grey bias=2250 scalebar=y color=j title="P-wave"')

Result('vs','grey bias=750 scalebar=y color=j title="S-wave"')


### Zoom input model

Flow('vp2','vp-cut','cp')

Result('vp2','window f2=1200 n2=470 | grey color=j scalebar=y title="P-wave input
model"')


##### Modeling

# Parameter setup

par = {

      'dim':2,

      'nshots':75,

      'dt':0.0004,

      'nt':7000,

      'surface':0,

      'local_models':1,

      'ghost_border':50,

      'amax':300,

      'kmax':10,

      'shotgeometry':'shots.rsf',

      'workingpath':'/work/austrhei/independence/original/'
```

```
}

par['receiver'] = {'xstart':180,'xend':380,'xinc':2,'z':2}

par['size']={'nx':400}

par['inc']={'x':5}

par['start']={'x':920}

par['end']={'x':1295}

par['source']={'x':180,'z':4}

msimmod.param(par)


# Wavelet

msimmod.wavelet('source',30.0,10000,500,par)

Result('source','graph title="Source wavelet"')


# Modeling

msimmod.split('rho','vp','vs',par)

msimmod.mod('source','rho','vp','vs',par)

msimmod.cat('data',par)


# Frequency spectra

Flow('fspectrum','source','spectra')

Result('fspectrum','window n1=300 | graph title="Frequency spectrum"')


# Plotting

Result('data','grey color=g scalebar=y')



End()
```

B.1.2 Modelling 2 and 3

```
 ##### Importing libraries

from rsf.proj import *

from rsf.recipes import msimmod


### Setup model

Flow('rho','rho-cut','window j1=1 j2=1')

Flow('vp','vp-cut','window j1=1 j2=1')

Flow('vs','vs-cut','window j1=1 j2=1')


Result('rho','grey bias=1750 scalebar=y color=j title="Density"')

Result('vp','grey bias=2250 scalebar=y color=j title="P-wave"')

Result('vs','grey bias=750 scalebar=y color=j title="S-wave"')


### Zoom input model

Flow('vp2','vp-cut','cp')

Result('vp2','window f2=1200 n2=470 | grey color=j scalebar=y title="P-wave input
model"')


##### Modeling
# Parameter setup
par = {
      'dim':2,
      'nshots':236,
      'dt':0.0001,
      'nt':15000,
      'surface':0,
      'local_models':1,
      'ghost_border':50,
      'amax':300,
      'kmax':10,
      'shotgeometry':'shots.rsf',
      'workingpath':'/work/austrhei/independence/original/'
}
par['receiver'] = {'xstart':180,'xend':380,'xinc':2,'z':2}
```

```python
par['size']={'nx':400}

par['inc']={'x':2}

par['start']={'x':920}

par['end']={'x':1392}

par['source']={'x':180,'z':2}

msimmod.param(par)


# Wavelet

msimmod.wavelet('source',30.0,10000,500,par)

Result('source','graph title="Source wavelet"')


# Modeling

msimmod.split('rho','vp','vs',par)

msimmod.mod('source','rho','vp','vs',par)

msimmod.cat('data',par)


# Frequency spectra

Flow('fspectrum','source','spectra')

Result('fspectrum','window n1=300 | graph title="Frequency spectrum"')


# Plotting

Result('data','grey color=g scalebar=y')



End()
```

B.2 Processing scripts

B.2.1 Modelling 1

```
from rsf.proj import *


#===================================================
# SConstruct for basic processing flow
#===================================================


#--- Resampling


Flow("shots","data","sfwindow j1=10 f1=500 | sfput o1=0 o2=0 o3=0 d3=25")


#--- QC plot of shot
Flow("shot","shots","sfwindow min3=1000 max3=1000")
Result("shot", "sfgrey scalebar=y title='shot'")


#--- Mute
Flow("shots-mute", "shots", "sfmutter half=n v0=1550 x0=0 t0=0.07 tp=0.18")


#--- QC plot of muted shot
Flow("shot-mute","shots-mute","sfwindow min3=1000 max3=1000")
Result("shot-mute", "sfgrey scalebar=y title='Muted shot'")


#--- Sort to cdp
Flow("cmps", "shots-mute", "shot2cmp half=n")


#--- QC plot of cmp
Flow("cmp","cmps","window f3=200 n3=1")
Result("cmp", "grey scalebar=y title='cmp'")


#=====Uncomment for velocity analysis===========
#--- Velocity analysis
#Flow("scns", "cmps", "vscan half=n v0=1200 dv=20 nv=100 semblance=y")
#Flow("vrms", "scns", "pick rect1=30 rect2=20 v0=1500")
```

```
#--- QC plot of velocity scan

#Flow("scn","scns","window min3=3000 max3=3000")

#Result("scn", "grey min=1500 color=j")

#=====Uncomment for velocity analysis==========


#=====Uncomment for known depth velocity model ===========

#QC-plot of the velocity model

Flow("vp-zoom","vp","sfwindow  min2=6000 max2=8365")

Result("vp-zoom","grey min=1480 bias=1500 scalebar=y color=j title='P-wave'")

#--- Convert depth velocity model to time

Flow("xaa", "vp", "depth2time dt=0.004 nt=650 velocity=vp.rsf")

Result("xaa","window max1=1.5 min2=6000 max2=8350|sfgrey bias=1480 color=j
scalebar=y title='P-wave'")

#--- Convert stacking velocities

Flow("xab", "xaa", "vint2vrms")

Flow("vrms", "xab", "window min2=5500 max2=8365 | sfput o2=0")

#=====Uncomment for known depth velocity model ===========


#--- QC plot of vrms

Result("vrms","grey min=1480 bias=1500 scalebar=y color=j title='vrms'")


#--- Nmo
Flow("nmos", ["cmps","vrms"], "sfnmo half=n velocity=${SOURCES[1]}")


#--- QC plot of nmo corrected cmp
Flow("nmo","nmos","window min3=1000 max3=1000")

Result("nmo", "sfgrey scalebar=y title='nmo'")


#--- Stack
Flow("stack", "nmos", "sfstack")

Result("stack", "sfgrey scalebar=y title='stack'")


#---- Migration
Flow("tcmp","cmps","transp plane=23 memsize=1")

Flow("migstack", ["tcmp","vrms"], "sfmig2 vel=${SOURCES[1]} half=n")
```

```
Result("migstack", "window max1=1.5 min2=500 max2=2840 |sfgrey scalebar=y
title='migstack'")

End()
```

B.2.2 Modelling 2 and 3

```
 from rsf.proj import *


#===================================================
# SConstruct for basic processing flow
#===================================================


#--- Resampling


Flow("shots","data","sfwindow j1=40 f1=500 | sfput o1=0 o2=0 o3=0 d3=10")


#--- QC plot of shot
Flow("shot","shots","sfwindow  min3=1000 max3=1000")
Result("shot", "sfgrey scalebar=y title='shot'")


#--- Mute
Flow("shots-mute", "shots", "sfmutter half=n v0=1550 x0=0 t0=0.07 tp=0.18")


#--- QC plot of muted shot
Flow("shot-mute","shots-mute","sfwindow min3=1000 max3=1000")
Result("shot-mute", "sfgrey scalebar=y title='Muted shot'")


#--- Sort to cdp
Flow("cmps", "shots-mute", "shot2cmp half=n")


#--- QC plot of cmp
Flow("cmp","cmps","window f3=200 n3=1")
Result("cmp", "grey scalebar=y title='cmp'")


#=====Uncomment for velocity analysis==========
#--- Velocity analysis
#Flow("scns", "cmps", "vscan half=n v0=1200 dv=20 nv=100 semblance=y")
```

```
#Flow("vrms", "scns", "pick rect1=30 rect2=20 v0=1500")


#--- QC plot of velocity scan

#Flow("scn","scns","window min3=3000 max3=3000")

#Result("scn", "grey min=1500 color=j")

#=====Uncomment for velocity analysis===========


#=====Uncomment for known depth velocity model ===========

#QC-plot of the velocity model

Flow("vp-zoom","vp","sfwindow  min2=6000 max2=8365")

Result("vp-zoom","grey min=1480 bias=1500 scalebar=y color=j title='P-wave'")

#--- Convert depth velocity model to time

Flow("xaa", "vp", "depth2time dt=0.004 nt=363 velocity=vp.rsf")

Result("xaa","window max1=1.4 min2=6000 max2=8365|sfgrey bias=1480 color=j
scalebar=y title='P-wave'")

#--- Convert stacking velocities

Flow("xab", "xaa", "vint2vrms")

Flow("vrms", "xab", "window min2=5500 max2=8365 | sfput o2=0")

#=====Uncomment for known depth velocity model ===========


#--- QC plot of vrms

Result("vrms","grey min=1480 bias=1500 scalebar=y color=j title='vrms'")


#--- Nmo

Flow("nmos", ["cmps","vrms"], "sfnmo half=n velocity=${SOURCES[1]}")

Result("nmos","sfgrey")


#--- QC plot of nmo corrected cmp

Flow("nmo","nmos","window min3=1000 max3=1000")

Result("nmo", "sfgrey scalebar=y title='nmo'")


#--- Stack

Flow("stack", "nmos", "sfstack")

Result("stack", "sfgrey scalebar=y title='stack'")
```

```
#---- Migration

Flow("tcmp","cmps","transp plane=23 memsize=1")

Flow("migstack", ["tcmp","vrms"], "sfmig2 vel=${SOURCES[1]} half=n")

Result("migstack", "window max1=1.0 min2=500 max2=2850 |sfgrey scalebar=y
title='migstack'")

End()
```
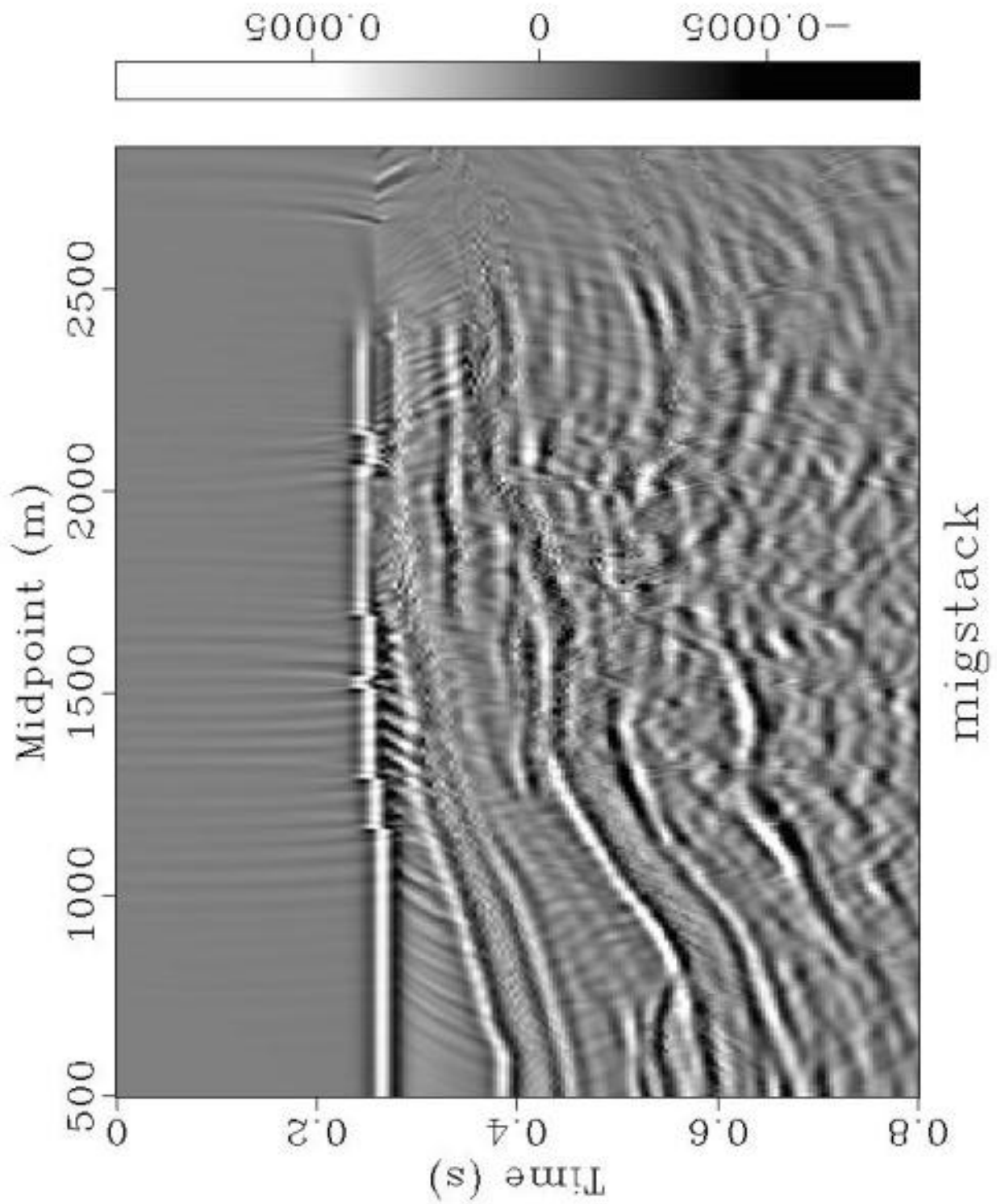
```
#---- Migration

Flow("tcmp","cmps","transp plane=23 memsize=1")

Flow("migstack", ["tcmp","vrms"], "sfmig2 vel=${SOURCES[1]} half=n")

Result("migstack", "window max1=1.0 min2=500 max2=2850 |sfgrey scalebar=y
title='migstack'")
```
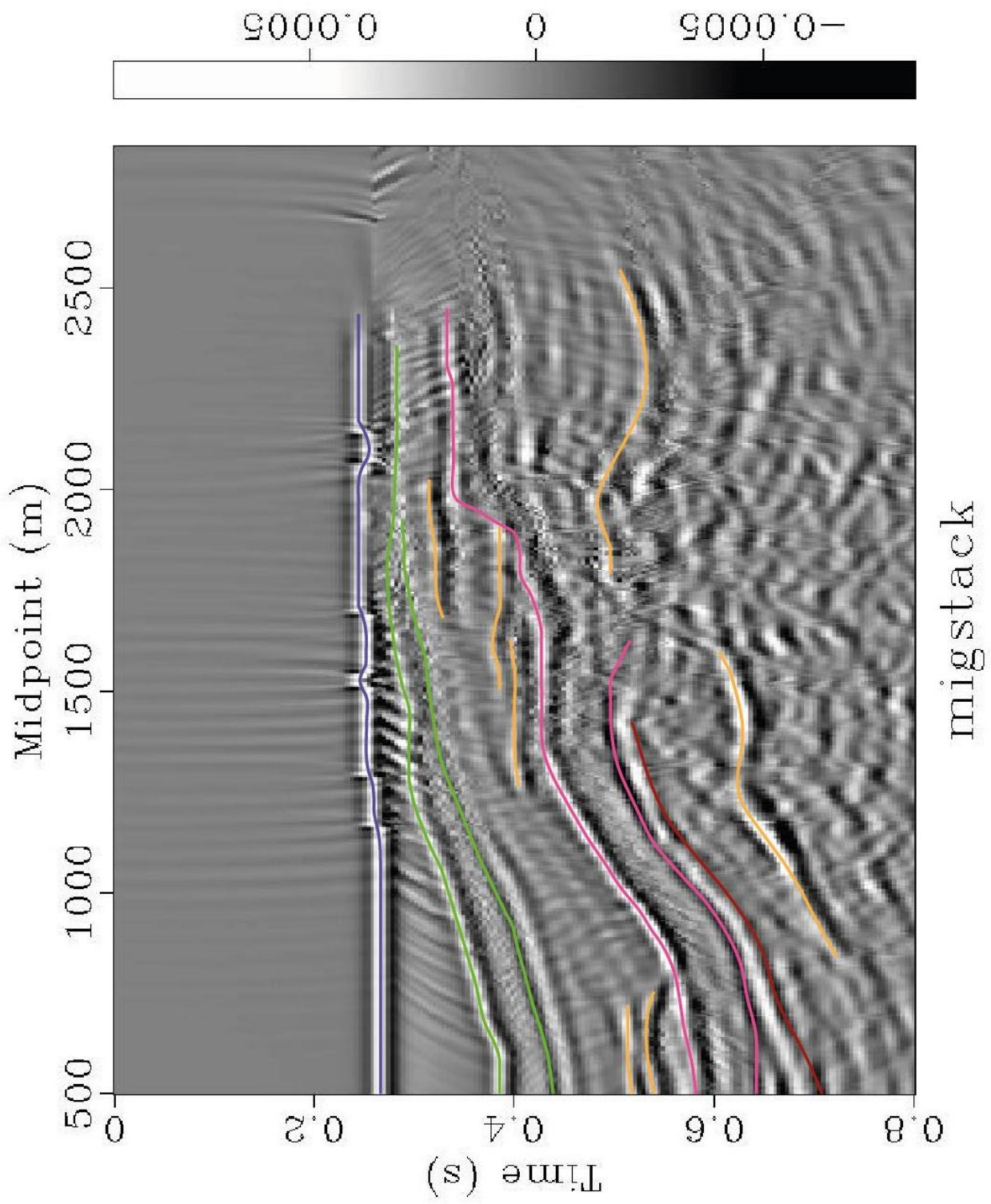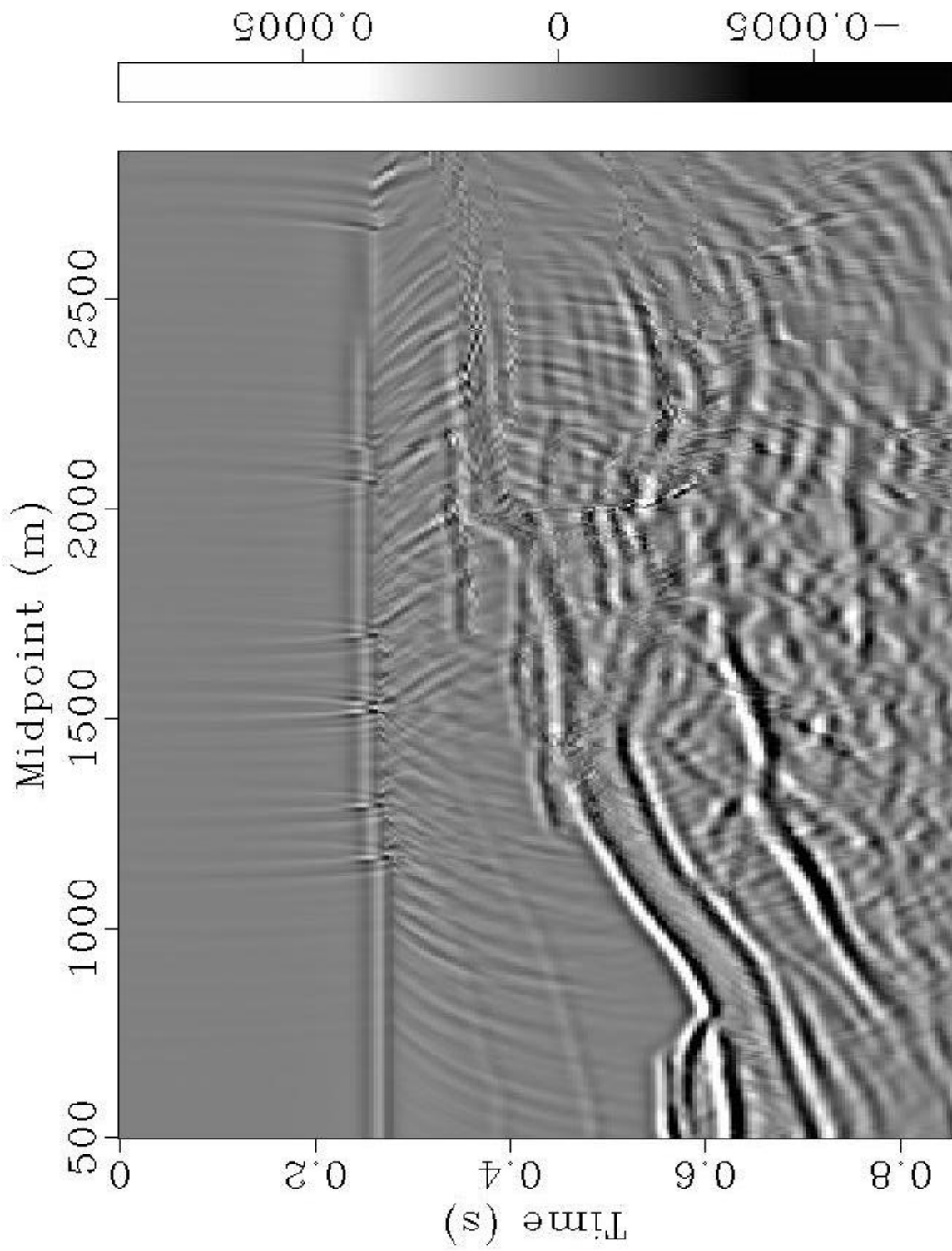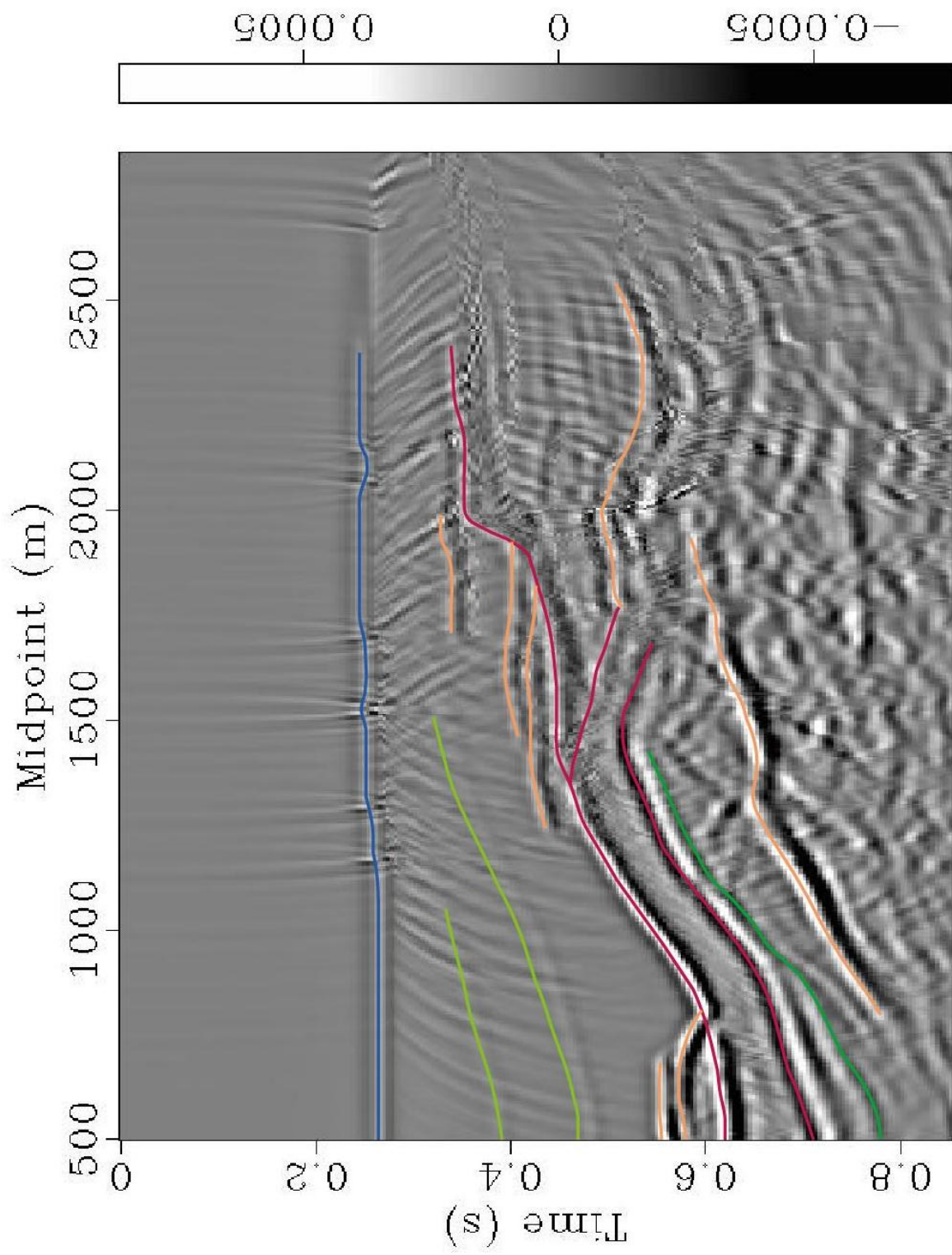
Figure C.1: Migrated section from modelling 2.

Figure C.2: Interpretation of the migrated section from modelling 2.

Figure C.3: Migrated section from modelling 3, where the plateau basalts have been replaced with sandsrtone.

Figure C.4: Interpretation of the migrated section from modelling 3, where the plateau basalts have been replaced by sandstone.